SBUF

ID: 13342

SKANSKA

LUNDS UNIVERSITET

MODELL FÖR PREDIKTERING AV SALTFROSTBESTÄNDIGHET HOS BETONG MED NYA BINDEMEDEL

Slutrapport

David Wahlbom

2022-06-17

SBUF stödjer
forskning & utveckling
som leder till
praktisk handling

Moisture uptake and salt frost deterioration of concrete

David Wahlbom

LUND
UNIVERSITY

Licentiate Thesis, Report TVBM - 3190, Division of Building Materials,
Faculty of Engineering, Lund University, Lund 2022

Faculty of Engineering, Lund University
Department of Building and Environmental Technology
Division of Building Materials

ISBN 978-91-8039-326-3 (Print)
ISBN 978-91-8039-327-0 (PDF)
ISSN 0348-7911 TVBM

Printed in Sweden by Lund University
Lund 2022

Preface

The work presented in this licentiate thesis has mainly been carried out at the Division of Building Materials, Lund University, starting 2017. Thanks to IFSTTAR in Paris, France for taking care of me the six month I was there. I also wish to express my acknowledgement to The Industrial-Academic Nanoscience Research Network for Sustainable Cement and Concrete, (Nanocem) and the Development Fund of the Swedish Construction Industry, SBUF and especially Hans Hedlund och Joakim Jeppsson from Skanska, for financing this project.

I would like to thank my main supervisors Katja Fridh and Lars Wadsö for their advice, discussions and support. Without you this project would not have been possible.

I would also like to thank all my co-supervisors and industrial advisors I have had during this project: Mette Geiker, Stefan Jacobsen, Teddy Fen-Chong, Patrick Dangla, Jan Skocek, Fabrizio Moro, Quoc Huy Vu, and Mohsen Ben Haha. It was an honor having such a large group of experts in this field, supporting me, giving me feedback and driving this project forward.

A special thanks to IFSTTAR, for the opportunity to spend five months in France to learn poromechanics and modelling, even though the performed simulations are not part of this thesis.

I also want to thank Stephen Hall and Jonas Engqvist at Solid Mechanics at Lund University for their help with the X-ray micro-tomography measurements.

To my friends, family and colleagues at the department, for supporting me through it all, thank you.

Summary

Concrete is one of the most used building materials in the world because it is flexible, durable so it can be used in different harsh environments, and can be made into almost any shape. A problem with concrete is that the cement industry releases 5-8% of the total man-made carbon dioxide emissions. These emissions can be reduced by using supplementary cementitious materials, such as ground granulated blast-furnace slag to replace a part of the cement in concrete. These materials change the material properties of the finished concrete, and a good understanding of how they change is needed for the proper uses of concretes containing supplementary cementitious materials.

For countries where the temperature often decreases below freezing temperatures, frost deterioration of concrete is an important durability issue. Structures exposed to a combination of high degree of saturation and low temperatures have an increased risk of suffering damage due to frost. This can result in both surface scaling and internal cracking, which can then lead to loss of concrete cover, reduced protection of the reinforcement, and possible loss of load bearing capacity. The deterioration is also accelerated in the presence of salt.

This thesis has focused on two different topics relevant to the study of frost deterioration of concrete. The first topic includes participating in further developing an existing frost deterioration model and providing input material parameters that can be measured experimentally. The second topic includes the planning and execution of experimental series to be used as verification of different parts of the mechanism of models of salt frost deterioration.

For the first topic, a cooperation with Daniel Eriksson at KTH, was initiated, as he had already developed a poromechanical frost model. This model was further developed to simulate the influence of multiple freeze-thaw cycles and an external salt-containing solution (Paper I). The results indicate that the model can also describe freeze-thaw induced absorption into air-entrained concrete that is initially capillary saturated. In the thesis it is also shown how some of the material parameters needed for poromechanical modelling of frost deterioration can be measured experimentally.

For the second topic, a simplified approach was used to divide the complex problem of frost deterioration into smaller parts. It was not the actual scaling damage that was studied, but length change, ice formation and liquid uptake due to freezing temperatures and presence of water. Such results can be used to test if a poromechanical model can capture the proper trends of these phenomena of frost damage mechanism.

The additional liquid uptake through cryosuction during freezing temperatures compared to room temperature was confirmed through the cryosuction experiments on different concretes (Paper II). The samples were capillary saturated at the start of the experiment to isolate the effect of cryosuction. In this study, the liquid uptake was not influenced by if the samples were in contact with salt solution or pure water, or by replacement of cement with ground granulated blast furnace slag, but samples with air entrainment agent had a tendency to have a higher liquid uptake than the samples without air entrainment agent. The results generally show larger spread and larger mean uptake for the cases with freezing temperatures compared to the case at constant room temperature, with some samples reaching much higher liquid uptakes than other samples. The liquid uptake in constant room temperature samples was significantly more uniform. We hypothesize that the higher liquid uptake in some samples was caused by the filling of stochastically distributed large pores in the freezing zone.

The further development of poromechanical models and the support they need from experimentalist to give relevant data for verification shows that a joint cooperation between modelling and experiments is the way forward if we want to improve the understanding of the mechanisms for frost deterioration. This study is therefore a small step towards a better understanding and improved tools for the management of future concrete production.

Sammanfattning

Betong är det mest använda byggmaterialet i världen på grund av att det är så flexibelt, beständigt - så att det kan användas i många olika miljöer - och kan ges nästan vilken form som helst. Ett problem är dock att cementindustrin står för 5-8% av de totala koldioxidutsläppen i världen, men dessa utsläpp kan minskas genom att använda olika tillsatsmaterial, såsom mald granulerad masugnsslagg för att ersätta en del av cementen i betong. Dessa tillsatsmaterial förändrar materialegenskaperna hos den färdiga betongen, och en god förståelse för hur de förändras krävs för att använda betong som innehåller tillsatsmaterial.

För länder där temperaturen ofta sjunker under noll grader, är frostbeständighet av betong en viktig beständighetsfråga. Betong som utsätts för en kombination av hög vattenmättnadsgrad och låga temperaturer har en ökad risk att drabbas av frostskador. Detta kan resultera i både avskalning och inre sprickor, vilket då kan leda till minskning av betongens täckskikt, minskat skydd för armeringen och eventuellt förlust av bärförmåga. Försämringen accelereras när salt är närvarande.

Denna avhandling fokuserar på två olika områden som är relevanta för studier utav frostnedbrytning av betong. Det första området innefattar deltagandet i vidareutvecklingen av en befintlig modell för frostnedbrytning och tillhandahålla indata för värden för materialparametrar som kan mätas experimentellt. Det andra området innefattar utformning och genomförande av experiment som kan användas som verifiering för olika delar för modeller för frostnedbrytning.

För det första området så inleddes ett samarbete med Daniel Eriksson på KTH, då han har utvecklat en poromekanisk frostmodell. Denna modell vidareutvecklades för att kunna simulera påverkan av flera fryscykler och med en saltlösning som extern vätskereservoar (Artikel I). Resultaten indikerar att modellen även kan beskriva vattenupptagning i betong med luftporbildare under frysning och som initialt är kapillärmättad. I avhandlingen presenteras även hur några av de materialparametrar som behövs för poromekanisk modellering av frostnedbrytning kan mätas experimentellt.

För det andra området delas det komplexa problemet med frostnedbrytning in i mindre delar. Det är inte skadorna från avskalning som studeras, utan längdändring, isbildning och vätskeupptagning på grund av låga temperaturer i kombination med

närvaro av vatten. Resultat kan användas för att testa om en poromekanisk modell kan fånga de rätta trenderna för dessa fenomen under ett frysförlopp.

Vätskeupptaget under frysning är högre jämfört med vätskeupptaget under rumstemperatur. Detta bekräftades genom experiment på olika betonger (Paper II). Provkropparna var kapillärmättade i början av experimentet för att isolera effekten av vätskeupptagning under frysning. I denna studie påverkades inte vätskeupptaget av om proverna var i kontakt med saltlösning eller rent vatten, eller om en del av cementet ersattes med mald granulerad masugnsslagg, men prover med luftporbildare hade en tendens att ha en högre vätskeupptag än proverna utan luftporbildare. Resultaten visar generellt större spridning och större vätskeupptag för proverna som utsätts för frysning jämfört med rumstemperatur. Vätskeupptaget för prover i rumstemperatur var betydligt mer enhetligt med mindre spridning. Vi antar att det högre vätskeupptaget i vissa prover orsakades av fyllning av stokastiskt fördelade stora porer i fryszonen.

Den fortsatta utvecklingen av poromekaniska modeller och det stöd de behöver från experimentalister för att ge relevant data för verifiering, visar att ett gemensamt samarbete mellan modellering och experiment är vägen framåt om vi vill förbättra förståelsen för mekanismerna för frostnedbrytning. Denna studie är därför ett litet steg mot en bättre förståelse och förbättrade verktyg för framtida betongproduktion.

Table of content

List of appended publications

I. Hygro-thermo-mechanical modeling of partially saturated air-entrained concrete containing dissolved salt and exposed to freeze-thaw cycles

D. Eriksson, D. Wahlbom, R. Malm, K. Fridh
Cement and Concrete Research, volume 141, 2021, 106314

I am the second author, my contribution is: Writing - Review & Editing. The first author is Daniel Eriksson, who did a major part of the work on this paper. His contribution is: Methodology, Software, Validation, Formal analysis, Writing - Original Draft, Writing - Review & Editing, Visualization

II. Cryosuction experiments on concrete containing ground granulated blast-furnace slag; influence of temperature, air entrainment and salt

D. Wahlbom, K. Fridh
Manuscript: Submitted to Nordic Concrete Research

I am the first author of this paper, my contribution is: Methodology, Experimental work, Analysis, Writing - Original Draft, Writing - Review & Editing.
Katja Fridh: Methodology, Writing - Review & Editing.

List of attended conferences

An abstract or report have been sent to the attended conferences. These are not appended as the relevant information is presented in this thesis.

2017 Aalborg, Denmark, Nordic Concrete Research Symposium

2017 Leimen, Germany, Nanocem consortium Spring meeting

2018 Zurich, Switzerland, Nanocem Spring Meeting

2019 Madrid, Spain, Nanocem Spring Meeting

1 Introduction

Concrete is the most used building material in the world and the cement industry releases 5-8% of the total man-made carbon dioxide emissions [1]. These emissions can be reduced by using SCM, supplementary cementitious materials, such as ground granulated blast-furnace slag (GGBS), fly ash, and silica fume to replace a part of the cement in concrete. When using different SCMs, the change in chemical and material properties needs to be taken under consideration, e.g., the hydration progress is slowed down and the pore structure of the concrete can become coarser, as in the case with carbonated concrete with high levels of granulated blast-furnace slagg [2, 3].

Frost deterioration of concrete is an important durability issue for structures exposed to a high degree of saturation and low temperatures. The deterioration is also accelerated with the presence of salt. This can result in both surface scaling and internal cracking, which can then lead to loss of concrete cover, reduced protection of the reinforcement and possible loss of load bearing capacity [4]. The degree of deterioration depends on the surrounding environment (e.g. temperature, rain, salt concentration) and the materials properties (e.g., permeability, pore size distribution, air void structure, and mechanical properties).

The concrete can be protected against frost deterioration by a proper air void system since this allows the pore liquid to move into the air voids and freeze without creating any pressure as explained by Powers and Helmuth [5]. This phenomenon has later been described by different models, some of them based on the poromechanical equations by Coussy [6, 7].

To make sure that new types of concrete are durable, an improved understanding of basic deterioration mechanisms is needed. It is also essential to recognize that more than one mechanism can contribute to frost damage and different mechanisms can be more or less dominant under certain climate conditions for materials with different properties.

1.1 Aim, research topics and limitations

As there is a lack of experimental data to use and test models of frost deterioration of concrete, the aim of this thesis is to support the development of models of such deterioration by experimental studies of the fundamental mechanisms. The thesis therefore presents experimental results that can be used as input data for frost deterioration models and/or testing part of the mechanism to better understand the complex process of frost deterioration of concrete.

The work of this thesis has focused on two different topics, for which I have sought to provide increased knowledge.

The first topic includes participating in further developing an existing poromechanical frost deterioration model in cooperation with Daniel Eriksson. The model was further developed to include freeze-thaw hysteresis, moisture uptake during multiple freeze-thaw cycles, non-saturated samples, and with salt in an external liquid reservoir.

The second topic includes the planning and execution of experimental series to be used as verification of models of salt frost deterioration. A simplified approach is used to isolate the problem of frost deterioration into smaller parts. It is not the actual scaling damage that is studied, but length change, ice formation and moisture uptake due to freezing temperatures and presence of water. This can be used to test if a poromechanical model can capture the trends of these phenomena.

The largest limitation in this work is that I do not study the actual frost damage process, but the mechanism behind it. This is a different approach compared to most other studies, but it is a fundamental way to approach modelling frost deterioration.

A second limitation is that some of the studies were made on mortars, instead of concrete, as mortar is easier to model.

A third limitation is that the effect of surface scaling due to the glue spall theory is not considered in this project.

2 Literature study

The aim of this literature study is to present relevant information about concrete as a material, and different theories on liquid uptake, frost damage and the effect of salt.

2.1 Concrete materials

Concrete is one of the most used building materials in the world because of its flexible use, its durability, that it can be made in almost any shape. There is also plenty of the necessary raw materials accessible all around the world. This thesis is focusing on the aspect of frost durability, and then properties like permeability, surface tensile strength, connectivity in the porous system and total air content are of importance when looking at the life expectancy for a concrete construction exposed to freezing temperatures.

2.1.1 Cement

Cement is made from the raw materials limestone ($CaCO_3$), clay and gypsum to give the product that is called Portland cement (PC) or CEM I according to the European standard EN 197-1 [8, 9]. The size of the cement grains is decided by the grinding process and with finer grains, there is more surface area per kg cement, and the reaction rate increases.

Cement chemists have a shorthand chemical notation which makes the writing of chemical formulas for cement reactions efficient. In this notation each oxide is denoted by a letter:

C - CaO
S - SiO_2

A - Al_2O_3
F - Fe_2O_3
H - H_2O

The chemical composition of the main clinkers are: alite (tricalcium silicate, C_3S), belite (dicalcium silicate, C_2S), aluminate (tricalicum aluminate, C_3A), and ferrite (calcium aluminoferrite, C_4AF) [10]. The different cement clinkers react at different rates in the exothermic hydration reaction. C_3S reacts early and thus contributes to early strength while C_2S reacts slower and contributes to the strength increase later in the hydration process. C_3A reacts immediately when in contact with water, but to avoid so called flash set, sulphate, often in the form of gypsum is added to the cement. C_4AF reacts slowly and does not contribute much to the final strength [10].

Calcium silicates C-S, react with water and form calcium hydroxide CH, and calcium silicate hydrate C-S-H-gel, which makes up the main part of hydrated cement paste, schematicly shown in Eq.1 without stoichiometric coefficients [10].

$$\text{C-S} + \text{H} \rightarrow \text{C-S-H} + \text{CH} \quad (1)$$

During the hydration, the cement grains are gradually dissolved and the C-H-S-gel is formed on the outside of each particle, which makes it interlocked with the C-S-H-gel from the surrounding grains. This mesh is what gives the concrete its strength, holds the aggregates in place and creates the porous system of gel-pores, capillary pores and air voids. The cement reaction is rapid after an initial induction period, but slows down as the water needs to penetrate deeper through the C-S-H-gel to the unreacted core for the reaction to continue [11].

2.1.2 Supplementary cementitious materials, SCM

The use of supplementary cementitious materials, SCM, when casting concrete changes, the chemical composition, the microstructure, and the strength development, and increases or decreases the concretes resistance to different aggressive agents [1]. A good understanding of these property changes is needed for the proper uses of concretes containing SCM [3]. The use of SCMs is increasing and the average percent of cement used as binder have gone down in the world, from 85% in 2003 to 77% in 2010 [12].

SCMs contain a reactive form of silicate and take part of the hydration process and will contribute to the strength of the concrete, but will not react on their own with water [12]. SCMs depend on C-H from the cement hydration to react and create a C-S-H-gel, so a certain amount of cement needs to have reacted before the SCM reaction can start, Eq. 3 [3].

$$\text{CH (from cement reaction)} + \text{S (from SCM)} + \text{H} \rightarrow \text{C-S-H} \quad (2)$$

Cement with SCM reacts more slowly than PC, as a certain amount of cement needs to have reacted first, and it takes longer time to reach the same strength compared to a CEM I cement, and the heat of reaction in the early stage is reduced [12, 13].

The two most common SCMs used in the concrete industry are ground granulated blast furnace slag, GGBS, and fly ash [12]. The GGBS, is created inside a blast furnace during the production of iron. Slag is formed on top of the melted iron as a by-product [14]. During production of GGBS, the slag needs to be cooled rapidly below 800 °C to get granular particles with an amorphous structure that gives the slag its reactivity [14]. Slowly cooling the slag results in an unreactive crystalline structure, which cannot be used as an SCM. The granular particles are then ground to a fine powder. The particle size of GGBS is similar to the size of cement grains, and GGBS can be ground to a smaller particle size to increase its reactivity. GGBS mainly consists of calcium oxide (CaO), silicon oxide (SiO_2), aluminium oxide (Al_2O_3) and magnesium oxide (MgO). Not all slag can be used for cement production, as it needs to have the approved chemical composition, been cooled rapidly and be reactive enough [14]. The GGBS composition is largely dependent on what iron ore that is used and the type of iron produced. The possible replacement

level is different for each SCM; GGBS is usually used with 20-70% replacement level of the cement but it can be up to 80-90% [3].

Fly ash consists of spherical particles formed as a by-product in coal power plants [9]. The particles are formed from rapid cooling of the exhaust gases. The fly ash is then gathered in mechanical or electrostatic filters in the chimney, to prevent it from getting released and pollute the surroundings. Not all fly ash can be used as SCM. Similar to the manufacturing of GGBS, it needs to be cooled rapidly to get the amorphous structure that gives its reactivity [15]. Fly ash particles have roughly the same size as cement grains. Fly ashes consist mainly of silicon oxide (SiO_2) and aluminium oxide, (Al_2O_3). According to the ASTM C618-19 standard [16], there are two classes of fly ash: class C-fly ashes with a high calcium content, and class F ashes with a low calcium content. Class F fly ash is more commonly produced and better suited as an SCM due to its higher content of silicon oxide. The quality of fly ash depends on the fuel for the coal power plant, and the burning conditions during combustion. The replacement level of fly ash is usually 10-25% [3].

2.1.3 Admixtures

Admixtures are used to change the properties of concrete, and are usually added in small doses, with a weight of less than 1% of the cement weigh. The basic functions of two types of admixtures are presented - air entraining agents and superplasticizers - as they are the only two admixture types used in the project.

2.1.3.1 Air Entraining Agents, AEA

The use of air entraining agents, AEA is recommended in concrete exposed to freezing, to increase the frost durability of the structure. The addition of AEA during the mixing of concrete creates a system of evenly dispersed and stable air bubbles with a diameter between 5 and -100 µm in the cement paste. This increases the total volume of air voids in the fresh concrete from between 1% and 3%, to between 4% and 10%, depending on the amount and quality of AEA [17, 18].

Air-entraining agents are surfactants that end up at the interface between air and water inside the cement paste and that stabilize the surface tension [19]. The surfactant molecules have one end that is hydrophilic and another end which is hydrophobic [19]. The AEA are separated into two main categories: soaps made from natural resins, e.g., root resins or gum resins, and synthetic surfactants, e.g., alkyl polyglycol ethers or alkyl sulphonates [20]. The role of AEA is only to produce these finer air bubbles and they do not react chemically with either cement or any other SCM [20].

2.1.3.2 Superplasticisers

Superplasticisers can be used to increase the workability of the concrete. Increased workability gives better flow, easier placing and it demands less vibration. The superplasticisers adsorb to the surface of cement grains in the fresh concrete, which disperse the grains and prevents early agglomeration [21]. Superplasticisers are separated into three categories: natural polymers e.g. lignosulphonates and casein, synthetic linear polymers, e.g., sulphonates and polymelamine sulphonates, and the newer comb-shaped copolymers, e.g., polycarboxylate ethers [17].

2.1.4 Aggregates

Aggregates take up about 75% of the weight of concrete, and different materials are used as aggregates depending on what are locally accessible. In Sweden, the bedrock consists largely of granite, which have high compressive strength and no porosity, and is well suited to be used as aggregate.

The choice of aggregates affects the workability and rheology of the concrete [22]. Both the shape and size of the aggregates and the particle size distribution are important to get a good rheology as it is the surface area of the aggregates that governs the amount of cement paste needed [22]. Aggregates with a small diameter have more surface and need more cement paste to create a good rheology than larger aggregates with less surface area per kg material. The rugged and hard edges of crushed stone create a stiffer rheology than when using natural gravel since the rounded and smooth surface of natural gravel creates less friction during mixing. Today, most aggregates in Sweden is crushed stone.

The final strength of concrete is a combination of the strength of the aggregates and the hardened cement paste [23]. For structures that will be exposed to freezing temperatures, frost resistant aggregates should be used. In general, a frost resistant aggregate has a high strength and low absorption [22]. If the aggregates have a high liquid absorption, then there is a risk for the liquid to freeze inside of the aggregates and create cracks, lowering its compressive strength.

2.2 Frost damage

This section will give a brief introduction to some of the different theories about frost deterioration, looking at both internal damage and surface scaling.

Internal damage can occur without visible surface damage, as cracks develop throughout the concrete as a result of a combination of freezing temperatures and a high degree of liquid saturation [24]. Internal damage results in higher permeability, lower E-modulus, and reduced load bearing capacity. It also opens up the material for other types of damage e.g. reinforcement corrosion [25].

Surface scaling is caused by a combination of freezing temperatures and a high liquid saturation in the surface, causing small flakes the surface to be spalled off. The damage is increased with the presence of low concentrations of salt [26, 27]. It can lead to reduced load bearing capacity and loss of concrete cover, which reduces the protection of the reinforcement [25].

Concretes that are properly air entrained gives an protective effect that decreases the mass of scaling and internal cracking [28] [29].

2.2.1 Hydraulic pressure theory and critical degree of saturation

The hydraulic pressure theory was presented by Powers in 1949 [28]. This theory describes the pressure on the solid matrix from the water expelled from pores due to the 9% increase in volume when water freezes into ice. Air voids are almost never saturated at non-freezing temperatures, and can work as expansion reservoirs where the liquid can be transported to and freeze without damaging the concrete, when the surrounding pores are saturated with liquid or ice [29], Fig. 1.

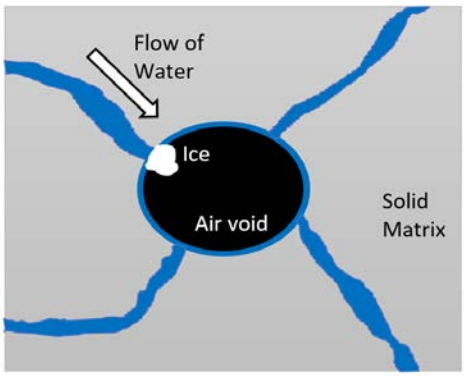

Figure 1. Liquid flows into the larger non-saturated air void from surrounding pores, where the liquid can freeze, figure adapted from [29].

The hydraulic pressure is connected to the distribution and distance between air voids, the so called spacing factor. The critical spacing factor is the longest distance that expelled water due to freezing has to move before it reaches an air void large enough to contain it without reaching the tension stresses that will damage the material [30]. The spacing factor is defined considering all the entrained air voids, but progressive saturation of those air voids, starting by the smallest one, has the same consequence as increasing the spacing factor [30], Fig. 2.

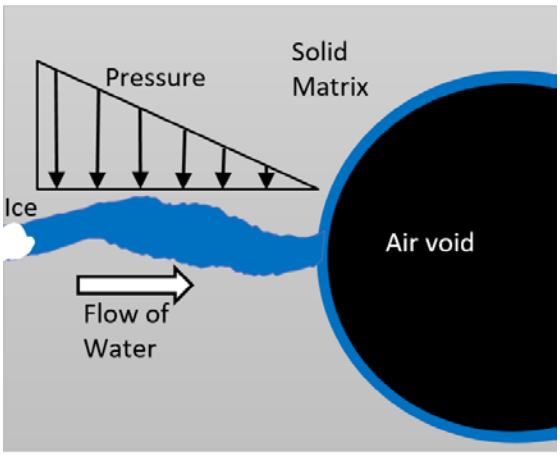

Figure 2. A schematic figure of the hydraulic pressure theory, when water freezes into ice. Figure adapted from [31].

Fagerlund presented the theory of critical degree of saturation in 1973 [32]. The critical degree of saturation is individual for each concrete and is a material parameter connected to how much liquid a porous material can contain without risk for frost damage. The amount of liquid is connected to how much space there is for ice to form, and how accessible this space is (spacing factor). If there is an external source of liquid, the pores that are still air-filled will slowly take up liquid through dissolution and diffusion of entrapped air. Therefore, to make a prediction of the future service life one possibility is to predict the long term absorption into the air void system [33].

2.2.2 Ice lens growth and cryosuction

Taber presented the theory of frost heave in soil in 1930 [34]. The theory described what occurs in a porous material when it is exposed to freezing temperatures on one side and non-freezing temperature in a liquid reservoir on the other during a long period of time. There will then be a transport of warmer unfrozen liquid towards the colder regions, where the liquid will freeze and form a macroscopic ice lens. The macroscopic ice lens can then continue to grow and shift the soil, causing damage on foundations of buildings or roads when the soil heaves. There needs to be a stable temperature gradient where the freezing front is located at roughly the same depth for an extended period of time and with a steady flow from the liquid reservoir, for the macroscopic ice lens to grow large enough [35]. The liquid reservoir in this case was the groundwater. Rosenqvist showed that hydraulic structures of concrete like hydro power plants also could experience similar conditions, facilitating macroscopic ice lens growth [36]. For a macroscopic ice lens to grow the concrete needs an external liquid reservoir, otherwise the growing ice lens will drain the surrounding pores of liquid and the growth of the ice lens will end [37]. It has been shown that a growing ice lens can create damage to concrete with high water/binder ratios because of its open pore system [35], Fig. 3.

Figure 3. Damage caused by macroscopic ice lens growth. Bottom of the sample were stored in unfrozen water, and the top of the sample were exposed to freezing temperatures, [35]. Figure used with consent from author M. Rosenqvist.

Powers and Helmuth [5] observed in freezing tests of both non-air-entrained and air-entrained cement pastes, that specimens with a well distributed air pore system contract more than pure thermal contraction during freezing. From their observations, Powers and Helmuth [5] proposed the theory of microscopic ice lens

growth in 1953. The theory is based on the fact that water has different freezing temperatures in pores of different sizes [38]. Formation of ice crystals starts from the largest pores containing liquid and becomes more difficult when the radius of the pores decreases [37]. Ice crystals in large capillary pores attract water from the gel and smaller capillary pores [36] [39]. A thin film of unfrozen water covers the interface between ice and the inside porous material, this thin film allows liquid to flow and supply the micro ice lenses [35]. The driving potential for the liquid transport is the difference in free energy between the ice and the liquid [34]. Unfrozen water at freezing temperatures has a higher free energy than the ice and will flow to the ice with lowest free energy. Ice in an unfilled air void is the ice that grow tensionless. When the ice in a pore reaches the pore wall it will exert pressure on the pore wall and its free energy will increase. The transport of water ceases when the free energy at the freezing and drying sites are equal (at equilibrium). Due to the drying effect of the pores containing unfrozen water, the material will shrink both as a result of the thermal contraction and the drying, explaining the increased shrinkage observed by Powers and Helmuth [5]. However, since the growing ice crystals in the larger pores exert a pressure on the solid matrix, the material will also expand. Depending on the size of the shrinkage due to drying and decreasing temperature and the size of the expansion due to ice pressure, the total volume change will be decided.

The phenomenon of liquid flowing to its crystalized form will occur, even if the crystalized phase decreases in volume compared to the liquid phase [40]. An experiment from Beaudoin and MacInnis using benzene instead of water during freeze testing in a sealed specimen of cement paste (without access to an external liquid reservoir) showed an increase in volume during freezing temperatures for benzene (below +6 °C) due to the pressure from the crystalized benzene in the air voids as these benzene crystals grow larger from liquid flowing from smaller surrounding pores [40], Fig. 4.

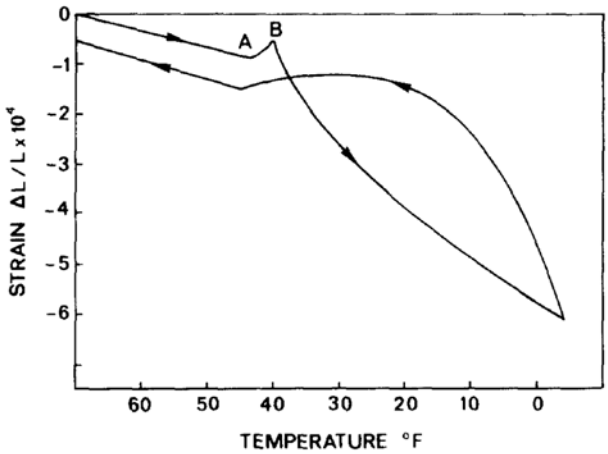

Figure 4. Length change depending on temperature on an benzene saturated sample of hardened cement paste, Figure adapted from [40]. (A) The sample starts to freeze and at (B), the sample have increased in volume due to the crystallization of benzene in the air voids.

When there is an external liquid reservoir, the microscopic ice lens mechanism will result in an increase in liquid uptake at freezing temperatures, compared to non-freezing temperatures,[35, 37, 41, 42]. The external liquid reservoir can continue to supply the microscopic ice lenses with liquid, when they have emptied the liquid in the surrounding smaller pores.

There is also an additional mechanism that increases the liquid uptake during temperature cycling: a pumping effect caused by the temperature gradient along the depth of the sample during freezing and thawing [43]. If the sample freezes outwards and in, then the hydraulic pressure from ice formation will push some liquid inwards, further into the sample, and at the same time the liquid will continue to flow towards the ice from the external liquid reservoir [43]. Some liquid will also flow from the warmer unfrozen inside of the material towards the freezing front closer to the surface of the sample.

When the temperature increases and the sample begins to thaw, the ice in the external liquid reservoir (if it was allowed to freeze) and the ice closest to the surface will start to thaw before the inside of the sample. This creates available unfrozen liquid, which will flow towards the ice in the colder regions due to the difference in free energy [44]. There is an increased liquid uptake when temperature gradient is high, due to the increased difference in free energy between ice and the warmer

unfrozen liquid [45] compared to the liquid uptake when liquid and ice have the same temperature.

The thawing acts like an additional water pump during multiple freeze-thaw cycles [46], increasing the liquid uptake and the degree of saturation in the pores after each cycle if there is an external liquid reservoir [31].

2.2.3 Glue spall theory

Valenza and Scherer presented the glue spall theory explaining the mechanisms behind frost salt scaling, FSS [47, 48]. This mechanism derives from the fact that ice and concrete have different thermal properties. Ice has a 5 times lager thermal expansion than the concrete, and this creates an increasing tensile stress in the ice formed in the outer solution when the temperature decreases [49, 50]. For low salt concentrations, that will create a crack in the ice that will propagate into the concrete surface, causing small flakes the surface to be spalled off. For high salt concentrations there will not be enough ice and for the case of no salt, the ice will be strong enough not to crack. This would explain the salt concentration pessimum. This theory also describes that the higher the tensile strength of the concrete surface is, the longer it can sustain the strain mismatch between the ice and the concrete, and the lower the temperature the more cracking. If the concrete is not properly air entrained, the thermal mismatch will cause spalling, particularly in combination with internal frost damage [4, 51]. The phenomenon can be demonstrated by pooling a solution on a block of concrete and subjecting it to freeze- thaw cycles [49]. Some studies have shown that the thickness of the solution affects the scaling, and it have been observed [50] that the scaling increases when the thickness of the solution increases.

Decrease in the tensile strength of the concrete surface should increase the damage and an increased porosity should result in a decrease in the tensile strength. But experiments show that a well-connected air-void system with large entrained voids (approximately 300 μm in diameter) results in a smaller difference between the thermal coefficients of the ice layer and concrete, as concrete contracts more when AEA is added than without AEA and ice in the air voids will also contribute to decrease the difference [29]. This could explain why entrained air decreases the mass of scaling.

2.2.4 The effect of salt

Pure water has a freezing temperature of 0 °C. When salt is added to the water, the freezing temperature of the water will decrease below 0 °C. That is why salt is used on roads to thaw ice and make the traffic more secure for cars or people walking during winter. One feature of frost salt scaling is that the damage is less if the external liquid is pure water than if it contains low concentation of salt [26, 50, 52-54], It becomes serious at salt concentrations of a few weight-%, and then decreases at concentrations above 6 weight-%. At high salt concentrations, the ice does not form a rigid enough structure to result in significant stress, so no damage occurs [49].

There are different salts that can be used for deicing, the two most common are sodium chloride and calcium chloride. As sodium chloride is used for standard salt frost scaling tests [55], we will start with that as an example, Fig. 5.

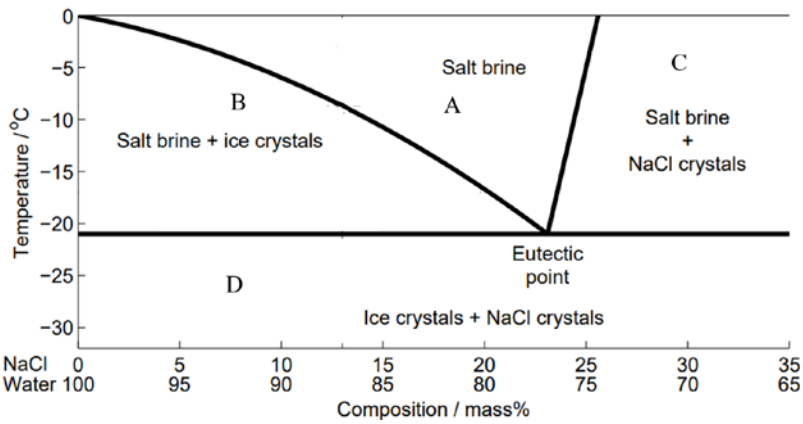

Figure 5. Phase diagram of water and NaCl.

The parts of interest in Fig. 5 are described below, to better understand how the concentration of NaCl affects the freezing temperature of a NaCl-water solution.

- Area A: Salt brine: This region consists of only a liquid brine. All the NaCl added can be dissolved in the liquid brine.

- Area B: Salt brine + ice crystals: At lower temperatures, ice crystals start to form and the rest of the water and NaCl form a liquid brine. When more ice

is formed due the decrease in temperature, the concentration of the remaining brine will increase.

- Area C: Salt brine + NaCl crystals: The concentration of NaCl is high enough so that the brine is not able to solve all the salt, and some of it will remain as salt crystals.

- Area D: Ice crystals + NaCl crystals: If the temperature is below -21.1 °C, we will always see a mixture of solid NaCl crystals and ice. There will never be any liquid whatever proportions of NaCl and water we have, separate NaCl crystals and ice crystals will be formed.

- Eutectic point: where three lines intersect, at temperature -21.1 °C and concentration 23.3%.

- The line between area A and B: This line could be called the freezing point depression curve and represent what temperature the different concentrations of brine will start to freeze.

In durability testing for frost salt scaling, there is an observed pessimum at low concentrations of salt, in the external liquid reservoir [47, 56]. The scaling damage is worse at around 3% NaCl than with pure water or at 6% NaCl concentration. Fagerlund [32] has proposed that the pessimum salt concentrations can be due to a combination of osmotic pressure and hydraulic pressure. The liquid is drawn in the pores because there is a difference in salt concentration, with higher concentration in the pores, thus the liquid is drawn into the pores to balance the concentrations. The hydraulic pressure arises from the liquid expulsion from these pores when more ice is formed. Salt frost attack with NaCl seems to be purely physical and not chemical, as the damage does not increase with higher concentrations of salt [26, 27].

The salt concentration in the external liquid reservoir seems more important to salt frost scaling than the salt concentration in the material. Salt solution inside the pores also lowers the freezing point of the liquid solution in the pores, compared to pure water, but has no clear effect on the frost salt scaling damage [37]. The pessimum is less defined for concrete with good resistance against salt frost scaling [37] such as concrete with low water binder ratio (around 0.30) [37], probably due to a

combination of higher surface strength, denser pore structure and less available freezable water [49].

If the external liquid reservoir is allowed to freeze, then the liquid uptake into the material increases if salt is present compared to the case of pure water. The liquid uptake increases because there is no solid ice layer at 0 °C preventing the liquid to be sucked into the material [26, 57].

Salts other than NaCl, like calcium chloride, $CaCl_2$, also show the same phenomenon with lowering the freezing temperature of water, and that low concentrations in the external reservoir are a pessimum for scaling damage. As mentioned above, substances like this are called de-icing agents. $CaCl_2$ function as a de-icing agent at lower temperatures than NaCl, as it has a eutectic point at -55 °C in the $CaCl_2$-water phase diagram [26]. $CaCl_2$ also creates scaling when used on roads, with a similar pessimum of 3-4% $CaCl_2$ concentration, and lower scaling with pure water or 10% $CaCl_2$ concentration [26, 27]. Other substances than salts functions as de-icing agents, like ethyl-alcohol or urea. All show the same phenomenon that a low concentration gives higher scaling than pure water or high concentration of the de-icing agent [26, 27].

As salt or any other de-icing agent keeps the water from freezing at 0 °C, it increases the liquid uptake into concrete during freezing temperatures, as the external reservoir does not form a solid ice layer that seals the boundary. This additional liquid uptake increases the degree of saturation and increase the risk of reaching the critical degree of saturation, that will cause internal damage to the concrete. The extended access to the liquid reservoir could also provide a constant stream of liquid to grow a microscopic ice lens, that would otherwise be cut off from the externa reservoir. The de-icing agent in the external reservoir affects the rigidity of the ice formed, and according to the glue-spall theory, it is the reason for its pessimum at low salt concentration [49].

3 Modelling

Modelling is important to understand the complex interactions between a porous material and water. There are many different interactions to consider e.g. physical interaction when the pore water phase changes into at a temperature which is a function of the pore radius, chemical interaction when cement paste constituents are dissolved in the pore water, and mechanical interaction between the freezing liquid and the surrounding material due to pressure from restrained expansion.

Several poromechanical models have been developed over the years to predict the impact of freezing in porous materials. The earlier models based on the poromechanical equations of Coussy [58-60] were 1D linear models suitable for cement paste, and had the limitation of only simulating fully saturated samples with no effect of repeated freeze-thaw cycling. One of these early models was developed at IFSTTAR, in France, by Dangla et al. and captures the thermodynamics of ice formation and its consequences such as hydraulic pressure and cryosuction [59, 61]. Mayercsik [62] developed a model to describe freezing of a non-saturated air pore system and the gradual increase in ice-saturation during temperature cycling. Eriksson at KTH in Sweden has made a hygro-thermo-mechanical multiphase model that can simulate air-entrained concrete (including aggregates) in 3D, phase changes and hydraulic pressure [39, 63]. This model was used in the present project to simulate the effect of dissolved salt for two experiments with air-entrained concrete during freeze-thaw, see Paper I in section 5.1.

In the following, the components of basic poromechanical approach based on the theory of Coussy [6] are described. The detailed information of the model, input data and boundary conditions used is presented in the paper in Appendix 1 (Paper I).

3.1 Ice-water equilibrium in pores

The freezing temperature of the water in a pore depends on the threshold pore size of the pore [64], and it is always lower than the freezing temperature of bulk water since the chemical potential of water in small pores is lower than that of bulk water. For a certain threshold pore size with a certain Kelvin radius R, the potentials of water and ice are in equilibrium only when the temperature reaches a certain temperature. At this temperature, it can be assumed that ice occupies all the pores with a Kelvin radius larger than R and that ice is not to penetrate further to smaller pores unless the temperature is decreased further.

The capillary pressure in a freezing pore is equal to the difference between ice and water pressures and can be expressed with the Thomson equation [6] which gives a relation between the temperature of freezing and the capillary pressure.

The difference in pressure between the ice phase and the liquid phase can also be described by Young-Laplace's equation [6]. The Young-Laplace equation describes the relationship between the threshold pore size and the capillary pressure that is needed for the pore water inside the pore to freeze.

The Thomson and Young-Laplace equations can be combined into the Gibbs-Thomson equation, that is used in poromechanical modelling to determine which pore sizes are filled with ice at a given temperature [6].

3.2 Water retention curve

The water retention curve expresses the degree of saturation as a function of the capillary pressure. The capillary pressure can be translated into a threshold Kelvin radius through Young-Laplace's equation, so the water retention curve is also a description of the pore size distribution.

For liquid-saturated porous materials, the van Genuchten equation is often used to express the relationship between pore capillary pressure and liquid saturation [65] based on fitting parameters depending on material used. It is used for all types of porous materials, even if it was first derived for soil.

As water freezes in pores, a liquid like layer is assumed to exist at the interface between ice and pore wall and this part of liquid phase is reported to be crucial for the freezing of the pore water [66], as the liquid like layer makes transportation of liquid water into already frozen pores further inside the material possible [66].

3.3 Ice saturation curve

A calculation of the amount of ice in a porous material during freezing is needed to simulate the effect of cryogenic swelling. A freezing temperature that corresponds to a pore threshold Kelvin radius can be calculated by using the water retention curve and the Gibbs– Thomson equation. This gives the amount of ice as a function of temperature and shows the amount of ice at a certain temperature.

3.4 Boundary conditions for mass and heat

The boundary conditions for poromechanical models describe the flow of mass and heat to or from the porous material. There are two cases for the mass boundary conditions, the drained and the undrained case. If there is no flow allowed to or from the porous material, it is an undrained case and if a flow is allowed, it is a drained case [6].

3.4.1 Conservation of fluid mass

The conservation of fluid mass describes that the total fluid mass in a volume of porous material remains the same during phase transitions and that the mass of water in a volume of a porous material only changes by the mass that enters/exits the volume [6]. For a fully saturated porous volume during freezing there can only be liquid water and solid ice in the pores, and for a non-saturated case there is liquid water, ice and water vapour.

3.4.2 Conservation of salt content

The conservation of salt content means that the total mass of salt in any volume of porous material remains the same during phase transitions and that the mass of salt in a volume of a porous material only changes by the mass that enters/exits the volume [6].

3.4.3. Heat equation

The heat equation describes the change of entropy in a system [67]. In thermodynamics, the entropy of a system can change if there is a flow of heat or a change in mass to or from the system [6].

3.5 Mass transport laws and heat transport law

The transport laws describe the flow of mass and heat inside the porous material. Darcy's law describes the pressure driven transport of fluid, Fick's describes the diffusion of salt, and Fourier's law describes the flow of heat.

3.5.1 Darcy's law

The flow of a fluid through a porous material can be described by Darcy's law [68]. Water changes its volume by 9% when it freezes into ice, this increase creates a viscous water flow from nucleation sites to unfrozen pores.

3.5.2 Fick's law

The transport of salt is assumed to take place by diffusion by Fick's Law [69], where the dissolved salt is transported in the water from higher concentration of ions to parts of the system where there is a lower concentration of salt until equilibrium is reached. The transport of salt can also occur due to Darcy's law.

3.5.3 Tortuosity Coefficient

Tortuosity is a term used to describe interconnectedness of the pore space as it affects transport process through porous material. The definition of tortuosity is the ratio of the shortest path of two connected points in a porous material and the straight distance between them [70]. This gives a sense of how twisted the path is between two connected points. A straight line has tortuosity equal to 1.

3.5.4 Fourier's law

Fourier's law states that that the heat flux through a material is proportional to the negative gradient in the temperature, so heat flows from areas with higher temperature to areas with lower temperature [71].

3.6 Stresses and strains, mechanics of freezing

When a porous material is exposed to freezing temperatures, the ice causes a strain in the material due to the 9% volume changes when water freezes. For a water saturated porous material under freezing, the pores are progressively invaded by ice and occupied by two phases: the liquid phase and the ice phase [6]. In poromechanical modelling, the strain is normally divided into the hydraulic strain, the cryogenic strain and the thermal strain.

- The hydraulic strain is the strain from the hydraulic pressure in the liquid caused by the volume change when water is transformed into ice. It depends on how much ice that is formed and if the liquid water is able to flow somewhere else.

- The cryogenic strain is the strain from the formation of ice and the 9% increase of volume during the phase change. The ice will cause a pressure on the pore wall if it does not have any room to expand.

- The thermal strain is due to the change in volume of ice, liquid and solid skeleton when the temperature changes, connected to the thermal expansion coefficient of each material.

4 Methods, materials and results

There are plenty of scaling experiments that test durability [4, 53], but the aim of this thesis is to investigate the mechanism behind the deterioration, and not to observe the damage they causes. A simplified approach is used to divide the problem of frost deterioration into smaller parts, and produce input data to possibly validate models that simulate the effect of freezing a porous material**.**

The first experimental series was performed to characterize different physical properties of mortar. Mortar is easier to simulate as it is more homogenous than concrete, as it does not contain the larger aggregates.

The second experimental series was performed to investigate the dilation and ice formation on fully saturated mortar samples during one freeze-thaw cycle, using the same mortar recipe as used in the first experimental series. This was to study how the temperature is affecting the formation of ice in different pores, and the shrinkage and the expansion due to the temperature and formation of ice in saturated mortar samples.

In the third experimental series we investigate how saturated the samples actually get with different conditionings, and the location of the water in the larger pores of the sample. The samples are with the same mortar recipe used in experimental series one and two. The level of saturation in the pores (larger than 0.1 mm) were studied with X-ray micro-tomography that scan small mortar samples to get a 3D model of the mortar sample where the different densities of the materials makes it able to separate what is cement paste, sand, air and water. The sample is analyzed as multiple images of thin horizontal sections of the whole sample.

The fourth and last experimental study investigated the additional liquid uptake in capillary saturated concrete samples during freezing. The materials contained different amount of GGBS and the experiment was made with different salt concentrations. The samples have access to an external liquid reservoir during different temperature conditions. The aim was to give input data to verify models that simulate frost deterioration when we have concrete, SCM, salt and the gradual

filling of the air pores during multiple freeze-thaw cycles with non-saturated samples [72, 73].

4.1 Investigation of physical properties

Several physical properties have been measured on samples of three different mortar recipes, Table 1, to give an accurate input data to simulate experiments with these materials.

All the three mortar recipes were the same, except for the amount of air entrainment agent used (Table 1). The mortars were mixed with a water cement ratio of 0.4 and the aggregate used was CEN standard sand according to EN-196-1 [74].

For each of the three recipes, mortars were cast in multiple 40 mm × 40 mm ×160 mm moulds, according to EN-196-1 [74] and one a larger block 400 mm × 400 mm × 200 mm. Samples were drilled and sawed to suitable sizes from the larger block.

Table 1. Mortar recipes.

Material	**W/C** -	**Cement** [1)] kg/m^3	**Aggregate** [2)] kg/m^3	**Air Content** Volume-%	**AEA** [3)]
M1	0.4	574	1377	3.9	-
M2	0.4	574	1377	7.0	0.03
M3	0.4	574	1377	9.8	0.075

[1)] CEM 1 42,5 N SR3 MH/LA. (Slite, anläggningscement, Cementa AB)

[2)] CEN Standard sand, EN 196-1 [74]

[3)] SIKA Air Pro, The amount of admixture was dosed in % of binder weight

4.1.1 Thermal conductivity and heat capacity

The thermal conductivity and the volumetric heat capacity were measured with a Hot Disk TPS 2500 S using single-sided measurements with an EPS-insulation with known properties on the other side, Fig. 6. The values are the average of 3 different areas on one sample with 3 measurements on each area. The mortar samples were rectangular prisms with dimension 40 mm × 40 mm ×160 mm mixed an cast in moulds according to EN-196-1 standard [74]. The samples were dried at 40 °C until the weight loss of the sample were less than 1 g of water during a week. The result are presented in Table 2 and can be used simulate the heat transport with Fourier's law [71].

Figure 6. Hot disk measurement, showing the sensor placed on the mortar prism. During the measurement, the sensor is placed between the prism and an EPS-insulation.

4.1.2 Porosity

The open porosity was measured by water saturation with vacuum and drying at 105 °C. The values are the average of 3 samples. The mortar samples were rectangular prisms with dimensions 40 mm × 40 mm × 160 mm mixed and cast in moulds according to EN-196-1 [74]. The samples were dried at 105 °C, then the samples were placed under vacuum suction of 5 Pa for 3 h before the samples were covered in deionized water. Then the vacuum pressure was released and the samples left to saturate for at least 24 h, Fig. 7. The open porosity is calculated from the difference in water mass between the oven dry mass and the water saturated mass. The results are presented in Table 2 and can be used to calculate a pore size distribution of the material with a fitting model, using the van Genuchten equation to get a water retention curve.

Figure 7. Porosity measurement, showing dried samples under vacuum; samples are later covered in deionized water.

4.1.3 Linear thermal expansion coefficient

The Linear thermal dilation coefficient was measured by the combined dilatometer and calorimeter described in section 4.2 below, during one 65 h freeze-thaw cycle. Sample size cylinders with length 150 mm and diameter 35 mm were drilled and sawed from the cast block 400 mm × 400 mm × 200 mm. The samples were dried at 40 °C until the weight loss of the sample were less than 1 g of water during a week. A thermo-element was placed on the surface to measure the temperature of the sample during the experiment. The sample were then sealed with a plastic film around the sample, but not on the top or bottom then placed in a calorimeter with a dilatometer on the top surface of the sample and subjected to the 65 h freeze-thaw cycle. The result are presented in Table 2 and can be used in simulation of the length change and stress of the solid matrix due to temperature during freezing and thawing.

4.1.4 Bulk and shear moduli of the material and of the solid matrix

The natural frequency was measured in a non-destructive method with a Grindosonic and the dynamic E-modulus was calculated from the natural frequency using ASTM E1875 [75]. The bulk and shear moduli were then calculated using self-consistent schemes [76].

The mortar samples are rectangular prisms with dimensions 40 mm × 40 mm ×160, mm mixed an cast in moulds according to EN-196-1 [74]. The samples were dried at 40 °C until the weight loss of the sample were less than 1 g of water during a week. The result of the bulk and shear moduli of the solid matrix are presented in Table 2 and are used to simulate the stresses and strains that occur in the material. The results are the average of 3 samples.

Table 2. Material parameters of mortar determined experimentally.

	Parameter	M1	M2	M3	Unit
Porosity	φ	0.18	0.22	0.25	-
Volumetric heat capacity	C_s	2.0×10^6	1.9×10^6	1.8×10^6	J/(m^3 K)
Thermal conductivity	λ_s	2.5	2.3	2.1	W/(m K)
Bulk modulus of the solid skeleton	k_s	2.7×10^{10}	2.7×10^{10}	2.7×10^{10}	Pa
Shear modulus of the solid skeleton	g_s	2.1×10^{10}	2.0×10^{10}	2.0×10^{10}	Pa
Thermal expansion coefficient	α_s	13.0×10^{-6}	12.9×10^{-6}	12.1×10^{-6}	1/K

4.2 Dilation and ice formation as a function of temperature

Water saturated samples of mortar with different amounts of air entrainment have been subjected to freezing, to study the length change and formation of ice during one freeze-thaw cycle. The experiment was peformed to simulate a simplified approach to frost deterioation, with only one freeze-thaw cycle and with fully water saturated mortar samples to not have to consider the air in the porous system, the effect of larger aggregates found in concrete or the effect of multiple freeze-thaw cycles.

The ice formation was measured with heat flow with calorimeter, as the freezing of liquid water into ice is an exotherm process and the dilation was measured with a linear variable differential transducer, an LVDT-sensor.

The dilation, or length change, of a sample during freezing is the combination of four phenomena: (1) The cryogenic swelling during the formation of ice and its 9% increase of volume during the phase change. The ice will cause a pressure on the pore wall if it does not have any room to expand. (2) The hydraulic strain from the increased pressure in the liquid, which will be high if the unfrozen water cannot flow into an empty pore or leave the material at the surface. (3) The thermal strain from the temperature change of the solid skeleton, the liquid and the ice. (4) The shrinkage due to the drying effect from liquid flowing from smaller pores into larger pores containing ice due to cryosuction (section 2.2.3). The combination of these strains will determine if the material will shrink or expand during freezing, and this can be measured with a LVDT.

In 1958 Verbeck and Klieger [77] developed a combined dilatometer-calorimeter to simultaneously measure the ice formation and strain in a sample. An instrument of this type is well suited for studies of internal frost destruction mechanisms in concrete, as it can detect internal cracking from frost damage, as internal damage can occur without visible surface damage [24]. The combined dilatometer-calorimeter used in this experiment was designed by Lindmark and further developed and investigated by Fridh, Lindmark, Wadsö in 2003 [78].

4.2.1 Materials

Sample cylinders with length 150 mm and diameter 35 mm were drilled and sawed from the cast block 400 mm × 400 mm × 200 mm.

4.2.2 Moisture conditioning and measurement preparations

The dilation and ice content was measured by the combined dilatometer and calorimeter [78] during one 65 h freeze-thaw cycle. The samples were dried at 40 °C until the weight loss of the samples was less than 1 g of water during a week. Then the samples were placed under vacuum suction of 5 Pa for 3 hours before the samples were covered in deionized water and the vacuum released for at least 24 hours. A piece of glass was glued on the top of the specimen to ensure free movement of the LVDT dilatometer. The samples were wiped on the surface with a damp cloth and a thermocouple was placed on the surface to measure the temperature on the sample during the experiment. The sample was then sealed with a plastic film around the sample, but not on the top or bottom, and then placed in a cylindrical invar vessel, Fig. 8. There is enough free space inside of the invar vessel for the sample to expand freely without putting pressure on the surrounding invar vessel.

Figure 8. Calorimetry and dilation experimental set-up. Sample with a piece of glass glued on top, to ensure free movement of the LVDT (left). Sample with a thermocouple on the surface of the sample and sealed with plastic (Middle). The sealed sample placed in an invar vessel (right).

The invar vessel was then placed in the vessel holder inside the instrument, with a LVDT dilatometer gauge on the top surface of the sample, Fig. 9. There are two identical calorimeters in the instrument, the sample in question being placed in one, and a reference sample in the other [78]. The reference sample was a dry sample of mortar, to reduce the influence of external disturbances.

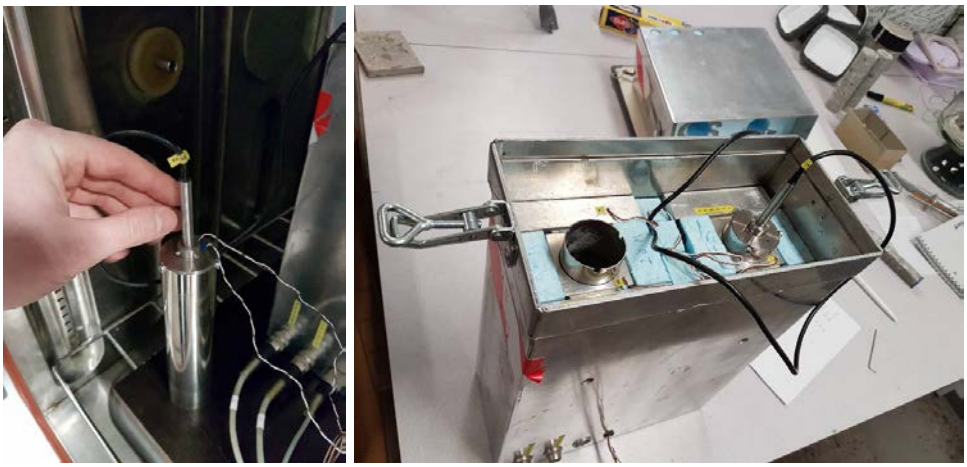

Figure 9. Calorimetry and dilation experimental set-up. An LVDT gauge is placed on top of the sample through the lid of the invar vessel (left). Invar vessel placed in one of the vessel holders of the instrument.

The instrument was then placed in a programmable low-temperature freezer with air as cooling and heating medium. A lid of insulation was placed on top and fastened with clamps on the sides, Fig. 10.

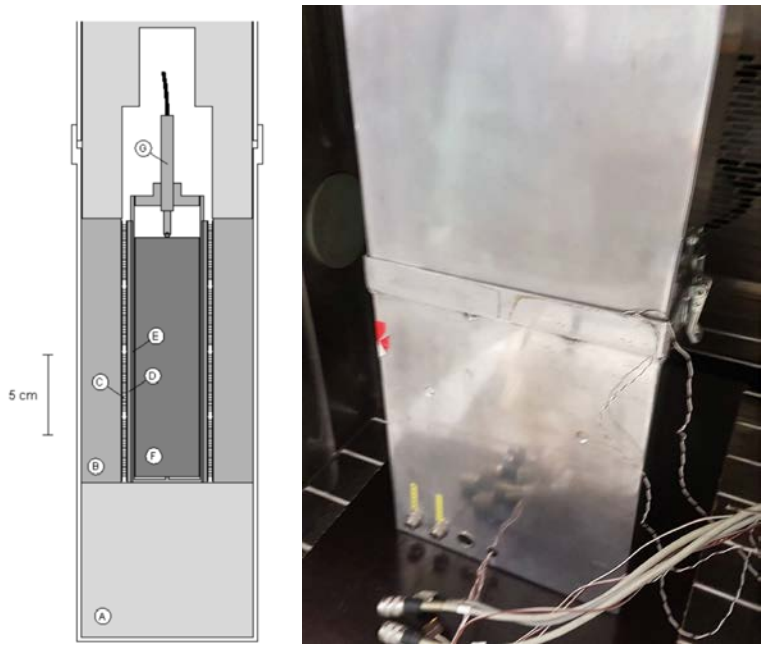

Figure 10. Calorimetry and dilation experimental set-up. A schematic figure of the combined calorimeter and dilatometer. (A) Insulation, (B) Heat sink, (C) Heat flow sensor, (D) Vessel holder, (E) Vessel, (F) Sample, (G) LVDT Dilatometer. Figure adapted from Fridh [78]. Note that the insulation lid on top is not placed yet (left). The instrument with a lid on top, placed in a programmable low temperature freezer (right).

The samples were subjected to a 65 h freeze-thaw cycle. The cycle went from 20 °C to -70 °C to 30 °C in 65 hours with a constant temperature cooling and heating rate of 3 °C/ h, Fig. 11.

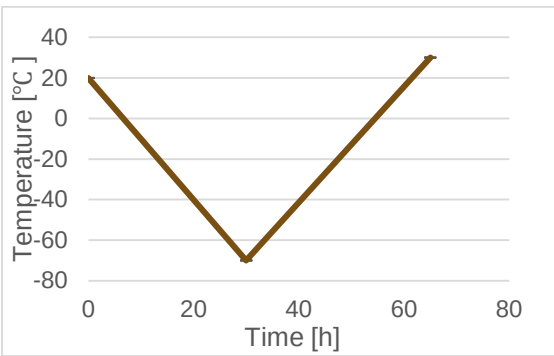

Figure 11. Temperature cycle for the dilation and ice formation experiment.

The result from the ice content calculations of the mortar samples are presented in Fig. 12. The results are presented in the mass-% of ice of the total water content in relation to the temperature. Normal bulk water starts to freeze at 0 ℃, but in these experiments ice starts to form at around -7 ℃. So there is a freezing point depression in the samples. The ice forms in the largest pores first due to a lower capillary pressure, and when the temperature decreases, the liquid in smaller pores is able to freeze. These samples have been dried and vacuum saturated before the experiment, so there is plenty of accessible liquid in the pores. Most of the ice forms between -7 ℃ and -15 ℃. The maximum ice content in the experiments are around 55%, so almost half of the water does not freeze, even at -50 ℃. The sample is cooled down to -70 ℃ but the ice formation between -50 ℃ and -70 ℃ is negligible. When the liquid starts to freeze into ice, the temperature will increase due to the exothermal reaction of liquid water freezing into ice. This can be observed in the mortar samples with air entrainment, M2 and M3 in Fig. 12. The use of air entrainment results in a higher porosity, Table 2, which leads to higher amount of water. The samples M2 and M3 contain more liquid that can freeze, and a system of entrained air pores, with roughly the same size, that freezes at the same temperature. This results in the increased temperature after the liquid starts to freeze at -7 ºC, marked with X, and Y- coordinates in Fig. 12.

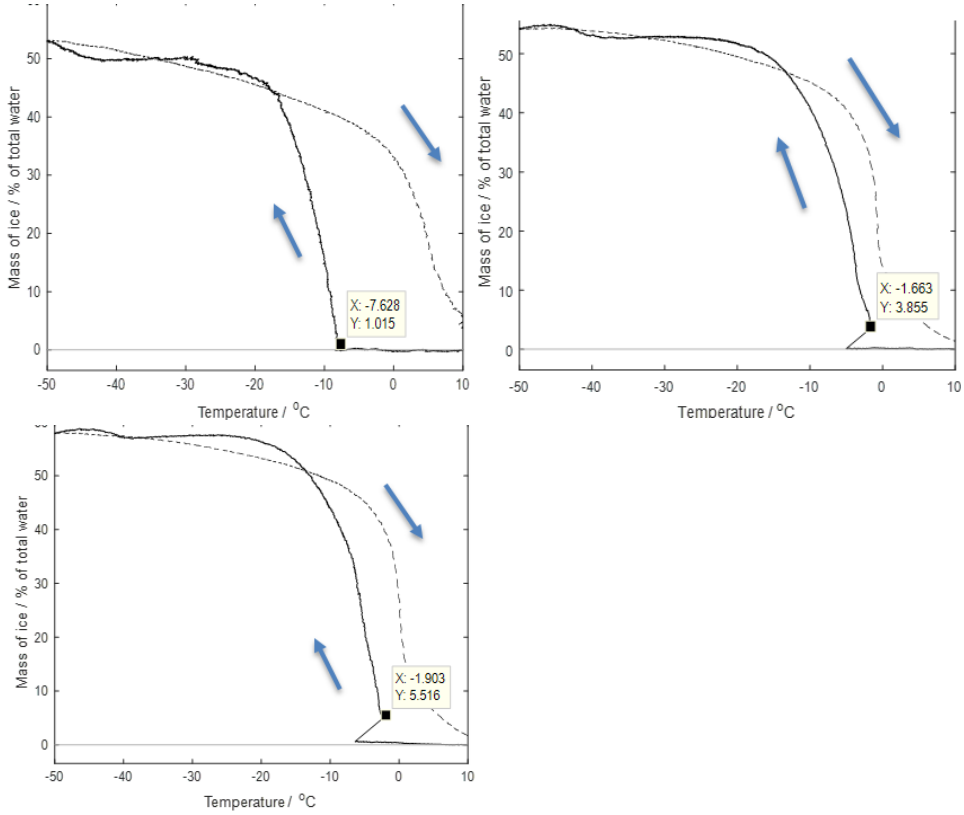

Figure 12. The ice content in mortar during one freeze-thaw cycle. The black line for freezing, and the dashed line is for thawing. Mortar M1 (top left), mortar M2 (top right) and mortar M3 (bottom left).

The result from the dilation of mortar are presented in Fig. 13. At first, the sample is contracting due to the thermal shrinkage of the mortar when the temperature is lowered from 20 °C to -7 °C. At -7 °C to around -15 °C the expansion increases most due to the preassure from the ice formation. At -15 °C to to -40 °C the dilation is almost constant due to that the thermal contraction and the swelling from the ice formation negates eachother. From -40 °C down to the lowest temperature of -70 °C, the sample is contracting due to the thermal shrinkage, as almost no more ice is formed. During thawing from -70 °C to +30 °C the ice starts to melt and the sample expands due to the increase in temperature. There is a large remaning dilation, at the end of the test. This shows that the materials have sustained internal damage and cracked, as the sample length after the freeze-thaw cycle is longer. If it were undamaged, the dilation before and after the freezing cycle would be the same.

The maximum dilation in the samples of mortar is increasing with an increased amount of air entrainment in the sample. The reason behind this is that with more air entrainment, there are more air voids in the sample and an increased porosity as seen in, Table 2. When the samples are fully water saturated, there are more water that can freeze, which results in the increased dilation. Although more entrained air voids should give protection of the sample by allowing the ice to have room to expand in the air filled entrained air voids [32], when the air voids are saturated with liquid they do not have a protecting effect.

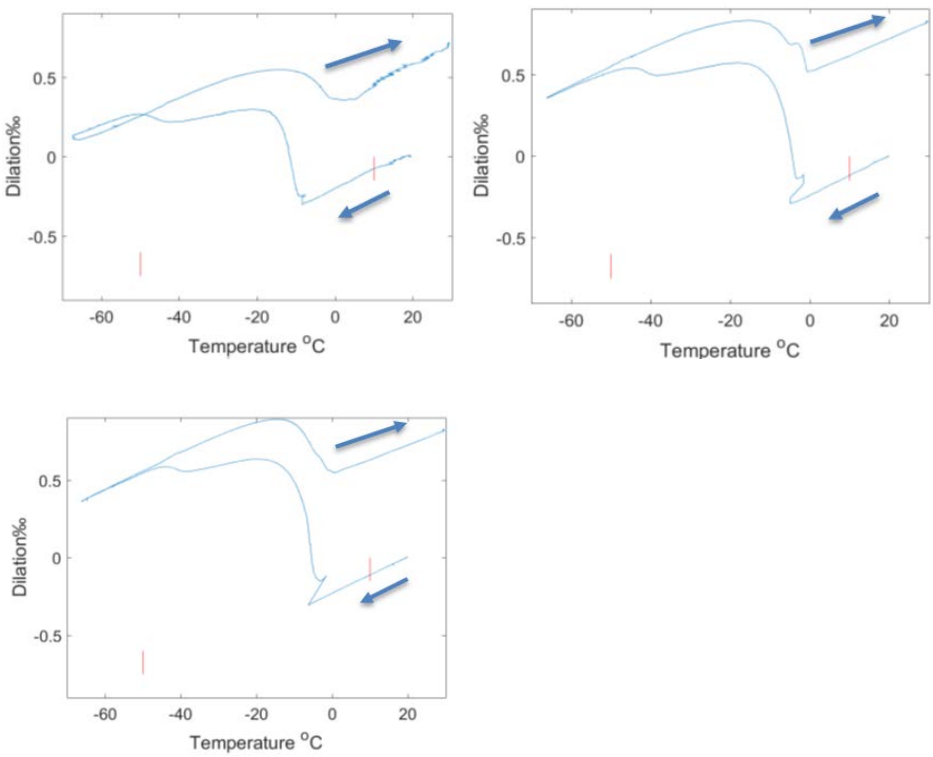

Figure 13. The dilation in mortar during one freeze-thaw cycle. Mortar M1 (top left), mortar M2 (top right) and mortar M3 (bottom left).

Comparing the ice formation and dilation in a combined calorimeter and dilatometer have shown to be a useful tool to study the internal damage of mortar samples. Most of the ice formation occurred at between -7 ℃ and -15 ℃, and this corresponds well with that the largest increase in dilation was the same temperatures.

Experiments like this can be used to verify models that simulate frost deterioration. Similar measurements with samples subjected to freeze-thaw by Fridh [78] were used to verifythe model simulated in Paper I [63].

4.3 Tomography

The inside of mortar samples has been scanned by X-ray micro-tomography to validate how saturated the mortar sample are during different moisture conditioning procedures. Mortar samples were placed in the X-ray micro-tomograph after different drying and saturation conditionings to examine the water content in the pores and if it is possible to fully water saturate samples of mortar with the used vacuum saturation method.

4.3.1 Materials

Sample cylinders with length 10 mm and diameter 10 mm were drilled and sawed from the cast blocks of 400 mm × 400 mm × 200 mm.

4.3.2 Method

The water content of pores in mortar samples have been investigated with X-ray micro-tomography with a Zeiss Xradia XRM520 Tomograph at the Division of Solid Mechanics, Lund University, Sweden. Samples were conditioned in four different ways before they were scanned with X-ray tomography: (1) capillary suction without drying, (2) drying at 40 ℃ in oven and then vacuum saturated with water, (3) drying at 105 ℃ in oven and lastly (4) drying at 105 ℃ in oven and then vacuum saturated with water.

The samples were vacuum saturated by drying in either 40 ℃ (condition 2) or 105 ℃ (condition 4) and then placed under vacuum suction of 5 Pa in a dry state for 3 hours before the samples were covered in deionized water, the vacuum released, and the samples were left to saturate for at least 24 hours.

The scanning in the X-ray micro-tomograph took 4 h for each sample and three samples were placed into a cylindrical tube and separated with metal discs and scanned in succession. In tomography, X-ray measurements are combined mathematically to produce cross-sectional images of specific areas of the sample, allowing the user to see inside the object without cutting it open. The images from

the scan of each sample are assembled from the X-ray tomography as circular sections from the top to the bottom of each sample. The samples were prepared in one of two ways to make them moisture sealed to retain the liquid water that had penetrated into the sample by capillary suction or vacuum saturation: either dried on the surface with a damp cloth and then sealed with a plastic film around the sample or submerged in water during scanning. Both preparations have equal effect but the submerged preparation minimized the risk of the sample drying as there is a small risk of drying through a tear the plastic film or if the plastic was not wrapped properly around the sample. There is an elevated temperature of 27 °C during the tomograph scanning

The result of an X-ray micro-tomograph measurement are 2034 horizontal sections of the sample in a colour scale from black to white depending on the density of the material. Parts with very low density are black and parts with high density are white. One section of a sample with the different components of mortar and their corresponding colour can be seen in Fig. 14. Air in the pores have very low density and are black, the water in the pores are dark grey, the sand grains has higher density than the water and is of a lighter grey and the cement paste have the highest density and are almost white. There is some variation in the colour for the different components in different images, due to the manual processing of the images.

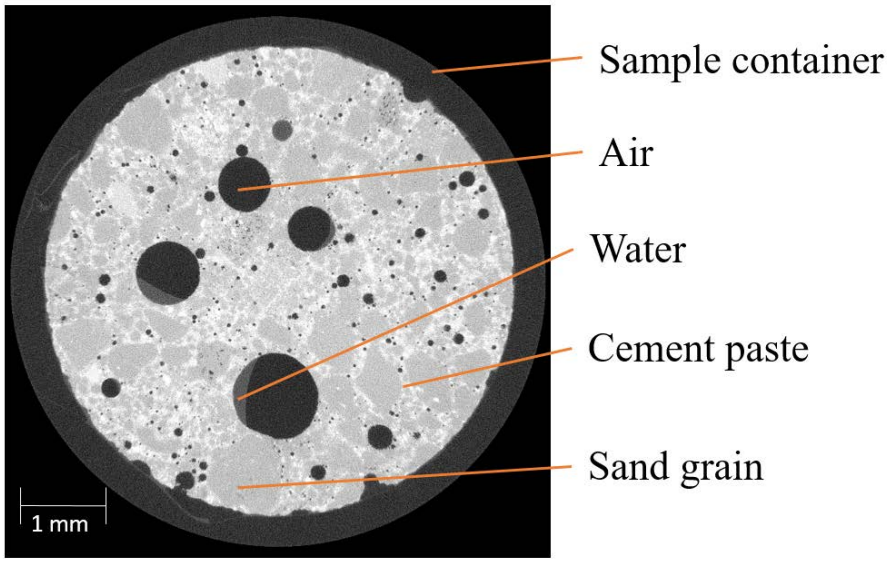

Figure 14. Tomograph description how result is presented.

4.3.3 Result

The tomography results have been processed in ImageJ, which is an image analysis software. The presented results for each tomograph experiment are only of one image out of 2034 and from this it is difficult to understand what the situation is in the whole observed pore or in the rest of the sample. A pore that looks like completely saturated with water on the selected image might have an air bubble visible in another section. An image of a horizontal section in a different part of the sample could indicate a slightly increased or decreased degree of saturation. The figures presented where chosen to represent the whole of the sample.

The samples exposed to capillary suction without drying (condition 1) were only used for that condition. For condition 2-4, the same sample was used for those conditions. The sample were dried at 40 ℃ then vacuum saturated and scanned in the X-ray micro-tomograph (condition 2), then dried at 105 ℃ and scanned in the

X-ray micro-tomograph (condition 3), then vacuum saturated again and scanned in the X-ray micro-tomograph one last time (condition 4).

4.3.3.1 Result: Capillary suction without drying

The sample cylinders were stored covered in 20 ℃ lime saturated water for 8 weeks to be saturated through capillary suction. The samples were dried on the surface with a damp cloth and then sealed with a plastic film around the sample before placed in the X-ray micro-tomograph. One sample of each mortar was used for the capillary suction. The samples were dried at 105 ℃ after the measurement to calculate the amount of water in the sample.

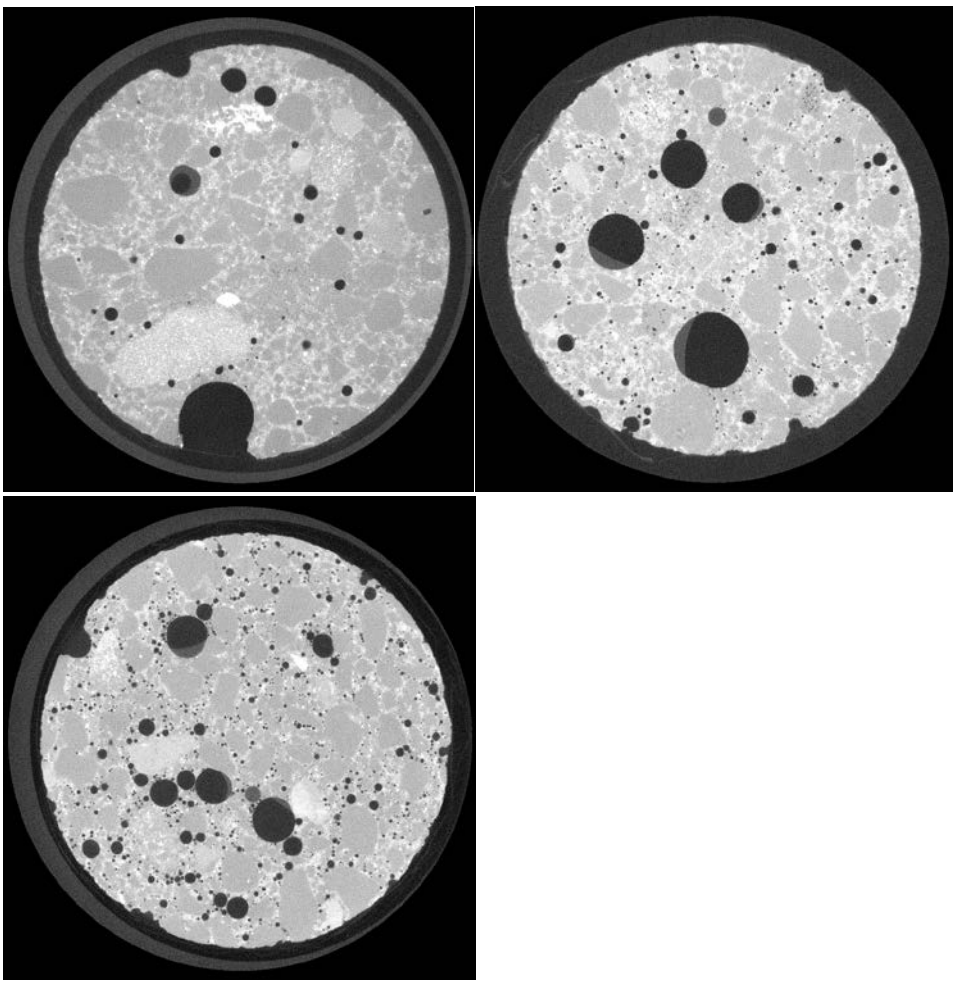

Figure 15. Capillary saturated mortar samples, Material M1 (top left), Material M2 (top Right) and Material M3 (bottom left).

All three of the samples M1, M2 and M3 are far from fully saturated, Fig. 15. A meniscus of water can be seen on the larger pores that are 1-2 mm diameter, and the

smaller pores with less than 1 mm diameter are often empty. Note that the samples used for the capillary suction (condition 1) are not the same as the one used in the other conditions (condition 2-4).

4.3.3.2 Result: samples dried at 40 °C and vacuum saturated with water

There is visibly more water in the samples in that have been dried at 40 °C and then vacuum saturated, Fig. 16, than the samples that were exposed to capillary suction. The drying and vacuum saturation conditioning increases the saturation of the samples compared to saturation by capillary suction as it is easier for the water to penetrate into the sample due to the low pressure inside the sample from the 3 h in 5 Pa vacuum.

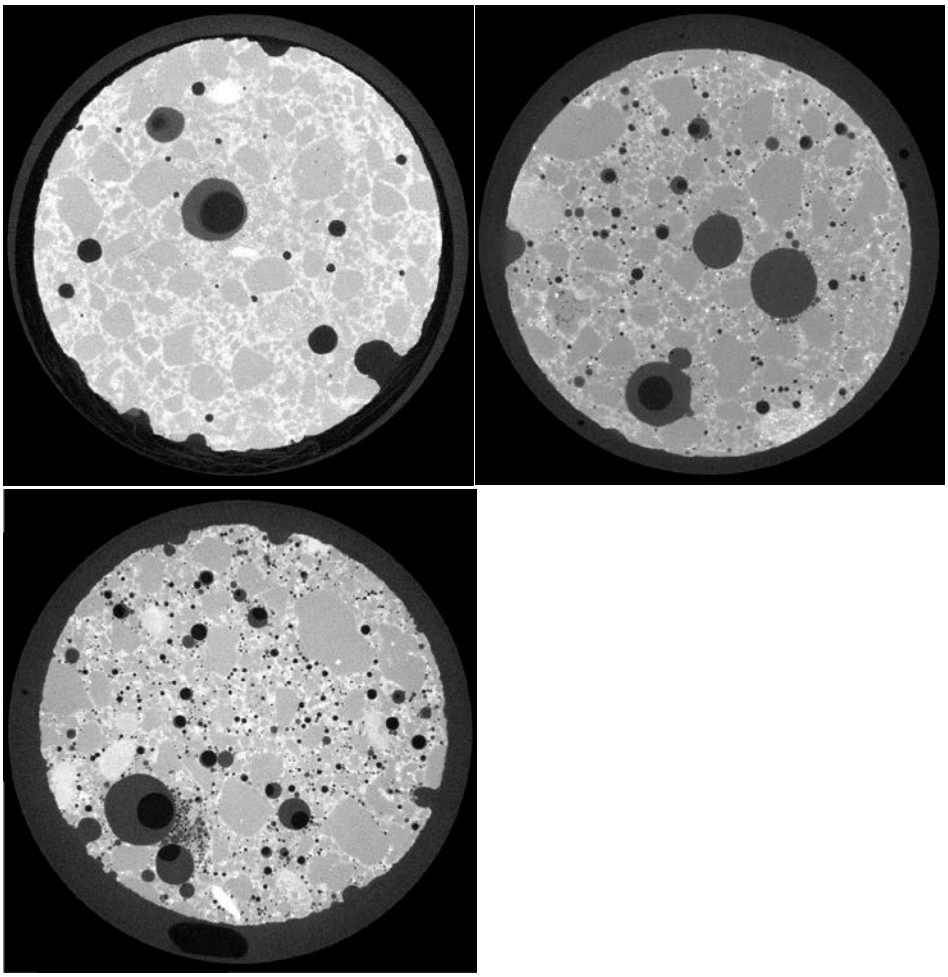

Figure 16. Samples dried 40 °C then vacuum saturated, Material M1 (top left), Material M2 (top Right) and Material M3 (bottom left).

4.3.3.3 Result: samples dried at 105 ℃

All of the pores are completely filled with air and no water, Fig. 17. This is expected as drying at 105 ℃ should get rid of the evaporable water that could be inside the pores. It also confirms that the part of the colour scale that we assumed was water, really is only water and nothing else with a similar density.

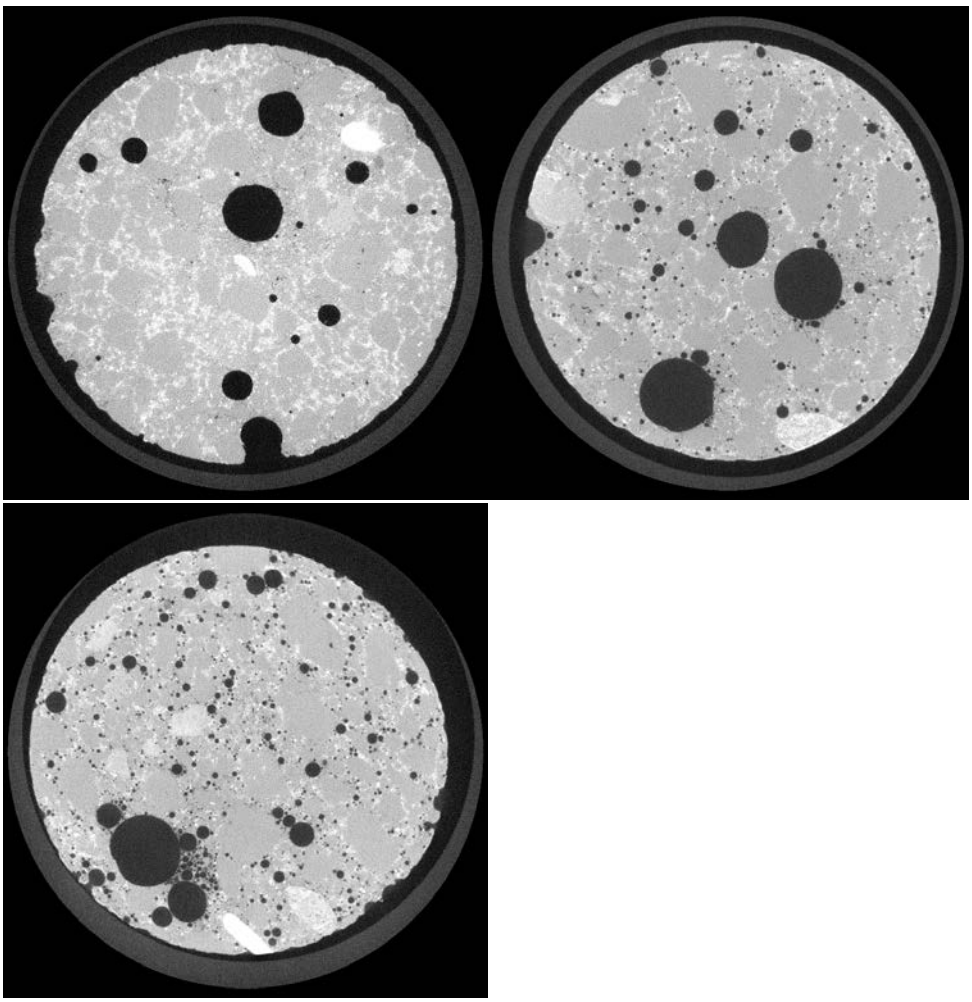

Figure 17. Samples dried 105 ℃, material M1 (top left), material M2 (top Right) and material M3 (bottom left).

4.3.3.4 Result: samples dried at 105 ℃ and vacuum saturated with water

To see if it is possible to fully saturate the samples with water, they were dried at 105 ℃ to not contain any evaporable water and then vacuum saturated with water. There is visibly more water in the samples that have been drying at 105 ℃ and then vacuum saturated, than in the samples that were exposed to capillary suction. The difference between drying the samples at 40 ℃ and dried at 105 ℃ before vacuum saturation with water is not as distinct as between the capillary suction and the dried at 105 ℃ and vacuum saturated samples. The vacuum saturated weights after dried at 40 ℃ and at 105 ℃ are similar. Even when the samples have been dried at 105 ℃ and saturated with liquid water, empty pores without liquid water or air bubbles in the pores can still be observed. This is most likely due to that when the material starts to saturate, some air becomes trapped and has to diffuse out of the sample through the water filled pores. It is clear that it is very difficult to fully saturate samples of mortar and the comparison with the poromechanical model which assume that the samples are fully saturated seems not to be entirely accurate. Howerever the degree of saturation is high enough to damage the material during freeze-thaw.

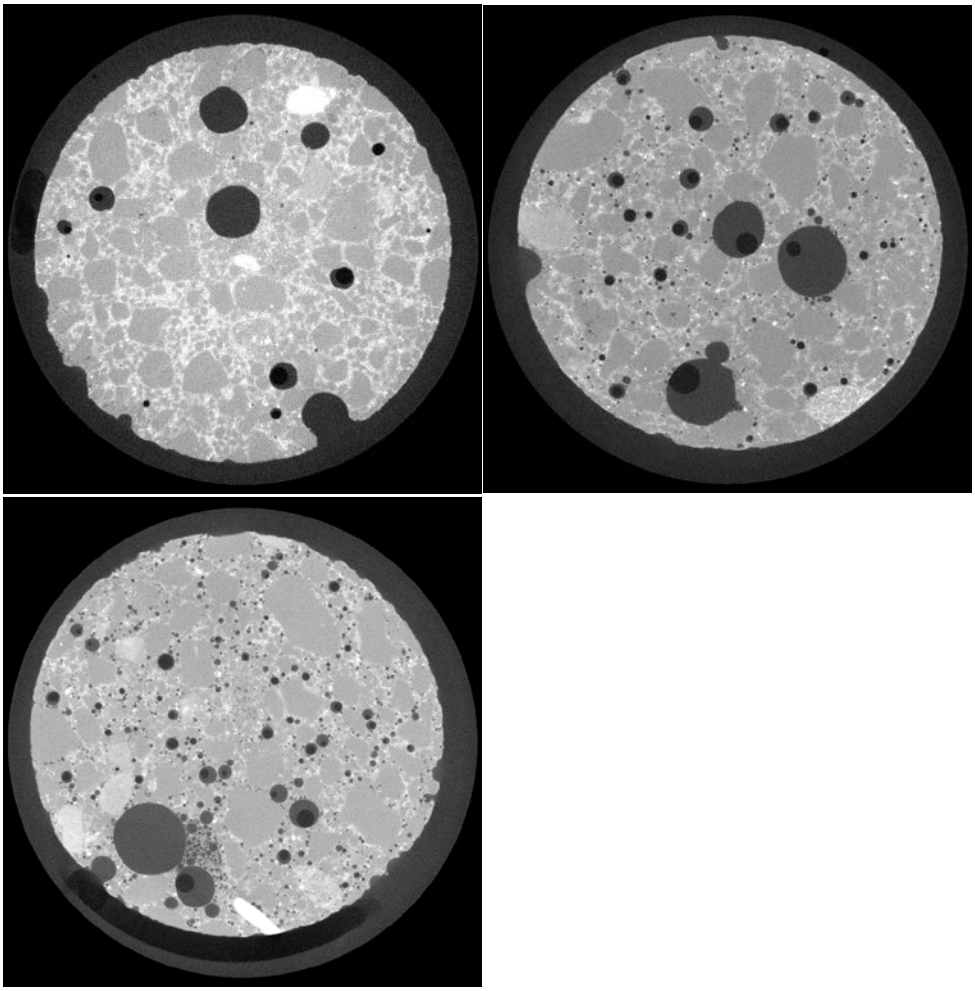

Figure 18. Samples dried 105 ℃ then vacuum saturated, material M1 (top left), material M2 (top Right) and material M3 (bottom left).

4.4 Cryosuction

Below is a brief description of the methods and material used in the cryosuction experiment. More detailed information of the results from these measurements is presented in Appendix 2 (Paper II).

The method was designed to study the liquid uptake in already capillary saturated samples of concrete with GGBS, investigating the effect of salt and three different temperature conditions. The three temperature conditions were: constant room temperature, constant freezing temperature and a cycling temperature between room temperature and freezing.

Six different concrete recipes were used as presented in Table 3. Two admixtures were used, an air-entrainment agent, Sika Air pro 5%, and a Super plasticizer, Sika Viscocrete RMC 520.

Table 3. Concrete recipe.

Material	**W/B** -	**Cement** [1)] kg/m^3	**GGBS** [2)] kg/m^3	**0-8 mm** kg/m^3	**8-11 mm** kg/m^3	**11-16 mm** kg/m^3	**SP** [3)]	**AEA** [3)]
1	0.4	430	0	966	285	536	1.1	-
2	0.4	430	0	966	285	536	1.1	0.45
3	0.4	280	150	966	285	536	1.1	-
4	0.4	280	150	966	285	536	1.1	0.45
5	0.4	129	301	966	285	536	1.1	-
6	0.4	129	301	966	285	536	1.1	0.45

[1]) CEM 1 42,5 N SR3 MH/LA. (Slite, anläggningscement, Cementa AB)

[2]) Merit 5000 from Merox

[3]) The amount of admixture was dosed in % of binder weight

Samples were capillary saturated before the experiment, to isolate the effect of additional liquid uptake in the specimens through cryosuction. They had a height of 50 mm and a diameter of 50 mm, and were drilled and sawed from a larger block. The samples were moisture sealed on top and sides, and the exposed bottom were put in contact with an external liquid reservoir with either deionized water or a 3% NaCl solution. The NaCl salt used were VWR chemicals GPR Rectapur sodium chloride. The liquid reservoir never freezes, and is controlled by a heating coil ensuring that the temperature never goes below +3 °C. There were two different set-ups, depending if the samples were exposed to freezing temperatures or not. The set-up for freezing temperature is shown in Fig. 19.

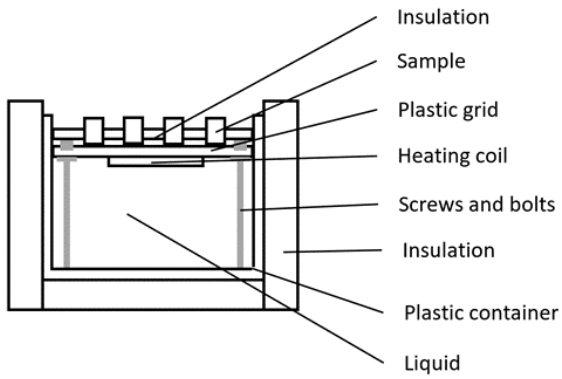

Figure 19. Cross section of set-up for freezing temperature.

The results show that the liquid uptake seems not to be influenced by if the samples are in contact with NaCl solution or pure water or by an increased amount of GGBS replacing cement. For the temperature, freezing temperature have a tendency to give higher liquid uptake than constant room temperature. Samples with AEA have a tendency to have a higher liquid uptake than the samples without AEA.

Salt frost scaling is correlated to liquid uptake, where a low liquid uptake from capillary suction results in higher frost scaling resistance [72]. The results of the present measurements will hopefully be of interest for researchers who build poromechanical frost models which needs experimental verification. More detailed information of the results from these measurements is presented in Appendix 2 (Paper II).

5 Summary of papers

This is a short summary of the two papers found in Appendices I and II in this thesis.

5.1 Summary of Paper I

Title: Hygro-thermo-mechanical modeling of partially saturated air-entrained concrete containing dissolved salt and exposed to freeze-thaw cycles

Authors: Daniel Eriksson, David Wahlbom, Richard Malm and Katja Fridh

Cement and Concrete Research, 2021, vol. 141, 106314(1-15).

This paper further develops the hygro-thermo-mechanical model based on the poromechanical equations of Coussy, to be able to simulate the response of air-entrained concrete exposed to freezing [39]. One of the new features of this model is the implementation of constitutive models describing the hysteresis of the freeze-thaw induced phase changes inside the pore space. This is of importance when simulating multiple cycles of freezing and thawing. The model was also further developed, to include the influence of salt in the pore liquid during freeze-thaw cycling. Unlike earlier models that consider the presence of salt on the freeze-thaw behaviour, the current model also includes the advection and diffusive transport of the salt connected to the freeze-thaw cycling. The behaviour of the model was verified using experimental data provided by Fridh [78]. In those experiments, the dilation of prismatic air-entrained concrete samples, pre-saturated with liquid solutions with different NaCl concentrations were measured during exposure to a freeze-thaw cycle.

The results show a good comparison between the experiments and the simulation during a freeze-thaw cycle, as can be seen in Fig. 7.4a (Paper I). The model is able

to replicate the small contractions of a specimen with an increasing concentration of salt in the pore liquid.

Another simulation shows the model's ability to describe the absorption of liquid from an external reservoir, during freeze-thaw cycling. The concrete was assumed to be capillary saturated with pure water, with the reservoir containing pure water or a liquid solution with different salt concentrations. two different boundary conditions were used on the exposed surface: an open boundary for the liquid flow or a boundary that closes when the formation of ice starts in the liquid reservoir.

The results from the simulations are presented in Fig. 7.4b (Paper I), which shows a higher rate of absorption for the open boundary case and an increasing salt concentration in the reservoir for both types of boundary conditions. The results indicate that the model can also describe freeze-thaw induced absorption into air-entrained concrete that is initially capillary saturated.

5.2 Summary of Paper II

Title: Cryosuction experiments on concrete containing ground granulated blast-furnace slag; influence of temperature, air entrainment and salt

Authors: *David Wahlbom, Katja Fridh*

Manuscript: *Submitted to Nordic Concrete Research*

This paper presents cryosuction experiments with liquid uptake measurements in concrete, to better understand the mechanisms behind frost deterioration. The material used was concrete with different air content and different replacement levels of ground granulated blast-furnace slag (GGBS). The objective of the experiment was to quantify the effect of cryosuction by exposing samples to three different air-controlled temperature conditions, a temperature cycling between -20 and +20 °C, a constant temperature of -20 °C and a constant temperature of +20 °C. Cryosuction is the process in which the absorption of liquid into a material is increased because of formation of ice below freezing temperatures. As liquid medium, deionized water and a 3% NaCl salt solution were used. The temperature in the liquid reservoir was never below +3 °C due to a heating coil, so the liquid reservoir never froze.

The materials were cast in molds, moisture sealed for 24 hours, then demolded and water cured in 20 °C lime saturated water for 2.5 months. Samples were then drilled and sawed to cylinders with sawed surfaces on top and bottom. The samples were then stored in 20 °C lime saturated water for an additional 3 months. The samples were moisture sealed on top and sides, leaving only the sawed bottom exposed. As the samples were preconditioned by capillary saturation, the moisture uptake that is studied in paper II is small, compared to the moisture content achieved during sample preparation.

The results are presented as liquid uptake per area from the sawed bottom as the function of time, Fig. 5 (Paper II).

There is an observed correlation between the capillary suction properties of a concrete surface and frost scaling resistance [79], where a low liquid uptake from capillary suction results in higher frost scaling resistance. The results from the present liquid uptake are discussed together with the results from scaling tests

performed by Strand [53], as the concrete material in the present study is cast with recipes similar to those used in that study, to compare the liquid uptake to the salt frost scaling in a representative material.

The results generally show larger spread and larger mean uptake for the cases with freezing temperatures compared to the case at constant room temperature, with some samples reaching much higher liquid uptakes than other samples. The liquid uptake in constant room temperature samples was significantly more uniform. We hypothesize that the higher liquid uptake in some samples was caused by the filling of stochastically distributed large pores in the freezing zone.

The results in Paper II also show that the liquid uptake seems not to be influenced by if the samples are in contact with NaCl solution or pure water. Also the liquid uptake does not seem to be influenced by an increased amount of GGBS replacing cement. For the temperature, freezing temperature have a tendency to give higher liquid uptake than constant room temperature. Samples with AEA have a tendency to have a higher liquid uptake than the samples without AEA.

The results of the measurements will hopefully be of interest for researchers who build poromechanical frost models which needs experimental verification [63].

6 Discussion

This chapter presents a discussion on the main topics of this thesis, connecting the observations from the four experimental series, the modelling part and the existing theories of frost deterioration.

The work of this thesis has focused on two topics:

- Further developing an existing frost deterioration model and providing input material parameters that can be measured experimentally. This resulted in Paper I, see appendix I, and is discussed in section 6.1 and 6.2 below.
- Planning and execution of experimental series to be used as verification of poromechanical models of salt frost deterioration. This resulted in Paper II, see appendix II, and is discussed in section 6.3 below.

6.1 Measured physical properties, and their role in modelling

One of the main objectives of this thesis was to simultaneously work on two quite different, but equally important parts while studying frost deterioration of concrete: experimental observations in the laboratory and using computer models to perform simulations with poromechanical models.

It is a complex task to simulate the frost deterioration of concrete. There are many different parameters to consider, so the aim should be to focus on the problem from the perspective of the most important mechanisms and analyze what material properties have the largest impact on them. In the end, the overall goal is to create an easy to use model that can give a good enough approximation of what happens in reality. To verify the models, controlled laboratory studies were performed to

isolate some phenomena or effect of a parameter, and also perform larger field studies in the environment and conditions that the material actually will be exposed to. All this to get the bigger perspective of what happens over longer periods of time as the service life of a concrete structure shall be 50 years or more.

If there is an established and verified model, it is easier and more cost efficient to perform computer simulation to predict the outcome of certain conditions and materials, than to do experiments that may take months or years to perform and require cost for material, equipment and space. As mentioned before, the models need to be verified to make sure that they can capture the behavior seen in the laboratory or in the field. The input data or the experimental result used to verify the model needs to be good enough and representative, and that can sometimes be difficult when testing concrete, as there are a vast number of different concretes, with different binders, water-cement ratios, admixtures, aggregates etc. Concrete is also a heterogeneous material composed of aggregates, cement paste, and reinforcement, and it can be difficult to separate the effect of each component on the total result. This also gives a natural spread in results of concrete specimens, even between specimens taken from the same batch.

Many different input parameters are needed for models. For the experiments simulated in Paper I there are 23 different input parameters in Table 1, Appendix 1. Some parameters have been studied more and are well known, e.g., properties of bulk water at room temperature and atmospheric pressure. Other parameters need to be determined for each different material when the material recipe changes. For example, the pore structure of concrete changes when GGBS is added. One person can spend many years, even decades to study only one of these parameters or one phenomena.

Many assumptions and simplification need to be made to be able to do a simulation, e.g., mathematical relationships are used for how one variable depends on some other variables, the shape of pores is assumed to be either cylindrical or spherical, and the boundaries of the sample have to be considered to be fully closed or fully open. When verifying the models, the experimental result also often need to be simplified using mean values, approximating trend curves and removing outliers.

In this study, the new features of the model described in paper I is the implementation of the hysteresis of the freeze thaw, and the model was also further developed to include the influence of salt in the pore liquid during freeze-thaw cycling.

In the present study, the following physical material properties were measured on mortars: thermal conductivity, heat capacity, linear thermal expansion coefficient, bulk and shear moduli of the material and of the solid matrix.

6.2 Porosity and the impact of drying

The result of a porosity measurement depends on the method, and how and if the samples are dried. The porosity of a porous material like concrete is divided into open porosity and closed porosity. The open porosity consists of pores that are connected to the outside of the material; they are therefore affected by external conditions. If we, e.g., dry the sample at 105 °C the open pores will dry out, if we put the sample in water, the open porosity can to be filled with that liquid again. The closed pores are not connected to the outside of the material, and will not take up the liquid we put the sample in. So when discussing porosity, it is important to specify which porosity is measured and with what method. To measure the total porosity including the closed pores, the sample can e.g. be cut up and the surface analyzed or ground so that there are no closed pores left in the material.

In this study, the open porosity has been measured by drying the samples and then vacuum saturating them with deionized water, as described in section 4.1.2. As the drying temperature affects the porosity result, porosity was measured after drying at 40 °C and 105 °C. For small samples, e.g., the rectangular 40 mm × 40 mm × 160 mm samples that were used for the porosity measurements in this study, drying at the higher temperature of 105 °C takes a couple of hours. When drying the same sample sizes at 40 °C, it takes several weeks for them to dry to an acceptable level. The chosen condition of an acceptable dry sample in this study was a weight loss of less than 1 g during 7 days when drying at 40 °C. The reason for drying at 40 °C, instead of drying at 105 °C, even though it takes much more time, is that the microstructure changes when drying at 105 °C. Drying at 105 °C damages the internal microstructure and will result in a not representative porosity [80]. The porosity result is higher when the samples have been dried at 105 °C than if the samples were dried at 40 °C before vacuum saturated with water.

Are open pores fully saturated when the samples are dried at 105 °C and then vacuum saturated? To answer this, we look at some of the tomography results from section 3.3, where we moisture conditioned the sample in four different ways and

observed the water inside of the samples. In Fig. 20, material M3 is conditioned in four different ways:

- Drying at 105 ℃.
- Capillary saturated without previous drying.
- Dried at 40 ℃ and vacuum saturated.
- Dried at 105 ℃ and vacuum saturated.

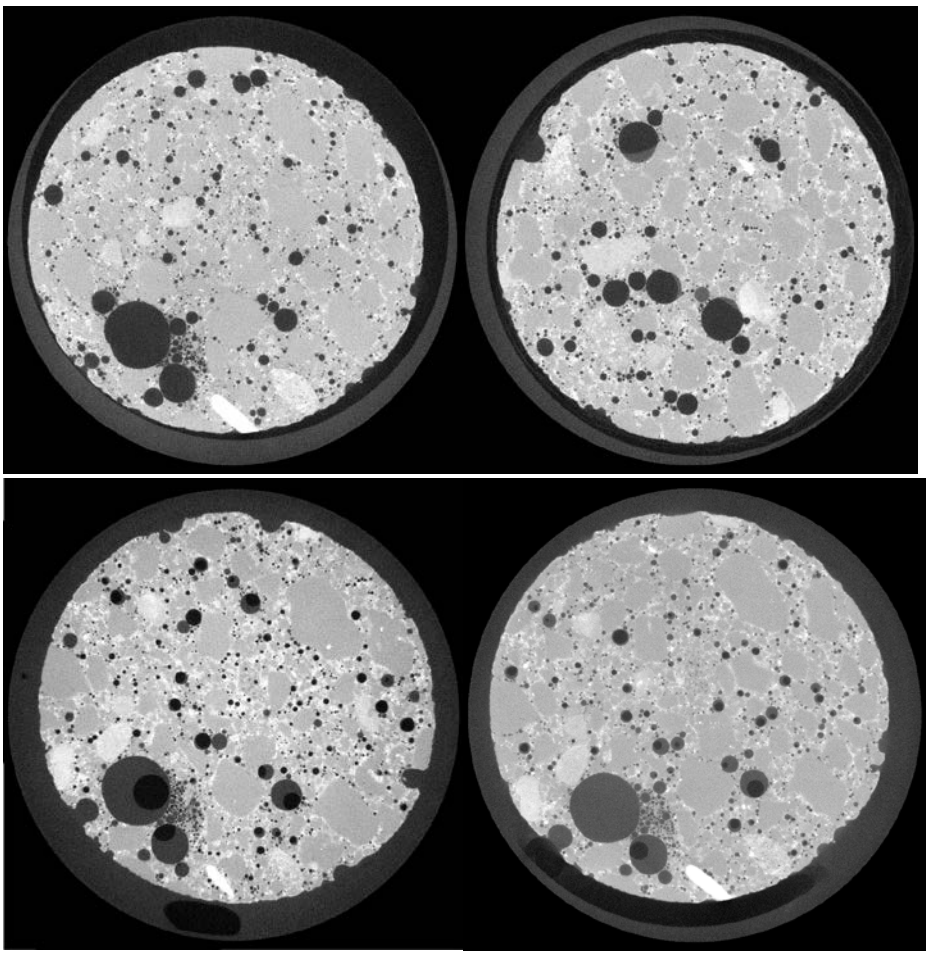

Figure 20. X-ray micro-tomography,with a Zeiss Xradia XRM520. The same material M3, exposed to four different conditions. Dried 105 ℃ (top left), capillary suction (top right), dried 40℃ + vacuum

saturated (bottom left), and dried at 105 ℃ + vacuum saturated (bottom right). Sample size is 10 mm in height and 10 mm in diameter.

It can be observed that drying at 40 ℃ and 105 ℃ before vacuum saturation create quite similar degrees of saturation, compared to only capillary suction. The case of drying at 105 ℃ before vacuum saturation have a slightly higher degree of saturation compared to drying at 40 ℃ before vacuum saturation. Empty pores without liquid water or air bubbles in the pores can still be observed. It is thus difficult to fully saturate samples. Even using drying at 105 ℃ (witch damages the microstructure and makes it more open) we only measure a major part of the open porosity with the method of drying at 105 ℃ and vacuum saturation, but not 100% of it. It is the open porosity that is of interest when considering frost deterioration in concrete, as it is that part of the porosity that actually interacts with the liquid, and can get progressively more saturated through capillary suction and cryosuction if in contact with an external liquid reservoir.

There are several material properties that depend on the moisture level in the samples. For example, the thermal conductivity and heat capacity (physical properties, section 3.1.1) depend on the moisture state, as water increases the ability to transfer and store heat. The compressive strength is also dependent on moisture level, and a completely dry sample has a higher compressive strength than a saturated sample [81]. This emphasizes the importance of presenting not only the results of a measurement, but also the method of the measurement and detailed description of the conditioning of the sample before testing.

6.3 Temperature, and its effect on ice formation

The experimental observations from the dilation, ice formation, tomography, and cryosuction are discussed here and connected to how the temperature affects the ice formation in mortar and concrete.

In the experiments on ice formation described in section 4.2, most of the ice forms between -7 °C and -15 °C. Such temperatures often occur in Sweden during wintertime, especially in the northern parts, and that is why frost deterioration is important to consider when building concrete structures in Sweden. This freezing point depression is typically not seen in field studies made on larger structures, the reason of this may be the large outer surface area of concrete structures [82].

One single freeze-thaw cycle is sufficient to damage a concrete structure, provided the moisture content is above a critical value, which is individual for each concrete [78]. This can be observed in results from section 4.2 on ice formation and dilation, Fig. 13. Drying a sample and then vacuum saturating it increases the moisture content in the sample, compared to capillary suction without drying, as seen in the tomography experiments in section 4.3. Using AEA also increases the moisture content in the sample when vacuum saturating, but it also increases the weight-% of freezable water, as is shown in Fig. 12.

Even if the critical degree of saturation is not achieved during the first freeze-thaw cycle, the added liquid uptake from cryosuction during multiple freeze-thaw cycles or long durations of freezing temperature can subject the concrete structure to a risk of increasing the saturation above the critical degree of saturation, if there is an external reservoir. The additional liquid uptake during freezing can be observed in Paper II.

In poromechanical modelling, there are three main mechanisms for internal damage at high liquid saturation. Firstly, the hydraulic strain [5] from the viscous flow of liquid water driven by the volume increase of water during freezing; secondly, the cryogenic strain from growing ice crystals that leads to stresses on the pore walls if the ice does not have room to expand freely; thirdly, the thermal strain from thermal expansion of all components. Measuring the dilation, e.g., strain of an experimental sample, is a method that can be used to detect internal cracking from frost damage, as damage will cause a remaining strain even if there is no visible surface damage [24, 56], Fig. 13.

The added liquid uptake from cryosuction compared to capillary suction is shown in Paper II. The samples were stored in lime saturated water 3 months before the experiment began so most of the pores that should be filled with liquid through capillary suction at room temperature, were already filled at the start of the experiment. The tomography pictures of capillary saturated samples, Fig. 15, shows that there is still plenty of unfilled space in the larger air voids where water can be transported to and freeze. So the additional liquid uptake during freezing temperatures compared to non-freezing temperatures may be due to hydraulic transport during freezing or micro ice lens growth in the pores.

In the present investigation, a study was made of where the freezing zone was located in the samples used in the cryosuction experiments. Temperatures in the center of a dummy sample at three different heights during freeze-thaw cycling were studied, Fig. 21.

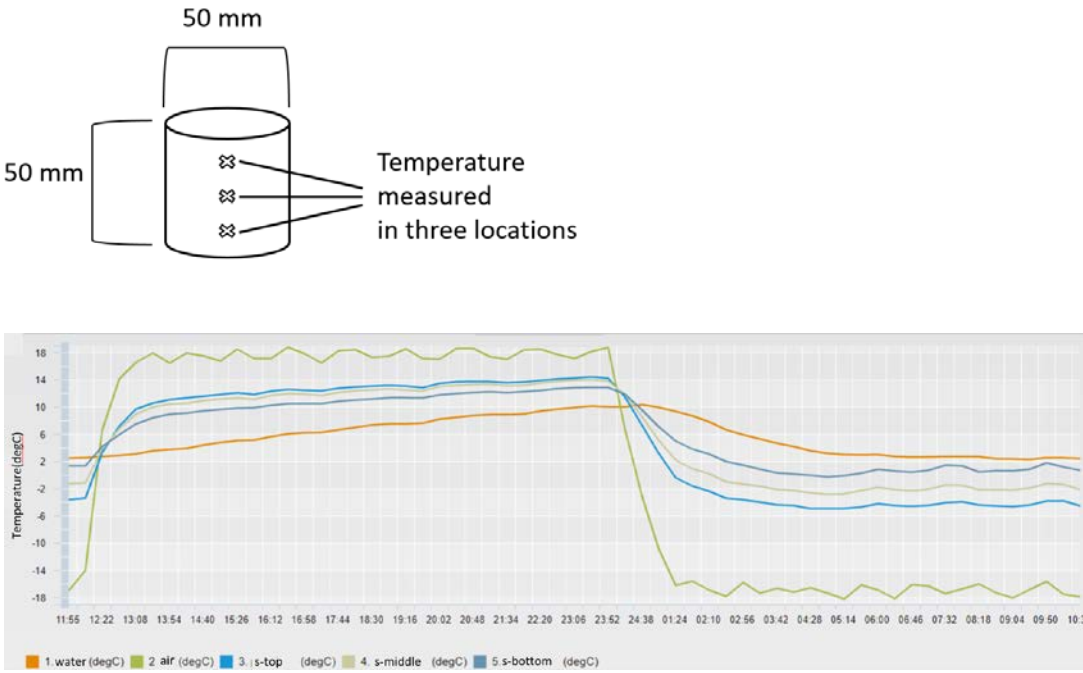

Figure 21. Placement of the temperature sensors in the sample (top), Temperature in the samples, air and water during temperature cycles (bottom).

The temperature is air controlled with a 24-hour cycle. At 12.00-00.00 the air is at room temperature and between 00.00- 12.00 the air is at freezing temperatures. When the temperature has become stable in the freezing part of the cycle (03.00-

12.00) it will have the same temperature gradient as the samples stored at a constant freezing temperature.

A relevant question is, is it really cold enough for a long time, so that the liquid can freeze in a large part of the sample? When observing the temperature measurement in the three points in the sample, it is about 0 °C, -2 °C, and -6 °C (bottom, middle, top). If the main part of the ice formation is between -7 °C and -15 °C as observed in the ice formation experiment in Fig. 12, only a relatively small part of the water will freeze, Fig. 21. The freezing parts of the sample will be located at the top of the sample were it is in direct contact with the circulating cold air.

The boundary condition of the samples during freezing is -20 °C air on the top, and +3 °C water on the bottom, Fig. 21. Water is more efficient to transfer heat than air, and the lower half of the sample was also surrounded by insulation. This means that the vertical temperature gradient through the sample was not linear, otherwise the middle of the sample would be around -8.5 °C. If that was the case, then around half the sample would be in the freezing zone below -7 °C, but in this case the temperature was -2 °C at the middle of the sample.

The results from the cryosuction experiment (paper II) showed that the moisture uptake of the samples exposed to freezing temperatures had a significantly higher spread, where some samples reaching much higher liquid uptakes than other samples. A hypothesis is that the higher liquid uptake in some samples was caused by the filling of stochastically distributed large pores (diameter of 1 mm or more) in the freezing zone. Observation and estimation of the large pores of 1 mm and larger on the surfaces of the samples have been performed, see Fig. 9 in Paper II. Several pores 1-5 mm diameter were found in all concrete samples. The samples that were exposed to cyclic temperatures had a larger spread in the results than the samples exposed to a constant freezing temperature. This is probably due to that the samples exposed to constant freezing temperature had a stable temperature gradient, while the samples exposed to cycling temperature conditions had a varying temperature gradient. The varying temperature gradient causes the freezing front of the sample to move back and forth in the sample, acting as cryo-pumps and in some cases saturating more of the larger air voids in the area were the freezing front is working. Please note that the samples were preconditioned to capillary saturation, so the moisture uptake studied in paper II is small, compared to the moisture content achieved during preparation of the same samples.

7 Conclusions

The overall aim of this thesis was to increase the knowledge of the mechanisms behind salt frost deterioration. In this thesis, the actual frost damage process is not studied, but the focus is on the mechanism behind it. This have been accomplished through studies of the following two topics:

(1) Participating in further developing an existing poromechanical frost deterioration model in cooperation with Daniel Eriksson, to consider what occurs during multiple freeze-thaw cycles in an air-entrained concrete. This includes the effect of hysteresis between freezing and thawing, the presence of an external reservoir that contains pure water or a liquid solution with different salt concentrations (Paper I). The results indicate that the model can also describe freeze-thaw induced absorption into air-entrained concrete that is initially capillary saturated. In the thesis it is also shown how some of the material parameters needed for poromechanical modelling of frost deterioration can be measured experimentally, but the results depend on e.g. drying condition.

(2) Plan, execute and analyse experiments on cryosuction in capillary saturated and un-carbonated samples (paper II). Cryosuction is the additional liquid uptake during freezing temperatures, compared to uptake at non-freezing temperature. The measurements confirmed the effect of cryosuction in samples exposed to freezing temperatures (cycled +20 °C/ -20 °C, constant -20 °C) as the liquid uptake was higher than for the samples exposed to constant +20 °C and the liquid uptake was not influenced by if the samples were in contact with NaCl solution or pure water. The liquid uptake was also not influenced by an increased amount of GGBS replacing cement, and samples with AEA had a tendency of higher liquid uptake than the samples without AEA.

8 Future research

These proposals for future research are based on the experimental work, and the need to further develop frost models.

8.1 Modelling

Expand the KTH model by Eriksson (paper I) to also include the glue spall theory, that focuses on the interaction between concrete and the external ice (with or without salt). The work of Sara Bahafid at NTNU, where she investigates the brine channels at the ice/concrete interface, is a good start [54].

Further expand the KTH model to be able to simulate the development of the damage during multiple freeze-thaw cycles. Internal damage can cause cracking, that results in, e.g., a more permeable microstructure. Surface scaling removes small pieces of material from the surface, decreasing the depth of the cover every cycle. It would be valuable to be able to model both these phenomena.

8.2 Experiments

Perform the dilation and ice formation experiments with partly saturated mortars, and compare the results with the results of fully saturated samples discussed in Section 4.2 to observe the protective effect of air voids. This would give additional results that could be simulated, to verify frost models.

Study the effect of the temperature gradient on cryosuction in samples that have a larger part of the sample in the freezing zone. This can be done by performing cryosuction experiments (Paper II) with longer samples, and have the temperature in the middle of the sample being around -7 °C, to be closer to the temperature where the freezing begun according to calorimetry measurements in this study.

Further observe the inside of the pores that are saturated by different methods and exposed to different temperatures. However, the pores that create internal damage to the material during freezing might be too small to be observed with X-ray micro-tomography in Lund. The research group have therefore reached out to ILL in Grenoble, France, where samples can be examined with higher resolution and complemented with neutron imaging.

9 Reference list

1. Scrivener, K.L., *Options for the future of cement.* The Indian Concrete Journal 2014
2. Gruyaert, E., P. Van den Heede, and N. De Belie, *Carbonation of slag concrete: Effect of the cement replacement level and curing on the carbonation coefficient – Effect of carbonation on the pore structure.* Cement and Concrete Composites, 2013. **35**(1): p. 39-48.
3. Lothenbach, B., K. Scrivener, and R.D. Hooton, *Supplementary cementitious materials.* Cement and Concrete Research, 2011. **41**(12): p. 1244-1256.
4. Jacobsen, S., D.H. Sœther, and E.J. Sellevold, *Frost testing of high strength concrete: Frost/salt scaling at different cooling rates.* Materials and Structures, 1997. **30**(1): p. 33-42.
5. Powers, H., *Theory of volume changes in hardened portlandcement paste during freezing. .* Proceedings, Highway Research Board 32, PCA Bull 46, 1953.
6. Coussy, O., *Mechanics and physics of porous solids*. 2010: Chichester, West Sussex, U.K. ; Hoboken, N.J. : Wiley, 2010.
7. Coussy, O. and P.J.M. Monteiro, *Poroelastic model for concrete exposed to freezing temperatures.* Cement and Concrete Research, 2008. **38**(1): p. 40-48.
8. Carpio, R., et al., *Alternative Fuels Mixture in Cement Industry Kilns Employing Particle Swarm Optimization Algorithm.* Soc. of Mech. Sci. & Eng, 2008. **30**.
9. *EN 197-1, Cement Composition, specifications and conformity criteria for common cements.* British standard institution 2011.
10. Odler, I., *Lea's Chemistry of Cement and Concrete.* Butterworth-Heinemann: Oxford., 1998. **Fourth Edition**(6 – Hydration, Setting and Hardening of Portland Cement): p. 241-297.
11. Liao, W., et al., *Hydration of Binary Portland Cement Blends Containing Silica Fume: A Decoupling Method to Estimate Degrees of Hydration and Pozzolanic Reaction.* Frontiers in Materials, 2019. **6**.

12. Juenger, M.C.G. and R. Siddique, *Recent advances in understanding the role of supplementary cementitious materials in concrete.* Cement and Concrete Research, 2015. **78**: p. 71-80.
13. Emborg, M. and S. Bernander, *Assessment of Risk of Thermal Cracking in Hardening Concrete.* Journal of Structural Engineering, 1994. **120**(10): p. 2893-2912.
14. Gruyaert, E., *Effect of Blast-Furnace Slag as Cement Replacement on Hydration, Microstructure, Strength and Durability of Concrete.* Ghent University, 2011. **Faculty of Engineering and Architecture**.
15. Siddique, R., *Performance characteristics of high-volume Class F fly ash concrete.* Cement and Concrete Research, 2004. **34**(3): p. 487-493.
16. ASTM-C618-19, *Standard Specification for Coal Fly Ash and Raw or Calcined Natural Pozzolan for Use in Concrete.* 2019.
17. Edmeades, R.M.P.C.H., *Lea's Chemistry of Cement and Concrete*. 1998,, Butterworth-Heinemann: Oxford. p. 841-905.
18. Gagné, R., *17 - Air entraining agents*, in *Science and Technology of Concrete Admixtures*, P.-C. Aïtcin and R.J. Flatt, Editors. 2016, Woodhead Publishing. p. 379-391.
19. Du, L. and K.J. Folliard, *Mechanisms of air entrainment in concrete.* Cement and Concrete Research, 2005. **35**(8): p. 1463-1471.
20. Gelardi, G., et al., *9 - Chemistry of chemical admixtures*, in *Science and Technology of Concrete Admixtures*, P.-C. Aïtcin and R.J. Flatt, Editors. 2016, Woodhead Publishing. p. 149-218.
21. Flatt, R. and I. Schober, *7 - Superplasticizers and the rheology of concrete*, in *Understanding the Rheology of Concrete*, N. Roussel, Editor. 2012, Woodhead Publishing. p. 144-208.
22. Ian Sims, B.b., *Lea´s Chemistry of Cement and concrete Chapter 16 concrete aggregates*, B.-H. Oxford., Editor. 1998.
23. Wu, K.-R., et al., *Effect of coarse aggregate type on mechanical properties of high-performance concrete.* Cement and Concrete Research, 2001. **31**(10): p. 1421-1425.
24. Stefan Jacobsen, D.B., Heikki Kukko, Tang Luping Katja Nordström *Measurment of internal cracking as dilation in the SS 13 72 44 frost test.* Byggforsk, 1999. **Nordtest Project 1389-98**.
25. Utgenannt, P., *The influence of ageing on the salt-frost resistance of concrete*. 2004, Lund University Open Access. p. 346.
26. Arnfelt, H., *Damage on Concrete Pavements by Wintertime Salt Treatment.* Statens Väginstitut, 1943.
27. Verbeck, G. and P. Klieger, *Studies of salt scaling of concrete* Highway Research Board bulletin, 1957.

28. Powers, *The Air requirement of frost-resistant concrete.* 1949.
29. Sun, Z. and G.W. Scherer, *Effect of air voids on salt scaling and internal freezing.* Cement and Concrete Research, 2010. **40**(2): p. 260-270.
30. Fagerlund, G., *The critical spacing factor : preliminary version.* Division of Building Materials, LTH, Lund University, 1993.
31. Zeng, Q., et al., *A study of the behaviors of cement-based materials subject to freezing.* 2010 International Conference on Mechanic Automation and Control Engineering, MACE2010, 2010.
32. Fagerlund, G., *Critical degrees of saturation at freezing of porous and brittle materials*. 1973, Division of Building Materials.
33. Fagerlund, G., *The long time water absorption in the air-pore structure of concrete.* Division of Building Materials, LTH, Lund University, 1993.
34. Taber, S., *The Mechanics of Frost Heaving.* The Journal of Geology, 1930. **38**(4): p. 303-317.
35. Rosenqvist, M., K. Fridh, and M. Hassanzadeh, *Macroscopic ice lens growth in hardened concrete.* Cement and Concrete Research, 2016. **88**: p. 114-125.
36. Rosenqvist, M., *Moisture Conditions and Frost Resistance of Concrete in Hydraulic Structures.* Licentiate Thesis, Building Materials, LTH, Lund University, 2013: p. https://lup.lub.lu.se/search/ws/files/3718424/4180251.pdf.
37. Lindmark, S., *Mechanisms of salt frost scaling on portland cement-bound materials: studies and hypothesis*, in *TVBM 1017*. 1998, Division of Building Materials. p. 272 pages.
38. Powers, *Structure and Physical Properties of Hardened Portland Cement Paste.* Journal of the American Ceramic Society, 1958. **41**(1): p. 1-6.
39. Eriksson, D., et al., *Freezing of partially saturated air-entrained concrete: A multiphase description of the hygro-thermo-mechanical behaviour.* International Journal of Solids and Structures, 2018. **152-153**: p. 294-304.
40. Beaudoin, J.J. and C. MacInnis, *The mechanism of frost damage in hardened cement paste.* Cement and Concrete Research, 1974. **4**(2): p. 139-147.
41. Sandström, T., *Durability of concrete hydropower structures when repaired with concrete overlays*. 2010, Luleå tekniska universitet.
42. Sandström, T., et al., *The influence of temperature on water absorption in concrete during freezing.* Nordic Concrete Research, 2012. **45**(1): p. 45-58.
43. Zhichao Liu, W.H.F.W., *Pumping effect to accelerate liquid uptake in concrete and its implications on salt frost durability.* Construction and Building Materials, 2018. **158**: p. 181-188.

44. Liu, Z. and W. Hansen, *A Hypothesis for Salt Frost Scaling in Cementitious Materials.* Journal of Advanced Concrete Technology, 2015. **13**(9): p. 403-414.
45. Faheem, A., *Influence of thermal boundary conditions and temperature distribution in concrete on frost scaling – experimental and numerical study.* Technical University of Denmark, Department of Civil Engineering, 2021. **Ph.D. thesis**.
46. Setzer, M.J., *Micro-Ice-Lens Formation in Porous Solid.* Journal of Colloid and Interface Science, 2001. **243**(1): p. 193-201.
47. Valenza, J. and G.W. Scherer, *A review of salt scaling: I. Phenomenology.* Cement and Concrete Research, 2007. **37**(7): p. 1007-1021.
48. Valenza, J. and G.W. Scherer, *A review of salt scaling: II. Mechanisms.* Cement and Concrete Research, 2007. **37**(7): p. 1022-1034.
49. John Valenza, G.W.S., *Mechanism for Salt Scaling.* The American Ceramic Society, 2006: p. 1161–1179
50. M-H Tremblay, F.L., J. Marchand, G. W. Scherer, J.J. Valenza, *Ability of the Glue Spall Model to Account for the De-Icer Salt Scaling Deterioration of Concrete*, in *International Congress; 12th, Chemistry of cement; 2007; Montreal, Canada in INTERNATIONAL CONGRESS ON THE CHEMISTRY OF CEMENT -CD-ROM EDITION- ; W4-07.3 Chemistry of cement*. 2007.
51. Jacobsen, S., E.J. Sellevold, and S. Matala, *Frost durability of high strength concrete: Effect of internal cracking on ice formation.* Cement and Concrete Research, 1996. **26**(6): p. 919-931.
52. Valenza, J. and G.W. Scherer, *Mechanisms of salt scaling.* Materials and Structures, 2005. **38**(4): p. 479-488.
53. Strand, M., *Experimental Study of De-icing Salt-frost Scaling in Concrete with Low-calcium Fly Ash or Slag: Influence of Drying and Carbonation, and Air Content Lund: Faculty of Engineering, LTH at Lund University.* 2018.
54. Bahafid, S., et al., *Revisiting concrete frost salt scaling: On the role of the frozen salt solution micro-structure.* Cement and Concrete Research, 2022. **157**: p. 106803.
55. C-672-92, A., *Standard test method for scaling resistance of concrete surfaces exposed to de-icing chemicals.* American Society for Testing and Materials. : p. p. 329–31.
56. Fagerlund, G., *Studies of the Scaling, the Water Uptake and the Dilation of Mortar Specimens Exposed to Freezing and Thawing in NaCl Solutions.* Freeze-Thaw and De-Icing Resistance of Concrete, Lund Institute of Technology: Lund, Sweden, 1992. **G. Fagerlund and M.J. Setzer, Editors**: p. 36-66.

57. Yuan, J., et al., *Mechanisms on the Salt–Frost Scaling of Concrete.* Journal of Materials in Civil Engineering, 2015. **29**: p. D4015002.
58. Yang, R., et al., *A micromechanics model for partial freezing in porous media.* International Journal of Solids and Structures, 2015. **75-76**: p. 109-121.
59. T. Fen-Chong, P.D., A. Fabbri, Paulo J.M. Monteiro, *Poroelastic contribution to freezing in cement paste.* Poromechanics V © ASCE 2013, 2013: p. 1505-1514.
60. Zeng, Q., et al., *A study of freezing behavior of cementitious materials by poromechanical approach.* International Journal of Solids and Structures, 2011. **48**(22): p. 3267-3273.
61. Teddy Fen-Chong, A.F., Mickael Thiery, Patrick Dangla, *Poroelastic Analysis of Partial Freezing in Cohesive Porous Materials.* Journal of Applied Mechanics, 2013. **Vol. 80**.
62. Mayercsik, N.P., M. Vandamme, and K.E. Kurtis, *Assessing the efficiency of entrained air voids for freeze-thaw durability through modeling.* Cement and Concrete Research, 2016. **88**: p. 43-59.
63. Eriksson, D., et al., *Hygro-thermo-mechanical modeling of partially saturated air-entrained concrete containing dissolved salt and exposed to freeze-thaw cycles.* Cement and Concrete Research, 2021. **141**: p. 106314.
64. Scherer, G.W., *Crystallization in pores.* Cement and Concrete Research, 1999. **29**(8): p. 1347-1358.
65. van Genuchten, M.T., . *closed-form equation for predicting the hydraulic conductivity of unsaturated soils. .* ASoil Sci. Soc. Am. , 1980. **J. 44,** : p. 892–898.
66. Toshiyuki Takamuku, M.Y., Hisanobu Wakita, Yuichi Masuda, and Toshio Yamaguchi, *Thermal Property, Structure, and Dynamics of Supercooled Water in Porous Silica by Calorimetry, Neutron Scattering, and NMR Relaxation.* J. Phys. Chem. B 1997. **101,** (No. 29): p. 5730-5739.
67. Biot, *Mechanics of Deformation and Acoustic Propagation in Porous Media.* Journal of Applied Physics 33, 1962. **4**.
68. Whitaker, S., *Flow in porous media I: A theoretical derivation of Darcy's law.* Transport in Porous Media, 1986. **1**(1): p. 3-25.
69. Milligen, B.P.v., et al., *On the applicability of Fick's law to diffusion in inhomogeneous systems.* European Journal of Physics, 2005. **26**(5): p. 913.
70. Clennell, M., *Tortuosity: A guide through the maze*. Vol. 122. 1997, Geological Society London Special Publications. 299-344.
71. Fourier, *Theorie analytique de la chaleur.* Paris, CHEZ FIRMIN DIDOT, PÈRE ET FILS, LIBRARIES POUR LES MATHÉMATIQUES, L'ARCHITEC'I'URE HYDRAULIQUE, 1822. **ET LA MARINE, RUE JACOB, N° 24**.

72. Liu, Z. and W. Hansen, *Sorptivity as A Measure Of Salt Frost Scaling Resistance Of Air-Entrained Concrete*. Vol. 629-630. 2014, Key Engineering Materials.
73. Liu, Z. and W. Hansen, *Moisture uptake in concrete under freezing–thawing exposure.* Magazine of Concrete Research, 2015. **68**: p. 1-13.
74. institution, B.s., *Methods of testing cement - Part 1: Determination of strength.* 2016.
75. ASTM-E1875, *Standard Test Method for Dynamic Young's Modulus, Shear Modulus, and Poisson's Ratio by Sonic Resonance,.* 2013.
76. Dormieux, L., D. Kondo, and F.-J. Ulm, *Non-Saturated Microporomechanics*, in *Microporomechanics*. 2006, John Wiley & Sons, Ltd. p. 237-266.
77. Verbeck, G.J. and P.C. Klieger, *Calorimeter-strain apparatus for study of freezing and thawing concrete.* Highway Research Board bulletin, 1958.
78. Fridh, K., *Internal frost damage in concrete - experimental studies of destruction mechanisms.* Division of Building Materials, LTH, Lund University, 2005. **Doctoral Thesis**.
79. Gagné, R., et al., *Study of the relationship between scaling resistance and sorptivity of concrete.* Canadian Journal of Civil Engineering, 2011. **38**(11): p. 1238-1248.
80. Pinto, S., A. Macedo, and R. Medeiros-Junior, *Effect of preconditioning temperature on the water absorption of concrete.* Journal of Building Pathology and Rehabilitation, 2018. **3**: p. 3.
81. Shen, J. and Q. Xu, *Effect of moisture content and porosity on compressive strength of concrete during drying at 105 °C.* Construction and Building Materials, 2019. **195**: p. 19-27.
82. Kaufmann, J., *Experimental identification of damage mechanisms in cementitious porous materials on phase transition of pore solution under frost deicing salt attack.* EMPA Dübendorf, Switzerland, 1999. **Doctoral Thesis**.

Appendix 1 - Paper I

Cement and Concrete Research 141 (2021) 106314

Contents lists available at ScienceDirect

Cement and Concrete Research

journal homepage: www.elsevier.com/locate/cemconres

Hygro-thermo-mechanical modeling of partially saturated air-entrained concrete containing dissolved salt and exposed to freeze-thaw cycles

Daniel Eriksson [a,*], David Wahlbom [b], Richard Malm [a], Katja Fridh [b,1]

[a] Division of Concrete Structures, KTH Royal Institute of Technology, Brinellvägen 23, 100 44 Stockholm, Sweden
[b] Division of Building Materials, Lund University, John Ericssons väg 1, 223 63 Lund, Sweden

ARTICLE INFO

Keywords:
Freezing and thawing (C)
Finite element analysis (C)
Absorption
Hysteresis
Salt

ABSTRACT

In cold regions, understanding the freeze-thaw behavior of air-entrained concrete is important for designing durable structures and assessing the remaining service life of existing structures. This study presents a hygro-thermo-mechanical multiphase model that describes the cyclic freeze-thaw behavior of partially saturated air-entrained concrete containing dissolved salt. An equilibrium and a non-equilibrium approach are adopted to model the ice formation, including the freeze-thaw hysteresis, inside the porous network. The model also considers the diffusive and convective transport of the dissolved salt coupled to the freeze-thaw processes. Two examples are presented to verify and highlight the capabilities of the model. The first example shows that the model is capable of reproducing the experimentally observed mechanical response of specimens containing NaC1-solutions of different concentrations. In the second example, a larger absorption of liquid from an external reservoir is obtained with an increasing salt concentration in the reservoir, which is consistent with experimental observations.

1. Introduction

The ability of concrete to withstand a harsh environment makes it suitable for structures that are difficult to maintain, such as bridges, hydropower dams, waterways, locks, and roads. In cold regions, frost deterioration is important to consider when designing new concrete structures or when assessing the remaining service life of existing structures [1–4]. For internal frost damage, there is a consensus that the material is damaged when the degree of liquid saturation reaches a critical level for the specific concrete mixture, commonly called the critical degree of saturation [5]. Fagerlund [1] proposed a service-life model to predict the time to reach the critical degree of saturation for air-entrained concrete exposed to an external reservoir containing pure water. The model considers a slow long-term absorption process of water into air voids caused by dissolution and diffusion of trapped air inside the voids [6,7]. Several experimental studies have, however, reported an increased absorption of water from external reservoirs during repeated freeze-thaw cycles compared to isothermal conditions, which is explained by a pumping effect caused by the freezing and melting of the pore water [2,8–13]. Under such exposure conditions, the critical degree of saturation can, thus, be reached after a shorter time than predicted by Fagerlund's model. If the reservoir contains a saline solution, scaling of the surface is usually also observed, and is often referred to as salt-frost scaling. Some researchers have proposed that a higher degree of saturation in the surface region caused by the dissolved salt in the reservoir and the pore liquid is the dominant mechanism responsible for the observed scaling [12,14–16]. Hence, to a certain degree, this implies that the underlying mechanism for internal frost damage is partly also the cause of scaling. On the other hand, the glue-spall theory suggests that the scaling is caused by the ice layer on the surface, which fractures during freezing and thereby propagates cracks into the surface material [17]. Nevertheless, to be able to choose an optimal material design for a specific application or study the different deterioration mechanisms, it is important to have models that account for the influence of the different complex physical phenomena related to frost action.

Several models in the literature aim to describe the freezing behavior of concrete containing pure water, see e.g. [18–25]. Many of these are limited either to fully saturated conditions or the effect of empty air voids is considered by using an approach where the material is modeled on the microscale by studying a single air void. To overcome the latter

* Corresponding author.
E-mail addresses: daniel.eriksson@byv.kth.se (D. Eriksson), david.wahlbom@byggtek.lth.se (D. Wahlbom), richard.malm@byv.kth.se (R. Malm), katja.frid@mau.se (K. Fridh).
[1] Present address: Department of Materials Science and Applied Mathematics, Malmö University, PO Box 71, 205 06 Malmö, Sweden.

https://doi.org/10.1016/j.cemconres.2020.106314
Received 8 July 2020; Received in revised form 10 November 2020; Accepted 17 November 2020
Available online 15 December 2020

limitation, Eriksson et al. [24] presented a multiphase model where the local flow of supercooled water to empty air voids was introduced on the structural scale and showed that it could replicate measured volume changes of air-entrained concrete during freezing. Moreover, Gong and Jacobsen [26] used a similar approach to model absorption of water during repeated freeze-thaw cycles from an external reservoir into air-entrained concrete that was initially capillary saturated with water. In the works by Zeng et al. [27,28], a model that considers the influence of dissolved salt during the freezing part of a freeze-thaw cycle was presented. This model is, however, also limited to fully saturated conditions on the structural scale and does not consider the diffusive or convective transport of the dissolved salt inside the material.

In this study, the purpose is to develop a hygro-thermo-mechanical multiphase model that describes the freeze-thaw behavior of partially saturated air-entrained concrete and which also considers the influence of dissolved salt. It should be noted that the scope is limited to internal physical processes, which means that any mechanical interactions with formed ice on the surface, as, e.g., suggested by the glue-spall theory, are not addressed. The work is based on an earlier published model by the authors but presents significant extensions and improvements compared to the original formulation [24]. An essential new feature of the model is the description of the ice formation, which considers both the dissolved salt and the hysteresis between freezing and melting of the pore liquid inside cement-based materials. In this regard, both an equilibrium and a non-equilibrium approach are adopted to derive adequate relationships. The two approaches are compared in a verification example, where measured longitudinal deformations of prismatic concrete specimens pre-saturated with water and different NaCl-solutions are compared to simulations with the proposed model. Furthermore, to account for the diffusive and convective transport of dissolved salt during freezing and thawing, a mass balance for the salt species is introduced. Although the model considers the internal physical processes, it can be used to study the influence of salt on the absorption of liquid into concrete from an external reservoir containing either pure water or a saline solution during repeated freeze-thaw cycles. These capabilities of the model are further explored in a second example. In addition to the effect of dissolved salt on the absorbed volume, the example also studies different types of boundary conditions at the exposure surface of the external reservoir.

2. Freezing and melting of saline solutions in concrete

The pore structure directly influences the amount of ice formed inside a porous medium at a certain freezing temperature. As described by e.g. Zeng et al. [27], a requirement for ice formation is that the chemical potential of the ice is either lower or equal to the chemical potential of the liquid water. However, due to the confinement of the water inside the pores, the chemical potential becomes lower compared to bulk water, meaning that the ice must first form in the larger pores and then progressively penetrate the smaller pores as the temperature decreases. The presence of salt ions in the pore liquid, however, further lowers the chemical potential, and thus results in even lower freezing temperatures of saline pore solutions compared to pure pore water, see e.g. [3,28,29]. This effect must of course be included in the model to sufficiently account for the presence of dissolved salt in the pore liquid under freeze-thaw conditions.

2.1. Modeling approaches of ice formation

The formation of ice is normally modeled by either assuming thermodynamic equilibrium between the two phases or by using a non-equilibrium approach where the imbalance of the chemical potentials is the driving force of the process kinetics of the ice formation [30]. The equilibrium approach requires that the chemical potentials are equal and is frequently used in the literature [21–23]. However, as pointed out by, e.g., Zuber and Marchand [20], this assumption is only valid if the rate of cooling is sufficiently low. The process of ice formation is, in a real case, better described by a process consisting of two stages, where the freezing first is initiated by heterogenous nucleation of ice crystals inside the pores. In the second stage, these crystal embryos continue to grow and progressively penetrate from larger to smaller pores in the porous network. It is this two-stage process that a non-equilibrium model typically describes better than an equilibrium-based model [16,31–33]. Nevertheless, if the rate of cooling is sufficiently low, models based on the two different approaches should give approximately equivalent results.

Based on the assumption of thermodynamic equilibrium, and as shown by e.g. Zeng et al. [27] and Lindmark [12] for cases with a saline pore solution, a relationship can be derived for the pressure difference between the two phases on the following form

$$p^i - p^l = \mathscr{S}_f\left(T_0 - T\right) - \left(1 - \frac{V_w}{V_i}\right)\left(p^l - p_0\right) + \frac{RTln(a^w)}{V_i} \tag{1}$$

where p^α is the pressure of the ice phase ($\alpha = i$) and the liquid phase ($\alpha = l$), $\mathscr{S}_f$ is the entropy of fusion, T_0 denotes the melting or freezing temperature of the bulk phases at pressure p_0 (normally 1 atm), T is the temperature and V_α is the molar volume of ice and water ($\alpha = w$). The last term on the right-hand side (RHS) takes dissolved salt into account, where R is the universal gas constant and a^w is the water activity, which depends on the concentration of salt in the liquid phase. In this study, a^w is evaluated using the semi-empirical relationship proposed by Lin and Lee [34], and also successfully used by e.g. Zeng et al. [27] to include the effect of salt on the freezing process. Due to the confinement of the phases inside the pores, the interface between them is curved, and hence the pressure difference can be expressed by the Young-Laplace law. Assuming the interface to be hemispherical yields

$$p^i - p^l = \frac{2\gamma_{li}}{r} \tag{2}$$

where γ_{li} is the interface energy and r is the radius of the interface. By substituting Eq. (2) into Eq. (1), one can obtain an expression for the equilibrium radius r_{eq} of the interface reading

$$r_{eq} = \frac{2\gamma_{li}}{\mathscr{S}_f\left(T_0 - T\right) - \left(1 - \frac{V_w}{V_i}\right)\left(p^l - p_0\right) + \frac{RTln(a^w)}{V_i}}. \tag{3}$$

Inside frozen pores, an unfrozen liquid-like layer exists between the ice crystals and the pore walls. The thickness of this layer, δ, is typically either considered to remain constant under freezing conditions, Brun et al. [35] e.g. found that $\delta \approx 0.8$ nm, or to follow a temperature-dependent relationship where δ decreases with a decreasing temperature. In a recent study by Zeng and Li [36], the physical origins of this layer were discussed based on the principles of thermodynamics, and it was theoretically shown that δ should decrease with a decreasing temperature. The study also compiled reported data of δ from a number of experimental and theoretical studies in the literature, which also consistently shows a decreasing value of δ with temperature. In the current study, a temperature-dependent relationship of δ proposed by Fagerlund [37] is adopted

$$\delta = 19.7 \cdot 10^{-10}\left(\frac{1}{|\theta|}\right)^{1/3} \tag{4}$$

where θ denotes the temperature in degrees Celsius and δ is obtained in meters. This relationship has also been successfully used in other models in the literature when modeling the behavior of cement-based materials exposed to freezing conditions, see e.g. [20,21,24,27]. Moreover, Zeng and Li [36] also used this relationship, together with three other from the literature, to show the significance of considering the unfrozen layer when evaluating both the volume of formed ice in the pore space and freezing-induced pressures in porous materials. Taking the thickness δ

into account, the critical pore radius r_p below which ice cannot form at certain state in the material is obtained as $r_p = r_{\text{eq}} + \delta$. Under the assumption of local thermodynamic equilibrium between the phases and using these definitions, the volume fraction of ice can, e.g., be estimated based on a measured cumulative pore size distribution $v(r)$ [18,21,23].

In the non-equilibrium approach to model ice formation, a relationship describing the thermodynamic imbalance between the phases must be established instead. This process affinity can then be used to model the kinetics of the phase transition between the liquid and solid state. Koniorczyk et al. [19] proposed a model based on this approach for porous materials, such as concrete, where the kinetics is characterized by a linear evolution law. The model has been further explored by Gawin et al. [30], who extended it to also consider initial supercooling of the liquid phase before initiating the nucleation of ice. However, neither of these studies consider dissolved salt in the liquid phase, and hence the kinetic description needs to be extended to also include this effect in order to fulfill the purpose of this study. Following the same principles as in the two aforementioned references, the rate of freezing is described by a linear law of the form

$$\dot{v}_i = \varepsilon k A_{li} = \frac{\varepsilon}{RT\tau_{fr}} A_{li} \tag{5}$$

where ε is the porosity, τ_{fr} is the characteristic time of freezing and A_{li} denotes the affinity. From the definition of chemical potentials and also considering dissolved salt in the liquid phase [27], the affinity can according to, e.g., Setzer [16] be expressed as

$$A_{li} = \mu_w\left(T, p^l, a^w\right) - \mu_i\left(T, p^i\right) = -\int_{T_0}^{T} s_w dT + \int_{p0}^{p^l} V_w dp + RT ln\left(a^w\right) + \int_{T_0}^{T} s_i dT - \int_{p0}^{p^i} V_i dp \tag{6}$$

where μ_α and s_α are the chemical potential and molar entropy, respectively. Substituting Eq. (6) into Eq. (5) and rearranging some of the terms as well as considering the conditions that must be satisfied for ice to form, one can obtain the following relationship for the rate of ice formation

$$\dot{v}_i = \begin{cases} \dfrac{\varepsilon V_i\left[\Delta p_{eq} - \Delta p_{fr}(S_l)\right]}{RT\tau_{fr}} & \text{if } \Delta p_{fr}(S_l) < \Delta p_{eq} \,\&\, T \le T_{fr,ini} \\ 0 & \text{otherwise} \end{cases} \tag{7}$$

where $T_{fr,ini}$ denotes initial supercooling and $\Delta p_{eq} = (p^i - p^l)_{eq}$ corresponds to the pressure difference between the phases under equilibrium conditions, and hence given by Eq. (1) in this study. The second pressure term, $\Delta p_{fr}(S_l)$, is determined by Eq. (2), but where the radius r is a function of the degree of liquid saturation S_l and corresponds to the size of the pore in which ice is currently forming. As proposed by Koniorczyk et al. [19], this relationship can, e.g., be determined from a measured sorption isotherm or a pore size distribution. The volume fraction of formed ice inside the material, at any point in time, is then obtained through time integration of Eq. (7).

2.2. Models considering freeze-thaw hysteresis

It is well-established that freeze-thaw cycles of cement-based materials typically show a hysteresis loop for the volume of formed ice inside the porous network. At the same freezing temperature, the observed volume of ice in the thawing part of a cycle is usually higher than during freezing. These hysteresis loops can, e.g., be observed in measurement results obtained from low-temperature calorimetry testing of cement-based materials. An example of such results from measurements performed by Sun and Scherer [38] using a differential scanning calorimeter (DSC) is shown in Fig. 1. The reason for observing this behavior can partly be explained by that the freezing temperature normally is

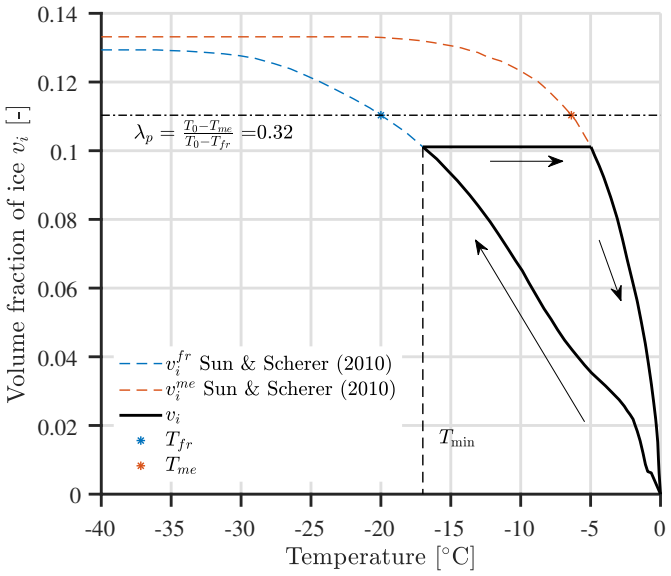

Fig. 1. Example of measured freezing and melting curves for mortar saturated with pure water from Sun and Scherer [38] together with a generic hysteresis loop following the model proposed by Gong and Jacobsen [26]. Furthermore, the calculation of λ_p in a single point using this type of measurements is illustrated.

controlled by the size of the pore entry, whereas the interior size of the pore body controls the melting temperature [20,26,33]. Moreover, the pore connectivity is also a contributing factor since a large pore might only be connected to smaller adjacent pores, which require a lower temperature for ice to penetrate them [33]. This type of blocking effect is also commonly referred to as the ink-bottle effect, see e.g. [39].

To model the behavior of concrete subjected to freeze-thaw cycles, it is of course necessary to account for the hysteresis. A suitable method to incorporate this in a model based on the equilibrium approach was proposed by Gong and Jacobsen [26], which utilizes a pore shape factor λ_p defined as

$$\lambda_p = \frac{\kappa_b}{\kappa_e} \approx \frac{T_0 - T_{me}}{T_0 - T_{fr}} \tag{8}$$

to describe the hysteresis loop. In the equation, κ_e and κ_b denotes the curvature of the interface between the ice and liquid phase at the pore entry and inside the pore body, respectively, i.e. the curvatures during freezing and thawing according to the description above. As described by, e.g., Sun and Scherer [33], this parameter reflects the shape of the pores and can provide a sufficiently good approximation of the relation between the size of the pore entries and the interior bodies. The approximative expression of λ_p given in Eq. (8) can be obtained through the use of Eq. (3) by omitting the effect of p^l and a^w as well as assuming that the entropy of fusion is a weak function of the temperature [33]. In the latter expression, T_{fr} and T_{me} are the freezing and melting temperatures corresponding to the same volume fraction of ice in a measured freeze-thaw curve. Consequently, it is possible to establish a relationship of λ_p that depends on the volume fraction of ice in the material directly from, e.g., low-temperature calorimetry measurements, see Fig. 1. Based on this, Gong and Jacobsen [26] proposed to describe a freeze-thaw cycle by first following the freezing curve v_i^{fr} until the minimum temperature $T_{\min}$ of the cycle is reached. Thereafter, the cycle continues by following a constant value of $v_i^{fr}(T_{\min})$ until reaching a temperature of $T = \lambda_p T_{\min}$, which follows from Eq. (8) by considering that $T_0 = 0\,^\circ$C. After reaching this temperature, the melting curve v_i^{me} is followed for the remaining part of the cycle. A complete generic hysteresis loop following this approach is illustrated in Fig. 1. Gong and Jacobsen [26] did, however, not consider a saline liquid solution, and hence their proposed

hysteresis model is in this study extended to also take dissolved salt into account. In addition, the dependence of p^l appearing in Eq. (3) is also considered.

A corresponding expression for the freeze-thaw loop, which also considers the dissolved salt, can be obtained from measured freezing and melting curves by utilizing that the temperatures can be converted into corresponding pore sizes. As described by, e.g., Sun and Scherer [33] and Wu and Johannesson [40], measured curves from low-temperature calorimetry can be utilized in thermoporometry to determine the size distribution of both the entries and the interior of the pores. Therefore, by following the outlined methods in the aforementioned studies, they can be expressed as functions of the pore size instead of temperature. Consequently, the equilibrium pore size r_p can be used directly to determine the volume fraction of ice in the material based on its current state, since r_p depends on T, p^l and a^w. An assumption regarding the transition between the freezing and melting curve in the hysteresis loop is, however, still required. Adopting the same type of assumption as Gong and Jacobsen [26] and also following the work by Sun and Scherer [33], it is assumed that the volume fraction of ice during the transition remains at a constant level, which is given by the minimum equilibrium pore size r_p^{min} reached during the freezing part of the loop. Based on this, the freeze-thaw hysteresis loops can be expressed as

$$v_i(T,p^l,a^w) = \begin{cases} v_i^{fr}(r_p) & \text{if } \dot{r}_p < 0 \\ v_i^{fr}\left(r_p^{\min}\right) & \text{if } \dot{r}_p \geq 0 \,\&\, \Delta v_i > 0 \\ v_i^{me}(r_p) & \text{if } \dot{r}_p \geq 0 \,\&\, \Delta v_i \leq 0 \end{cases} \tag{9}$$

where $\Delta v_i = v_i^{me}(r_p) - v_i^{fr}(r_p^{min})$. An example of a complete freeze-thaw loop using the extended hysteresis model according to Eq. (9) is illustrated in Fig. 2. In the example, an initial NaCl concentration of 6.5% by weight was assumed, which yields a water activity $a^w \approx 0.96$ according to the semiempirical relationship proposed by Lin and Lee [34] mentioned in Section 2.1. Moreover, it has been assumed that $p^l = p_0$, which means that the freezing and melting relationships, corresponding to the two curves in Fig. 1, are instead represented by two surfaces in the $T - a^w$ space. As can be seen in the figure, the loop, described by Eq. (9),

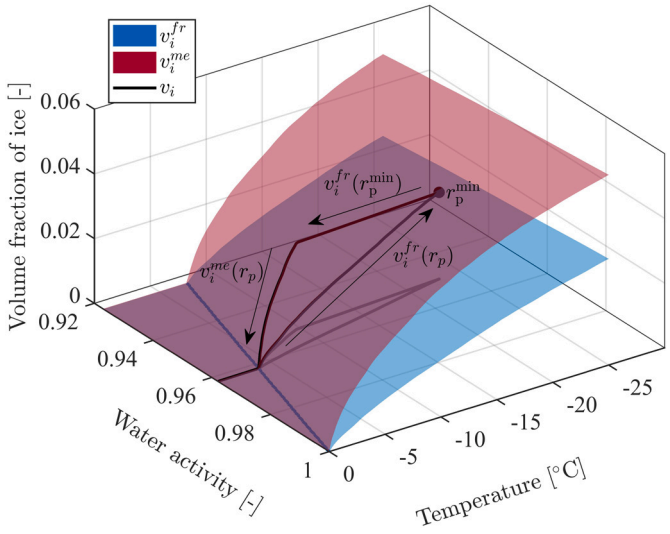

Fig. 2. Example of calculated ice formation in a freeze-thaw cycle using the extended hysteresis model based on the equilibrium approach, where an initial NaCl concentration corresponding to $a^w \approx 0.96$ has been assumed and that $p^l = p_0$. Note that the grey line in the figure corresponds to the projection of v_i on the $T - a^w$ plane. The arrows, together with their annotations, indicate the direction of the loop and the active term in Eq. (9).

first follows the freezing surface $v_i^{fr}(r_p)$ until reaching a point corresponding to the minimum penetrated pore size r_p^{min} of the loop. During the thawing phase of the loop, there is first a transition part between the freezing and melting surfaces where the ice content remains at a constant level determined by $v_i^{fr}(r_p^{min})$. When the melting surface is reached, the ice content is given by $v_i^{me}(r_p)$ for the remaining part of the loop. When freezing saline solutions, it is well-known that the dissolved salt is not incorporated into the ice crystals [3,41]. Hence, the concentration of salt in the remaining unfrozen solution increases as the liquid phase changes into its solid state. This phenomenon was considered in this illustrative example and can be observed in the plotted projection of v_i on the $T - a^w$ plane in the figure, where a^w continuously changes during the freezing and melting processes. The implementation of this phenomenon in the governing mass balance equations of the model developed in this study is further explained in Section 3.

In the non-equilibrium approach, the pore shape factor λ_p can be utilized to capture the hysteresis in freeze-thaw cycles. As shown by Koniorczyk et al. [19], the pressure corresponding to Δp_{fr} during the melting-phase of a cycle is given by $\Delta p_{me} = \lambda_p \Delta p_{fr}$. Using this definition as well as Eqs. (5) and (6), where the latter equation introduces the effect of a saline liquid pore solution, it is possible to obtain an expression for the rate of melting on the following form

$$\dot{v}_i = \begin{cases} \dfrac{\varepsilon V_i \left[\Delta p_{eq} - \Delta p_{me}(S_l)\right]}{RT\tau_{me}} & \text{if } \Delta p_{me}(S_l) > \Delta p_{eq} \,\&\, \dot{T} > 0 \,\&\, S_i > 0 \\ 0 & \text{otherwise} \end{cases} \tag{10}$$

where τ_{me} is the characteristic time of melting and S_i is the degree of ice saturation. Through the combined use of Eqs. (7) and (10), the freeze-thaw cycles including the hysteresis can be described by the non-equilibrium approach. As mentioned earlier, if the rate of temperature change is sufficiently small, the two described approaches to model the freeze-thaw cycles should give approximately the same results [18,30]. In Section 5.1, both approaches are further explored by comparing obtained simulation results to investigate differences when modeling the freeze-thaw behavior of air-entrained concrete that is partially saturated with a saline liquid solution.

3. Governing balance equations

To describe the behavior of partially saturated air-entrained concrete subjected to freeze-thaw actions and the influence of dissolved salt, the material is treated as a multiphase porous medium. In the developed model, the porous medium is assumed to consist of four phases: liquid (l), ice (i), gas (g) and solid (s). The presence of dissolved salt ions in the material is accounted for by considering the liquid phase to consist of the two species liquid water (w) and dissolved salt (Sa). The model is limited to conditions where the concrete is at least capillary saturated, which means that the capillary pores are always saturated with liquid and ice or just one of the two phases, depending on the state of the material. Following this assumption, the gas phase, which consists of air, can be considered to be trapped inside the air voids. Furthermore, it is well-established that the diffusive transport of trapped air through the liquid phase inside air-entrained concrete is a very slow process, see e.g. [6,7,42]. Therefore, both the diffusive and the advective transport of the gas phase are neglected in the model. The governing balance equations of mass, energy and linear momentum for the model are all obtained using general macroscopic balance equations derived for a generic porous medium. These can be derived using e.g. the hybrid mixture theory (HMT) or the thermodynamically constrained averaging theory (TCAT), which both starts at the microscale and then uses averaging procedures over a representative elementary volume (REV) to derive the macroscopic equations [43–45].

The general mass balance equation for an arbitrary phase α can be written as

$$\frac{D^{\alpha}(\eta^{\alpha}\rho^{\alpha})}{Dt}+\eta^{\alpha}\rho^{\alpha}\nabla\cdot\mathbf{v}^{\alpha}=\sum M^{\pi\to\alpha} \tag{11}$$

where the operator D^{α}/Dt denotes the material time derivative with respect to phase α, η^{α} is the volume fraction, ρ^{α} is the density, $\mathbf{v}^{\alpha}$ is the velocity and $M^{\pi\to\alpha}$ are source or sink terms taking phase changes into account. In porous media theory, it is customary to express the movement of fluid phases relative to the solid phase. Hence, to derive the final forms of the mass balance equations, the relative velocity $\mathbf{v}^{\alpha\pi}=\mathbf{v}^{\alpha}-\mathbf{v}^{\pi}$ of a phase α relative to another phase π is introduced as well as

$$\frac{D^{\alpha}f^{\pi}}{Dt}=\frac{D^{\pi}f^{\pi}}{Dt}+\nabla f^{\pi}\cdot\mathbf{v}^{\alpha\pi} \tag{12}$$

which can be obtained from the definition of material derivatives and where f^{π} is an arbitrary differentiable function [44].

Through the use of the general mass balance above and expressing the time derivatives relative to the solid phase, the mass balance of the dissolved salt can be written as

$$\begin{aligned}&\varepsilon\rho^{lSa}\frac{D^{s}S_{l}}{Dt}+S_{l}\rho^{lSa}\frac{D^{s}\varepsilon}{Dt}+\varepsilon S_{l}\frac{D^{s}\rho^{lSa}}{Dt}+\nabla\cdot\mathbf{J}^{Sa}+\\&\varepsilon S_{l}\rho^{lSa}\nabla\cdot\mathbf{v}^{s}+\nabla\cdot\left(\varepsilon S_{l}\rho^{lSa}\mathbf{v}^{ls}\right)=0\end{aligned} \tag{13}$$

where ε is the porosity and S_l is the degree of liquid phase saturation, which in general is defined as $S_f=\eta^{f}/\varepsilon$ for a phase f occupying the porous network. According to above, there are three phases occupying the pore space (l,i,g) and thus the relationship $S_l+S_i+S_g=1$ must hold. In Eq. (13), ρ^{lSa} denotes the mass concentration of dissolved salt in phase l and is given by

$$\rho^{lSa}=c^{Sa}M_{Sa} \tag{14}$$

where c^{Sa} is the concentration of salt expressed in mol/(m^3 interstitial liquid) and M_{Sa} is the molar mass of the salt. The term $\mathbf{J}^{Sa}$ describes the diffusive mass flux of dissolved salt through phase l and appears when developing Eq. (11) on the following form

$$\mathbf{J}^{Sa}=\varepsilon S_{l}\rho^{lSa}\mathbf{u}^{Sa}=\varepsilon S_{l}\rho^{lSa}\left(\mathbf{v}^{Sa}-\mathbf{v}^{l}\right) \tag{15}$$

where $\mathbf{u}^{Sa}$ is the diffusive velocity of the dissolved salt. Furthermore, it should be noted that there are no source or sink terms in the mass balance, which means that the concentration of salt in the liquid phase during freezing will increase since the volume fraction of liquid pore water decreases. As mentioned in Section 2.2, this is a well-known phenomenon when freezing saline solutions, and physically means that the salt is not incorporated in the forming ice crystals [3,41]. Following the work by Zeng et al. [27], who also accounted for the increased concentration of salt during freezing in a similar manner but under the assumption of sealed conditions, the eutectic phase appearing at −21.3°C in NaC1-solutions is not considered. Moreover, it should be emphasized that models including both the convective and diffusive transport of dissolved salt coupled with the freeze-thaw process, as done in this study, are scarce in the literature. By including these, the proposed model is capable of describing the redistribution of salt ions within the material induced by the freeze-thaw actions as well as, e.g., accounting for absorption of additional salt from an unfrozen external reservoir.

The mass balances of the liquid water species (w) and the ice (i) is obtained using the same principles. It is, however, assumed that the ice phase does not flow in the porous medium, and thus it follows that $\mathbf{v}^{i}=\mathbf{v}^{s}$. Performing the derivation steps individually for each of the two phases and then summing their contributions yields

$$\begin{aligned}&S_{l}\rho^{lw}\frac{D^{s}\varepsilon}{Dt}+S_{i}\rho^{i}\frac{D^{s}\varepsilon}{Dt}+\varepsilon\rho^{lw}\frac{D^{s}S_{l}}{Dt}+\varepsilon\rho^{i}\frac{D^{s}S_{i}}{Dt}+\\&\varepsilon S_{l}\frac{D^{s}\rho^{lw}}{Dt}+\varepsilon S_{i}\frac{D^{s}\rho^{i}}{Dt}+\left(\varepsilon S_{l}\rho^{lw}+\varepsilon S_{i}\rho^{i}\right)\nabla\cdot\mathbf{v}^{s}+\nabla\cdot\left(\varepsilon S_{l}\rho^{lw}\mathbf{v}^{ls}\right)=0.\end{aligned} \tag{16}$$

where ρ^{lw} denotes the mass concentration of species w in phase l.

As discussed above and also done by Eriksson et al. [24], both diffusive and advective transport of the gas phase is omitted in the model. Moreover, the density of the gas is assumed to remain constant. Based on these assumptions, the following mass balance of the gas phase can be obtained

$$S_{g}\rho^{g}\frac{D^{s}\varepsilon}{Dt}+\varepsilon\rho^{g}\frac{D^{s}S_{g}}{Dt}+\varepsilon S_{g}\rho^{g}\nabla\cdot\mathbf{v}^{s}=-\frac{M^{l}_{\mathrm{ap}}}{\rho^{i}}\rho^{g}. \tag{17}$$

where M^{l}_{ap} denotes a sink or source term accounting for the mass of gas that is either replaced by expelled supercooled liquid that is transported to the air voids during freezing or the release of gas in the air voids when ice is melting and the liquid phase is transported elsewhere in the material. The assumption of a constant gas density means also that the gas pressure inside the air voids is assumed to remain constant. Therefore, this suggests that the gas phase is enclosed into the ice that is formed inside the air voids during freezing and then released during melting. If water is sucked into the concrete from an external reservoir and accumulated during repeated freeze-thaw cycles, the assumption of constant gas pressure also implies that an equivalent volume of gas must be transported out of the material. As mentioned, this transport is, however, not explicitly included in the developed model.

For the solid phase, one obtains the following mass balance

$$\frac{D^{s}\varepsilon}{Dt}=\frac{(1-\varepsilon)}{\rho^{s}}\frac{D^{s}\rho^{s}}{Dt}+(1-\varepsilon)\nabla\cdot\mathbf{v}^{s} \tag{18}$$

where $(1-\varepsilon)$ corresponds to the volume fraction of the solid phase η^{s}.

The energy balance for the whole porous medium is obtained by summing the contributions from each considered phase and can be written as

$$\left(\rho C_{p}\right)_{\mathrm{eff}}\frac{D^{s}T}{Dt}=-\nabla\cdot\mathbf{q}-\left(\varepsilon S_{l}\rho^{l}C_{p}^{l}\mathbf{v}^{ls}\right)\cdot\nabla T+\varepsilon\rho^{i}\Delta H\frac{D^{s}S_{i}}{Dt}. \tag{19}$$

In the equation, T is the temperature, $\mathbf{q}$ denotes the conductive heat flux, which is described by Fourier's law, and $\Delta H=333\,\mathrm{kJ/kg}$ is the latent heat of fusion. The term $(\rho C_p)_{\mathrm{eff}}$ corresponds to the effective heat content and is defined as

$$\left(\rho C_{p}\right)_{\mathrm{eff}}=(1-\varepsilon)\rho^{s}C_{p}^{s}+\varepsilon S_{l}\rho^{l}C_{p}^{l}+\varepsilon S_{i}\rho^{i}C_{p}^{i}+\varepsilon S_{g}\rho^{g}C_{p}^{g} \tag{20}$$

where C_p^{α} is the specific heat capacity of phase α.

The linear momentum balance for the whole medium is derived in the same way as the energy balance, and can be written as

$$\nabla\cdot\mathbf{t}-\rho\mathbf{g}=0 \tag{21}$$

where $\mathbf{t}$ denotes the total stress tensor, $\mathbf{g}$ is the gravitational acceleration vector and ρ is the volume averaged density of the porous medium, given by

$$\rho=(1-\varepsilon)\rho^{s}+\varepsilon S_{l}\rho^{l}+\varepsilon S_{i}\rho^{i}+\varepsilon S_{g}\rho^{g}. \tag{22}$$

A choice of primary variables must be made for the set of governing equations presented above to describe the state of the material. In this study, the concentration of dissolved salt c^{Sa}, water pressure p^{l}, degree of gas saturation S_g, temperature T and displacement vector $\mathbf{d}$ have been chosen. Furthermore, it is also necessary to introduce additional variables for the two approaches discussed in Section 2 to describe the freeze-thaw hysteresis. For the equilibrium approach, an internal variable r_p^{min} is defined that keeps track of the minimum pore size reached in each freeze-thaw cycle, which then can be used in Eq. (9) to determine v_i. In the non-equilibrium approach, however, v_i is used as a state variable, and it is determined by the relationships defined in Eqs. (7) and (10). Additionally, there are more unknowns in the set of equations that must be defined, either directly as physical constants or by using constitutive relationships to relate them to the primary variables.

4. Constitutive relationships

In addition to the relationships described in Section 2, the most important remaining constitutive relationships used in this study to model the freeze-thaw behavior of air-entrained concrete that contains a saline solution are presented in the following. It should be noted that for many of the relationships, there exists several other versions in the literature that could also be applied. However, the relationships used herein have been successfully used in similar previously published models, although not all necessarily aimed to describe the freeze-thaw behavior.

4.1. Mass transport

Because of the freezing and thawing of the liquid phase inside the concrete material, hydraulic pressure gradients arise and causes a flow of the unfrozen liquid through the porous network. This flux can be quantified through the generalized Darcy's law [19,21,46], by which the relative velocity of the liquid phase can be expressed as

$$\varepsilon S_l \mathbf{v}^{ls} = -\frac{k_r^l \mathbf{k}}{\mu^l}\left(\nabla p^l - \rho^l \mathbf{g}\right) \tag{23}$$

where μ^l denotes the dynamic viscosity of the liquid, $\mathbf{k}$ is the intrinsic permeability tensor whereas k_r^l is the relative permeability. The latter parameter takes into that the effective permeability is influenced by the presence of other phases in the porous network. In this study, the relationship proposed by van Genuchten [47] is used to describe the variation of k_r^l, which has also been used in previously published freeze-thaw models by, e.g., Koniorczyk et al. [19], Gong and Jacobsen [26], and can be written as

$$k_r^l = \sqrt{S_l}\left[1 - \left(1 - S_l^{(1/m)}\right)^m\right]^2. \tag{24}$$

The parameter m is a model parameter which usually varies between 0.42 and 0.57 and is determined through fitting of experimental data [26,32].

It is well-known that the presence of an adequately distributed air void system in concrete has a beneficial effect on the frost resistance. According to Powers' hydraulic pressure theory [48], this is because the hydraulic pressure that arises due to the volume expansion of the liquid during freezing is reduced since the air voids can act as reservoirs for the expelled liquid. Moreover, the air pressure inside empty or partially saturated air voids can usually be assumed to be equal to the atmospheric pressure. Hence, ice crystals that grow and bulge into these air voids are subjected to the same pressure level. Consequently, to maintain the thermodynamic equilibrium between the phases in the vicinity of the air voids in a material that is at least capillary saturated, the liquid phase must be depressurized below the atmospheric pressure. In the literature, this negative liquid pressure is commonly called the cryo-suction pressure, and it will also influence the local flow of unfrozen supercooled liquid in connection to the air voids when the material is subjected to freezing conditions [3,22,32]. Furthermore, already in the 1950s, Powers and Helmuth [49] observed that partially saturated air-entrained concrete contracts more than the pure thermal contraction of the material when frozen. The under-pressure in the pore liquid is also believed to be the cause of this observed phenomenon [3,21,22]. To quantify the local flow of the liquid phase in connection to the air voids, a relationship proposed by Eriksson et al. [24] is adopted for the source term M_{ap}^l appearing in Eq. (17). This relationship is based on the model proposed by Powers [50] to define his spacing factor. Moreover, it considers both the aforementioned pressure contributions and assumes a linear pressure gradient on the local scale. Using the notations in this study, the relationship can be written as

$$M_{ap}^l = \frac{\rho^l \mathbf{k} k_r^l \left(p^l - p_{ap}^l\right)}{\mu^l (La/9 + 0.5) L^2} \tag{25}$$

where L denotes Powers' spacing factor, a is the specific surface area of the air voids and p_{ap}^l corresponds to the cryo-suction pressure in the vicinity of the air voids. The magnitude of p_{ap}^l can be obtained by combining Eqs. (2) and (3) as well as recalling that ice crystals growing into air voids are under atmospheric pressure

$$p_{ap}^l = -\frac{2\gamma_{li}}{r_{eq}} + p_0. \tag{26}$$

The values of L and a are given by the size distribution of the air void system and its current degree of saturation. As the degree of saturation in the air void system increases, the value of L also increases and rapidly approaches ∞ when the air voids start to reach full saturation [1]. Consequently, when the air void system is fully saturated in the model, M_{ap}^l has a value close to 0 according to the expression in Eq. (25), and there is no beneficial influence of the air void system in the model at this state. A thorough description of how to determine L and a is given by Eriksson et al. [24]. It should be noted, however, that the following frequency function proposed by Snyder [51] is used throughout this study to represent the air void size distribution

$$f(r) = \frac{exp\left(-\frac{ln(r/r_0)^2}{2\sigma_0^2}\right)}{\sqrt{2\pi}\sigma_0 r_0 exp(\sigma_0^2/2)} \tag{27}$$

where σ_0 and r_0 are two model parameters used for fitting measured data. In the study by Eriksson et al. [24], only freezing was considered, and hence it is necessary to assume an appropriate behavior of M_{ap}^l during the thawing part of a cycle. Gong and Jacobsen [26] used a similar approach to account for the effect of air voids in capillary saturated concrete but subjected to full freeze-thaw cycles. The only difference in their definition of the local flow is that they do not require a linear pressure gradient on the local scale. The supercooled liquid entering the air voids under freezing conditions phase changes almost immediately [22]. However, Gong and Jacobsen [26] assumed the local flow of liquid to be active during both the freezing and thawing part of a loop, thus allowing supercooled liquid to flow both towards and from the air voids under freezing conditions. Simulations performed in the study by Gong and Jacobsen [26] do, though, indicate that this assumption gives reliable results that show good agreement with measurements. Therefore, the same assumption for M_{ap}^l is also adopted in this study.

Based on the above and the requirement in the model of at least capillary saturation in the material, the degree of ice saturation is in this study defined as

$$S_i = v_i \Big/ \varepsilon + \left(\frac{\varepsilon_{ap}}{\varepsilon} - S_g\right) \cdot (v_i > 0) \tag{28}$$

where ε_{ap} is the volume fraction of air voids and $(v_i > 0)$ denotes a boolean expression. The last term on the RHS corresponds to ice in the air voids, which is assumed to form or melt when this occurs in the largest capillary pores. This assumption is consistent with the work by Eriksson et al. [24], and also means that v_i describes the volume fraction of ice in the gel and capillary pores, which are defined as all pores having a radius <10 μm [52].

The diffusive mass flux of dissolved salt through the liquid phase is described by Fick's first law of diffusion and can be expressed as

$$\mathbf{J}^{Sa} = \varepsilon S_l \rho^{lSa} \mathbf{u}^{Sa} = -\rho^l \mathbf{D}_d^{Sa} \nabla \frac{\rho^{lSa}}{\rho^l} \tag{29}$$

where $\mathbf{D}_d^{Sa}$ denotes the diffusivity tensor. Following the work by Lin et al.

[53], the diffusivity of chloride ions through a partially saturated pore network can be defined by adopting a multi-factor law to account for the effect of temperature and S_l on the diffusive transport, see also e.g. [54,55]. Moreover, and as also done by Valenza and Scherer [3], it is assumed that the diffusivity of sodium and chloride ions are similar. Based on this, the diffusivity tensor for dissolved NaCl can be written as

$$\mathbf{D}_{\mathrm{d}}^{Sa} = \varepsilon D_{\mathrm{d},0}^{Sa} S_l^n exp\left[\frac{U}{R}\left(\frac{1}{T_0}-\frac{1}{T}\right)\right]\mathbf{I} \tag{30}$$

where $D_{\mathrm{d},0}^{Sa}$ denotes a reference diffusion coefficient, n is a model parameter, T_0 is a reference temperature, U=35 kJ/mol [55] is the activation energy of the diffusion process and $\mathbf{I}$ is a unity tensor.

4.2. Mechanical behavior

The solid phase is in this study assumed to behave as an isotropic linear elastic material with the strains remaining small. Using Hooke's law to describe the effective stress in the solid phase and also accounting for thermal strains, the total stress tensor in Eq. (21) can be expressed as

$$\mathbf{t} = \mathbb{D}_{\mathrm{e}} : (\mathbf{e} - \mathbf{e}_{\mathrm{th}}) - bp^s\mathbf{I} \tag{31}$$

where $\mathbb{D}_{\mathrm{e}}$ is a fourth-order elasticity tensor, $\mathbf{e}$ is the total strain tensor and $\mathbf{e}_{\mathrm{th}}$ is the thermal strain tensor. The parameter b denotes Biot's coefficient and is defined as $b = 1 - (K_T/K^s)$, where K^s and K_T are the bulk modulus of the solid skeleton and the drained material, respectively. The thermal strains are governed by the volumetric thermal expansion coefficient of the porous medium, which should consider the contributions from both the solid phase and the current degree of ice saturation in the pores [38]. In this study, a volume averaging approach used by Fridh [4], and similar to the expression used by Sun and Scherer [38], is adopted to define the thermal expansion coefficient on the following form

$$\alpha = \frac{\alpha^s K^s(1-\varepsilon) + \alpha^i K^i S_i \varepsilon}{K^s(1-\varepsilon) + K^i S_i \varepsilon} \tag{32}$$

where α^{π} and K^{π} denotes the volumetric thermal expansion coefficient and bulk modulus of phase π, respectively. The pressure p^s in Eq. (31) corresponds to the average internal pressure on the pore walls and is governed by the pressures in the phases that currently occupy the material. Eriksson et al. [24] proposed a relationship for p^s in air-entrained concrete with an empty or partially saturated air void system by adopting a volume averaging procedure from the work by Zuber and Marchand [20,21] that utilizes the size distribution of the pore system. This relationship is used in this study also and can be written as

$$p^s = \frac{1}{\varepsilon}\left[\int_{r_p}^{0} p^l \frac{dv(r)}{dr}dr + \int_{r_{\mathrm{sat}}^a}^{r_p} p_{\mathrm{wall}}^i \frac{dv(r)}{dr}dr\right] \tag{33}$$

where r_{sat}^a corresponds to the size of the largest fully saturated air voids and $v(r)$ denotes a cumulative size distribution of the pore system, i.e. the cumulative volume fraction of pore space as a function of the pore size r. The pressure p_{wall}^i denotes the pressure exerted on the pore walls by the presence of ice crystals inside the pores. In a single frozen pore, the pressure can, according to, e.g., Scherer [31], be expressed as

$$p_{\mathrm{wall}}^i = p^l + \gamma_{li}(\kappa_{\mathrm{e}} - \kappa_{\mathrm{b}}) \tag{34}$$

where κ_{e} and κ_{b} are the curvatures of the crystal at the pore entry and inside the pore body, respectively. The magnitude of the pressure, thus, depends on the shape of the pores, which can be described by the pore shape factor λ_p defined in Eq. (8) [33]. During ice formation, the ice propagates into smaller pores as the temperature decreases and r_p in Eq. (33) corresponds to the size of the pore entry at the ice front. As described by Sun and Scherer [38], the pressure on the walls in each pore containing ice is governed by the difference in curvature between the ice front and the curvature of the crystals inside the pore body. Assuming the ice-liquid interface at the ice front to be hemispherical and using the definition of λ_p to express the curvature inside the pores as $\kappa_{\mathrm{b}} = \lambda_p\kappa_{\mathrm{e}}$, the pressure in each pore can, using Eq. (34), be written as

$$p_{\mathrm{wall}}^i = p^l + \gamma_{li}\left(\frac{2}{r_p-\delta} - \lambda_p(r)\frac{2}{r-\delta}\right) \tag{35}$$

where r denotes the size of the pore entry and $\lambda_p(r)$, e.g., can be evaluated from low-temperature calorimetry measurements [38].

The effect of the cryo-suction pressure p_{ap}^l, defined in Eq. (26), on p^s is included through the liquid phase pressure p^l, which is one of the chosen primary variables of the governing mass balance equations given in Section 3. The mass balances include the source term M_{ap}^l, which describes the local flow of the liquid phase in connection to the air voids and depends on p^l and p_{ap}^l. Therefore, when solving the system of the coupled governing equations of the model, p^l is dependent on p_{ap}^l, and thus also the pressure p^s is influenced by the cryo-suction of the air voids through Eq. (33). As thoroughly described in the study by Eriksson et al. [24], by including the cryo-suction pressure using this approach, the response of air-entrained concrete can be modeled on the structural scale. In other models proposed in the literature, modeling of the response of partially saturated air-entrained concrete is often limited to the microscale through studying single air voids, see e.g. [21,22,25].

4.3. Equations of state

The dependence of the liquid phase density on T, p^l and c^{Sa} is described by adopting an expression given by Zeng [56]

$$\rho^l = \rho_0^l\left[1 - \alpha^l\left(T - T_0\right) + \frac{(p^l - p_0^l)}{K^l}\right] + \left(M_{Sa} - \rho_0^{lw}V_{\phi}\right)\left(c^{Sa} - c_0^{Sa}\right) \tag{36}$$

where p_0^l and p_0^{lw} are the reference densities of the liquid phase l and the pure water species w in phase l at the reference state (T_0, p_0^l, c_0^{Sa}), respectively, and V_{ϕ} denotes the apparent molar volume of the salt. Moreover, since the species Sa and w occupy the same volume inside the porous medium, the definition $\rho^l = \rho^{lw} + \rho^{lSa}$ can also be introduced [56].

The ice and solid phase densities are defined on an equivalent form

$$\rho^i = \rho_0^i\left[1 - \alpha^i\left(T - T_0\right) + \frac{1}{K^i}\left(p^i - p_0^i\right)\right] \tag{37}$$

$$\rho^s = \rho_0^s\left[1 - \alpha^s\left(T - T_0\right) + \frac{1}{K^s}p^s + \frac{1}{3\eta^s K^s}I_1^s\right] \tag{38}$$

where I_1^s is the first invariant of the effective stress tensor [44]. An expression for the pressure in the ice phase can be obtained by combining Eqs. (2) and (3), which yields $p^i = p^l + 2\gamma_{li}/r_{\mathrm{eq}}$, see e.g. [20,21].

5. Numerical examples

Two different examples are solved using the proposed model. The purpose of the first one is to verify that the model is capable of capturing observed behavior of air-entrained concrete subjected to freezing temperatures and partially saturated with saline solutions of different concentrations. To this end, an experiment performed by Fridh [4] is simulated in which the longitudinal deformations of concrete specimens subjected to a freeze-thaw cycle were measured. The specimens had been partially pre-saturated with either water or a NaCl-solution. The experiment is simulated using both the equilibrium and the non-equilibrium approach for the ice formation described in Section 2. The second example aims to investigate the influence of different concentrations of dissolved salt in an external reservoir on the absorbed volume

of liquid into air-entrained concrete during repeated exposure to freeze-thaw cycles.

The system of governing equations presented in the previous sections are solved numically using the commercial FE-code Comsol Multiphysics [57]. The implementation follows standard procedures of the finite element method (FEM), see e.g. [58], where the model equations first are converted into weak form and Green's first identity is used to reduce the order of differentiation. The discreatized equation system is then obtained by the standard Galerkin method.

5.1. Example 1: freeze-thaw behavior of concrete containing NaCl-solutions

Fridh [4] presented results from a large number of experiments related to the freeze-thaw behavior of different concretes subjected to various conditions. In this verification example, one of the performed experiments is simulated, which aimed to investigate the influence of dissolved NaCl in the pore liquid. The considered experiment was performed on air-entrained concrete with a water-cement ratio (w/c) of 0.6 and an air void content of 6%. The specimens had a prismatic shape with the dimensions 20 × 20 × 170 mm. All tested specimens were partially pre-saturated by storing them in baths containing lime-saturated water or a NaCl-solution with a concentration of 2%, 4.5%, or 11% by weight for approximately 4.5 years. Two specimens of each type were prepared and tested. To maintain the moisture state in the specimens during testing, they were sealed by wrapping them in plastic foil. All specimens were mounted in a measuring frame and placed in a climate chamber where the air temperature was changed with a rate of 3.6 °C/h. The complete freeze-thaw cycle had a duration of 24 h and is shown in Fig. 6. Furthermore, the degree of liquid saturation was measured and found to be approximately 0.88 in all specimens except for the two stored in a 4.5% NaCl-solution. Those two were more or less fully saturated, and consequently, the measured deformations significantly deviated from the other specimens showing a substantial expansion instead of contraction. Since the aim of this example is to investigate the influence of the presence of dissolved salt on the behavior during a freeze-thaw cycle, the 4.5% specimens are omitted in the simulations.

The specimens are discretized with 750 quadrilateral elements, and a plane stress formulation is used to calculate the deformations. For the displacement and temperature fields, the boundary conditions are applied as Dirichlet conditions. However, concerning the liquid pressure, a boundary flux for the pure water defined as $q^{lw} = \rho_{\infty}^{lw}\beta_l(p^l - \rho_{\infty}^l)$ is applied, where ρ_{∞}^l corresponds to the pressure in the climate chamber and is assumed to remain at 1 atm throughout the freeze-thaw cycle. Since the specimens are frozen in air, the transfer coefficient β_l should be defined so that water can be transported out of the model domain but not be absorbed. Hence, β_l is set to ∞ when $p^l \geq \rho_{\infty}^l$ and to 0 if $p^l < \rho_{\infty}^l$ [24]. Because the pure water can only be transported outwards, the parameter ρ_{∞}^{lw} here denotes the mass concentration of pure water at the boundary inside the specimens. Due to the ambient conditions in the experimental setup, there is no diffusive flux of dissolved salt over the boundary. The convective flux should, though, be considered and is applied using the same type of boundary condition as for the pure water species. The convective boundary flux of salt is defined as $q^{lSa} = \rho_{\infty}^{lSa}\beta_l(p^l - \rho_{\infty}^l)$, where ρ_{∞}^{lSa} denotes the mass concentration of salt at the boundary inside the specimens. The initial values of p^l and S_g are set to 1 atm and 0.12, respectively, where the latter corresponds to the S_w obtained after the preconditioning procedure of the specimens described above. The corresponding initial concentrations, c^{Sa}, of dissolved NaCl in the pore solution for the three considered cases are 0, 350 and 2030 mol/m^3. The initial temperature is set to 19°C, which corresponds to the start temperature of the applied freeze-thaw cycle, see also Fig. 6. The dimensions of the specimens and applied boundary conditions are also shown in Fig. 3. Moreover, it should be noted that the influence of the cryo-suction pressure from the air voids is introduced through the source term M_{ap}^l in the model proposed in this study. A more thorough description of this is given in Section 4.2.

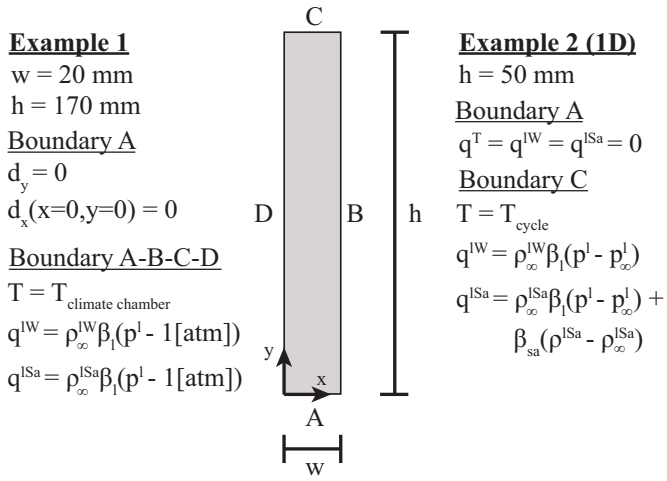

Fig. 3. Geometry and applied boundary conditions in Examples 1 and 2.

In the study by Fridh [4], low-temperature calorimetry was used to measure the amount of ice as a function of temperature inside the concrete during both freezing and thawing. This data can be utilized to obtain some of the required input for both the equilibrium and the non-equilibrium approach described in Section 2 to model the ice formation. Following the methods outlined by, e.g., Sun and Scherer [33] and Wu and Johannesson [40], the measurement data can be converted to describe the ice content as functions of the size of the pore entries (freezing) or the interior of the pores (thawing). By considering the thickness of the unfrozen layer δ, the amount of ice can instead be converted into a corresponding pore volume, hence yielding a cumulative pore size distribution. To model the formation and melting of ice following the equilibrium approach, see Eq. (9), the latter step is not required since v_i^{fr} and v_i^{me} are given directly by the first step. The two functions used in the simulations are shown in Fig. 4 and were obtained from the measurement data based on the assumption of spherically shaped pores [33]. To determine the pressure term Δp_{fr} in the non-equilibrium approach, the obtained function v_i^{fr} is used together with Eq. (2) in the current study. Furthermore, the pore shape factor λ_p is determined directly from the data presented by Fridh [4] through the use of Eq. (8). Both these functions are plotted in Fig. 5. As described in Section 4.1, it should be noted that the ice content given by these relationships corresponds to the ice in the capillary pores of the developed model. The size distribution of the air void system was also measured, and Powers' spacing factor was determined equal to 160 μm. It should be noted that Fridh [4] also characterized the material by measuring several other properties. Some of these and all other relevant input parameters and properties used in this example are summarized in Table 1.

The longitudinal deformations obtained from the simulations using both the equilibrium and the non-equilibrium approach are shown in Fig. 6, together with the experimental results from Fridh [4]. As can be observed in the figure, the strains obtained in the simulations replicate the experimental observations both during the freezing and thawing part of the temperature cycle rather well. In the experiments, the liquid phase is subjected to some supercooling before the ice starts to nucleate, which is indicated by the bumps in the graphs around 6 h. The supercooling is, however, not considered in the current simulations, and hence the numerical results show a smoother behavior around the points of nucleation. After these points, the compliance between the simulation and the measurement results is very good, where an increased concentration of NaCl results in less contraction of the specimens. During the part of the cycle where the temperature is held constant at −23 °C, the simulations,

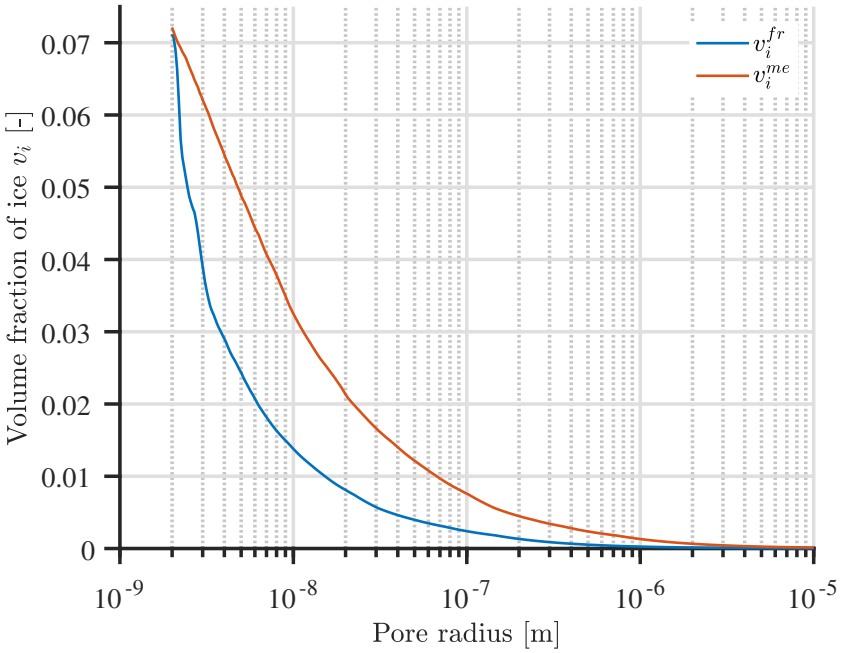

Fig. 4. Volume fraction of ice in capillary pores during freezing and thawing as function of r_p obtained from low-temperature calorimetry measurements performed by Fridh [4] and used as input in the simulations based on the equilibrium approach.

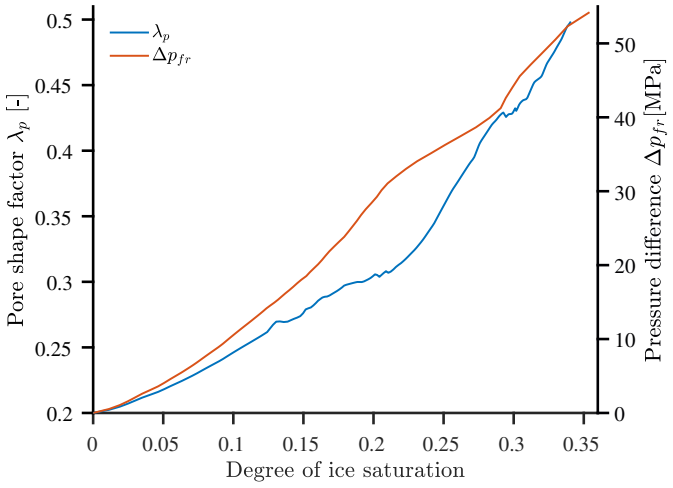

Fig. 5. Pore shape factor λ_p and pressure difference Δp_{fr} as function of the degree of ice saturation in the capillary pores obtained from the measurement results presented by Fridh [4], and used as input data for the simulations based on the non-equilibrium approach.

however, show a bit larger contraction than the experiments. There are several possible explanations for this, e.g., uncertainties regarding the initial state of the specimens (e.g., initial T and S_w) and in the input data. During this part of the temperature cycle, the experimental results also show a significantly larger scatter between the two specimens containing water than in the other two studied cases. Regardless of these differences, the general trends observed in the experiments are captured by the simulations, where samples containing a small concentration of NaCl or water show a larger contraction. The model also captures the slight continued contraction of the specimens when the temperature is held constant. According to the simulations, the primary reason for the smaller contraction obtained for specimens containing NaCl is the magnitude of the cryo-suction pressure p_{ap}^l. With an increasing salt concentration, the magnitude of p_{ap}^l is decreasing, and the specimens contract less. The total observed strains in the simulations are, of course, also affected by the other contributions in the model, e.g. the thermal strains and the pressure from ice crystals, but the main cause of the smaller contraction is the effect of dissolved salt on p_{ap}^l. During the thawing phase of the cycle, the agreement between the simulations and the experimental results increases again. It should be noticed that similar experimental observations, as reported by Fridh [4] concerning the effect of dissolved salt in the pore liquid on the freeze-thaw deformations, have also been reported elsewhere, see, e.g., Liu and Hansen [15,29]. Although the simulations do not match the experiments perfectly, the results demonstrate that the model is capable of reproducing the overall mechanical response of specimens containing water or NaCl-solutions of different concentrations. If one considers the uncertainties regarding some of the material properties and typical sensitivities in experimental measurements, the agreement between the experiments and the simulations must be considered as satisfactory. Furthermore, the physical parameters of the liquid phase generally depend on the current salt concentration, e.g. the dynamic viscosity, heat capacity, thermal expansion coefficient and density. However, as can be noted in Table 1, the influence of the salt concentration on the physical parameters was not considered in the current formulation of the model except for the liquid phase density, see Eq. (36). For example, a higher viscosity caused by an increasing salt concentration may induce higher pressures in the material and also a slower pressure relaxation. Hence, to improve the accuracy and applicability of the model further, future extensions of the model formulation should aim to add the influence of varying salt concentration also on the other physical parameters, where, e.g., the work presented by Zeng [56] can be used as a basis.

Comparing the deformations obtained by the equilibrium and the non-equilibrium approach for the ice formation, it can be concluded that they yield almost identical results in the current example. As mentioned earlier in Section 2, the motivation of using a non-equilibrium approach is that it more physically correct describes the process of ice formation, especially if the rate of freezing is not sufficiently low [19]. In addition to the deformation plots, the volume fraction of ice in the capillary pores obtained by the two approaches as a function of the temperature in the midpoint of the specimens is shown in Fig. 7. As can be observed, there

Table 1
Input parameters used in the two numerical examples. The parameters are based on the data presented by Fridh [4], but additional references are given in the parameter column where necessary. Note that θ denotes the temperature in °C.

Parameter	Notation	Unit	Value
Total porosity	ε	–	0.22
Air void porosity	ε_{ap}	–	0.06
Water-ice surface energy [35]	γ_{li}	N/m	0.0409
Entropy of fusion of ice [35]	$\mathscr{S}_f$	MPa/K	1.2
Characteristic times for freezing and melting [30]	τ_{fr}, τ_{me}	s	60, 15
Young's modulus	E	GPa	30.5
Poisson's ratio	ν	–	0.2
Bulk modulus of drained material	K_T	GPa	$E/[3(1-2\nu)] = 16.9$
Bulk modulus of s [38]	K^s	GPa	$K_T\frac{(1+\varepsilon)}{(1-\varepsilon)} = 26.4$
Bulk modulus of l, i [59]	K^α	GPa	2.2, 8.3
Volumetric thermal expansion of s	α^s	1/K	$36.5 \cdot 10^{-6}$
Volumetric thermal expansion of l [60]	α^l	1/K	$(-9.2 + 2.07\theta) \cdot 10^{-5}$
Volumetric thermal expansion of i [61]	α^i	1/K	$157.6 \cdot 10^{-6} + 0.5556 \cdot 10^{-6}\theta + 2.655 \cdot 10^{-8}\theta^2 + 7.11 \cdot 10^{-10}\theta^3$
Thermal conductivity of s [62], l, i, g [59]	λ^α	W/m·K	1.2, 0.56, 2.16, 0.024
Heat capacity of s [63], l [64], i, g [59]	C_p^α	J/kg·K	740, 4210, 2110, 1006
Density of s [4], i, g [59]	p_0^α	kg/m^3	2650, 917, 1.2
Reference density of l: 0%, 1–6%, 11% NaCl [65]	p_0^l	kg/m^3	998.4, 1005.3, 1012.4, 1019.7, 1026.9, 1034.2, 1041.5, 1078.5
Apparent molar volume of NaCl [28]	V_ϕ	ml/mol	$13.072 + 0.287\theta - 0.922 \cdot 10^{-2}\theta^2 - 1.991 \cdot 10^{-4}\theta^3$–$2.226 \cdot 10^{-6}\theta^4 + 6.321 \cdot 10^{-7}\theta^5$
Parameter m in Eq. (24)	m	–	0.55
Intrinsic permeability [21]	k	m^2	$3.55\varepsilon^{3.6} \cdot 10^{-18} = 1.5 \cdot 10^{-20}$
Dynamic viscosity of l [66]	μ^l	Pa·s	$4.601{\cdot}10^{-8} exp\left(\frac{3068.6}{\theta+123.15} - \frac{3.3775{\cdot}10^5}{(\theta+123.15)^2} + \frac{1.4781{\cdot}10^7}{(\theta+123.15)^3}\right)$
Reference diffusion coefficient [67]	$D_{d,0}^{Sa}$	m^2/s	$2.17 \cdot 10^{-12} \exp((w/c)/0.279) = 1.9 \cdot 10^{-11}$
Air void size distribution $L = 160\,\mu m$	–	–	$r_0 = 0.035\ \mu m$, $\sigma_0 = 1.52$

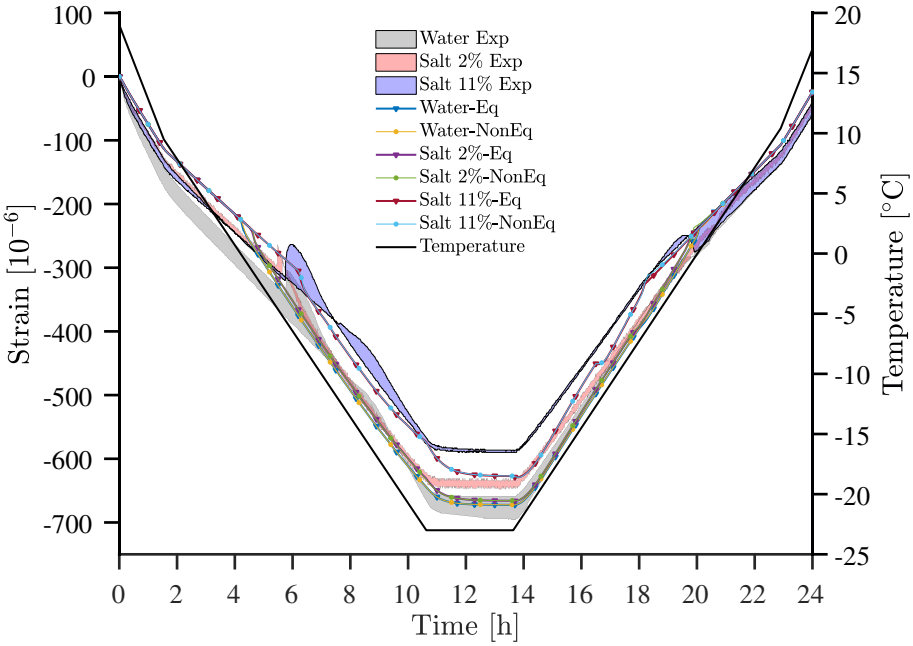

Fig. 6. Comparison of longitudinal deformations obtained from the simulations with the measurements performed by Fridh [4], together with the temperature cycle in the climate chamber. In the legend, Exp denotes experimental results whereas Eq and NonEq corresponds to simulation results using the equilibrium and the non-equilibrium approach, respectively.

are no major differences between the obtained results, but some additional ice is formed when using the equilibrium approach for the specimens containing water and 2% NaCl. Based on the findings in this example, it seems that a freezing rate of 3.6 °C/h is sufficiently small to use either of the two approaches. According to Fagerlund [68], a normal rate of freezing in northern Europe is typically below 3 °C/h, and hence it should be possible to use either approach also in real-world applications. As discussed and investigated by Koniorczyk et al. [19] and Gawin et al. [30], the ice formation in the non-equilibrium model is affected by the characteristic times τ_{fr} and τ_{me}. It should, thus, be noted that the values used in this example correspond to the typical values used in the study by Gawin et al. [30]. They do, however, also mention other benefits with the non-equilibrium approach such as less tendencies of numerical instability, which of course is also an important aspect to consider although no such issues were encountered in this example.

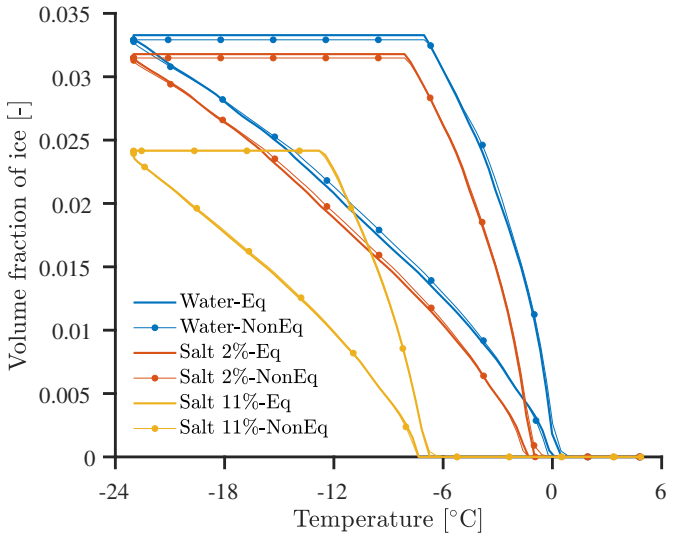

Fig. 7. Comparison of ice content in the capillary pores as a function of temperature from the simulations using the equilibrium (Eq) and non-equilibrium (NonEq) approach.

5.2. Example 2: absorption of liquid

The second example aims to investigate the absorption of liquid into air-entrained concrete from an external reservoir containing different concentrations of dissolved NaCl. The primary purpose is to study the influence of the salt on the absorbed volume of liquid when the material is subjected to repeated freezethaw cycles. The same concrete material as in Example 1 is also studied in this example, but here the concrete is assumed to be initially capillary saturated with pure water in all studied cases. In addition to the case where the reservoir contains pure water, the concentration of NaCl is varied between 1 and 6% by weight in the reservoir. A total of 40 freeze-thaw cycles are applied in each simulation, where each applied temperature cycle follows the one used in Example 1. All simulations are performed using the equilibrium approach to describe the ice formation.

The setup of the model in this example is inspired by the work performed by Gong and Jacobsen [26], who simulated the absorption of pure water into air-entrained concrete due to cyclic freeze-thaw conditions using a one-dimensional modeling approach. They also performed a thorough sensitivity analysis of some important parameters, which mostly also applies to cases involving dissolved salt. In this example, the reservoir of liquid is located on a single boundary surface, which is also subjected to the temperature cycle. This type of external wet frost exposure on concrete surfaces is common in cold regions, and especially in combination with salts since they are used as deicers on, e.g., roads and bridges. A one-dimensional model is also employed herein, which means that it could, e.g., represent a vertical strip in a roadway or a specimen where all sides in the length-direction are moisture sealed and heat insulated. The length of the specimens is set to 50 mm. On the boundary opposite to the exposure surface, adiabatic conditions are applied, and it is also assumed to be moisture sealed. The temperature cycles are applied using Dirichlet conditions on the exposure surface, whereas p^l and c^{Sa} are prescribed by applying fluxes through the use of mixed-type boundary conditions. For the pure water species, this means a similar formulation as in Example 1, but in this example, ρ_∞^{lw} denotes the mass concentration in the reservoir. Because of the reservoir, the total flux of the salt species over the boundary should also take the diffusive transport into account and is, thus, defined as $q^{lSa} = \rho_\infty^{lSa}\beta_l(p^l - \rho_\infty^l) + \beta_{Sa}(\rho^{lSa} - \rho_\infty^{lSa})$. The first term on the RHS corresponds to the convective flux of salt and the second term to the diffusive flux, where ρ_∞^{lSa} is the mass concentration in the reservoir and β_{Sa} is a transfer coefficient over the boundary. In addition to varying the NaCl-concentration in the reservoir, two different conditions for the mass fluxes over the boundary are also studied. In the first condition type, denoted CB (Closed Boundary) in the following, the flux of liquid is assumed to stop when the temperature on the boundary reaches the freezing temperature of the solution corresponding to its initial NaCl-concentration. This condition, thus, implies that all liquid in the reservoir is assumed to phase change into ice. Therefore, the values of β_l and β_{Sa} is set to 0 when there is ice on the surface and to ∞ otherwise. However, as discussed earlier, salt ions are generally not incorporated into ice crystals, and thus there might remain a solution on the surface with a higher concentration of NaCl that can be absorbed by the concrete under freezing conditions [29]. To model these open surface conditions, henceforth denoted OB (Open Boundary), the values of β_l and β_{Sa} are set to ∞. The current mass concentration ρ_∞^{lSa} of the remaining saline solution in the reservoir can be determined from the liquidus curve in the phase diagram for NaCl-solutions by using the lever rule [3]. Since the remaining solution in the reservoir is in contact with the formed ice on the surface, the pressure ρ_∞^l in the reservoir corresponds to a cryo-suction pressure on the surface given by Eq. (26), see e.g. [3,38]. The applied boundary conditions and dimensions used in this example are also summarized in Fig. 3.

Fig. 8 shows the volume of absorbed liquid over the exposure surface into the specimens after each freeze-thaw cycle and for all analyzed cases. For the case with pure water, only the CB conditions have been analyzed since all the water in the reservoir should freeze at the same temperature. Gong and Jacobsen [26] also performed simulations for this type of conditions and additionally complied results from a number of experiments where the absorbed volume of water had been measured. For a similar material and freezing rate as studied herein, the measurements showed an absorption rate of $0.69 \cdot 10^{-9}$m/s whereas their simulation gave a rate of $0.24 \cdot 10^{-9}$m/s. Calculating the corresponding rate based on the current results yields a value of $0.23 \cdot 10^{-9}$m/s, which indicates that the developed model in this study is also capable of describing the freeze-thaw induced absorption of water. The results also show that the absorbed volume of liquid increases with a higher concentration of NaCl in the reservoir regardless of the applied boundary condition type. For the CB conditions, the larger absorbed volume is primarily a result of the reservoir being open for longer durations in the freeze-thaw cycles. Furthermore, the internal parts that contain less or

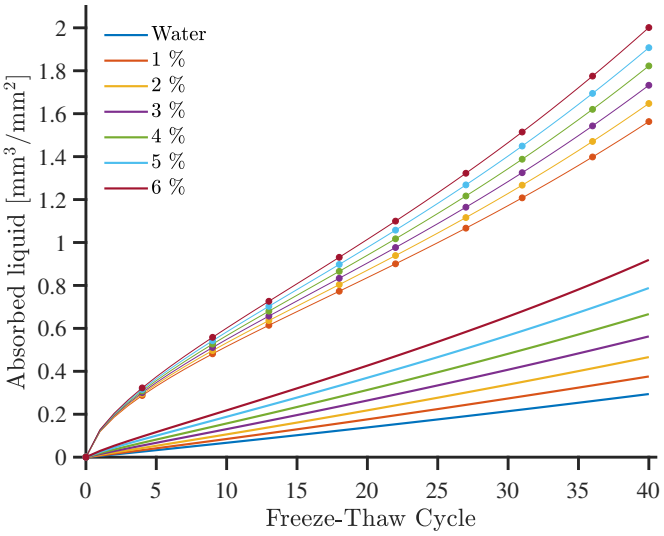

Fig. 8. Volume of liquid absorbed over the exposure surface in all analyzed cases in Example 2. Lines without markers show the results for CB conditions, while lines with markers correspond to the cases with OB conditions. Note that the absorbed volume is expressed as mm^3 per mm^2 concrete in contact with the reservoir.

no NaCl will freeze and melt at higher temperatures, thereby contributing to an increased suction of the liquid into the material while the reservoir is unfrozen. However, and as can be expected, applying the OB conditions results in more liquid being absorbed by the specimens because they always have access to the reservoir. The increasing absorption with a higher concentration of NaCl in the reservoir is mainly because a larger pressure gradient arises in the specimens as the concentration increases. Another contributing factor is that the effective permeability is slightly higher in the regions containing more dissolved salt since less volume of ice forms there. Furthermore, Liu and Hansen [69] performed measurements under similar conditions as in this example with reservoirs containing both water and a solution with 3% NaCl. It should be noted, though, that they used a cooling and heating rate of 10 °C/h in the measurements. Concerning the absorbed volume of liquid, the simulations using the CB conditions show the best compliance with their measurements. For a concrete with a w/c of 0.45 and 5.1% air, they measured a value of approximately 0.39 mm after 20 cycles, whereas our results show an absorbed volume of 0.27 mm for 3% NaCl. Moreover, although there is some scatter in their measurements, a general trend can be observed in the data with an increased absorption in the specimens exposed to NaCl after 20 cycles. At this stage, the specimens exposed to a saline reservoir had, on average, absorbed approximately 0.16 mm more liquid while the simulations show a difference of 0.13 mm. For subsequent freeze-thaw cycles, the measured differences generally become smaller, and eventually, the relationship becomes the opposite for some of the tested specimens. Liu and Hansen [69] do, however, mention that the liquid in the scaled off material is not included in their evaluation of the absorbed volume, which could explain this observation since the specimens exposed to NaCl show a more severe scaling of the exposure surface. In addition, the results show that the scaling of the surfaces increases in connection to the point where the shift of the aforementioned trend initiates. Nevertheless, as can be seen in Fig. 8, the OB conditions yield a significantly larger absorbed volume of liquid. Thus the results, furthermore, indicate that the CB conditions generally seem to represent the real conditions better.

Another phenomenon that might influence the absorption of liquid from the reservoir is the osmotic transport of pure water inside the material. Osmosis is the natural transport of the solvent molecules, typically water, through a semipermeable membrane allowing these to pass through while blocking the transport of the solute particles. It is the gradient of the chemical potential that drives the flow of the solvent through the membrane [70]. As described in Section 2, the presence of dissolved salt ions lowers the chemical potential of the liquid compared to pure water. Consequently, pure water is transported from regions with a lower salt concentration to regions with a higher concentration. Koniorczyk and Gawin [71] described that cementitious materials, because of their well-developed microstructure, may act as semi-permeable membranes, and thereby at least partially blocking the movement of the solute particles. Hence, the presence of a NaCl-solution on the surface can induce a flow of water towards the surface region to dilute the solution and thus also influence the liquid absorption. The osmotic transport was not explicitly considered in the current model formulation but can be added in future extensions of the model, e.g. based on the work presented by Koniorczyk and Gawin [71]. However, further experimental work is also needed to study the significance of this transport mechanism on the liquid absorption during freeze-thaw exposure. Moreover, because of the cryo-suction by the air voids, the degree of saturation of the capillary pores can decrease if the air voids are not close to the exposed surface, which may induce additional transport processes to restore equilibrium. As mentioned in Section 3, the proposed model formulation is limited to conditions where the capillary pores are always saturated with liquid and ice or just one of the two phases. Hence, this effect is not explicitly considered in the current model. It should be noted that the same assumption of capillary saturation also was made in the model developed by Gong and Jacobsen [26] mentioned above.

The distribution of S_l along the length of the specimens is another interesting parameter to study and is shown in Fig. 9 along the first 11 mm from the exposure surface. For the CB conditions, the obtained distributions after 10 cycles are shown for all analyzed concentrations. However, for the OB conditions, only the case with 3%, after both 1 and 10 cycles, is plotted because all remaining analyzed concentrations show an almost identical distribution at this stage. As can be observed for the CB conditions, the addition of salt alters the distribution of liquid, and S_l remains at a level close to capillary saturation over a distance of 1.5 mm before starting to increase. Without salt in the reservoir, the specimen absorbs water also at the exposed surface. In the cases with salt in the reservoir, this means there is a small or no local flow of liquid to the air voids closest to the surface. The reason for this can be explained by studying the distribution of the pressures p^l and p^l_{ap}, which are governing the local flow defined in Eq. (25), over the same length from the exposure surface. The obtained pressure distributions at the time 10 h during freeze-thaw cycle 10 for the cases with pure water and 3% NaCl-solution in the reservoir and the CB conditions applied are plotted in Fig. 10. As can be seen for the case with 3% NaCl in the reservoir, the pressure difference close to the surface is small, and the local flow of liquid to the air voids is thus also small. The decreasing magnitude of p^l_{ap} in this region is caused by the salt that has been transported into the specimen from the reservoir. The bump in p^l at approximately 3 mm is caused by the ice formation inside the pore space. Hence, the pressure difference, driving the flow to the air voids, is significantly larger and thus results in a substantially higher absorption rate of liquid in this region. Closer to the exposure surface, the ice formation process is depressed because of the dissolved salt in the pore liquid. For the case with pure water in the reservoir and the CB conditions applied, the magnitude of p^l_{ap} is primarily determined by the temperature, and the ice formation process close to the surface is not depressed because of any dissolved salt. Consequently, and as indicated by the pressure distributions in Fig. 10 and shown by the distribution of S_l in Fig. 9, there is thus a larger absorption of liquid close to the exposure surface. It should be noted that the same type of phenomenon from the presence of salt also can be observed for the OB conditions, where S_l is lower on the exposure surface than at a greater depth after one cycle in Fig. 9. However, because of the significantly higher absorption rate using these boundary conditions, the ice formation causes p^l to become larger than p^l_{ap} also closer to the

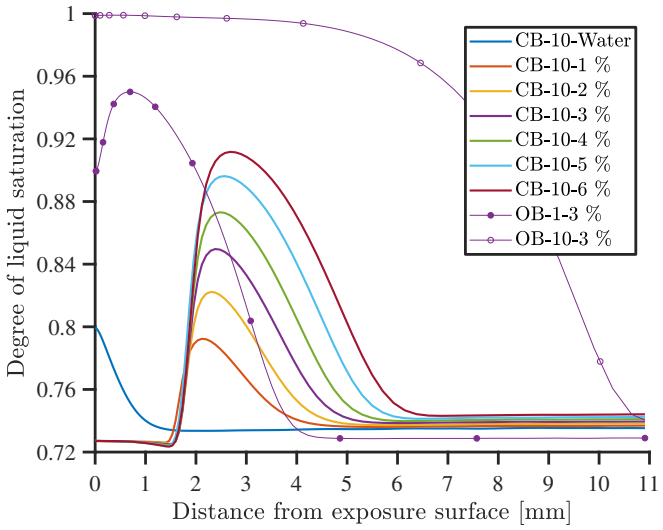

Fig. 9. Distribution of S_l along the first 11 mm of the specimens from the exposure surface. The notations in the legend denotes the following: Boundary condition type - Number of cycles - NaCl concentration in the reservoir. Note that the distributions are plotted at the end of the applied freeze-thaw cycles, i. e. after full thawing of the formed ice.

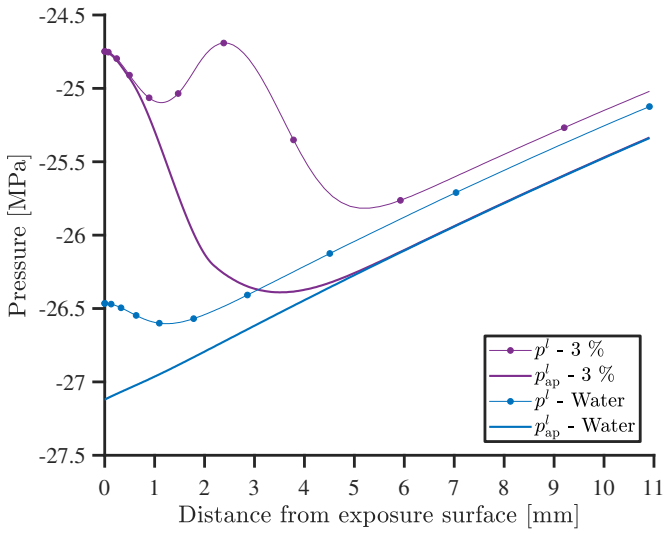

Fig. 10. Distribution of p^l and p^l_{ap} along the first 11 mm of the specimens from the exposure surface with the CB conditions applied. The distributions are plotted for the cases with water and 3% NaCl-solution in the reservoir at the time 10 h in freeze-thaw cycle 10.

exposure surface. The pressure difference is though still larger at approximately 1 mm, which yields a larger absorption at this location than at the surface. Moreover, due to the higher absorption rate with the OB conditions, the specimen becomes fully saturated at the exposure surface already after ten cycles.

The qualitative comparisons of the obtained simulation results with both other simulations and performed measurements in the literature indicate that the proposed model is capable of describing freeze-thaw induced absorption of liquid into air-entrained concrete. The results also indicate that the model is capable of considering the influence of dissolved salt on the absorbed volume of liquid. There are, however, uncertainties when making qualitative comparisons and, thus, further experimental work is necessary to fully verify these capabilities of the model.

6. Discussion

Finding an accurate representation of the real boundary conditions is challenging but also important to obtain reliable results. The two boundary condition types tested in Example 2 give quite different results and can be regarded as two extremes since they correspond to either a fully closed (CB) or open (OB) reservoir during freezing temperatures. However, the real boundary conditions are more likely to be somewhere in between these two extremes. For example, Valenza and Scherer [17] discuss the existence of brine pockets in the ice layer, which during freezing can crack and make the liquid inside these available for absorption. Therefore, further experimental work is necessary to study the effect of different salt concentrations in the reservoir on the boundary conditions and the absorbed volume of liquid. Preferably, the experiments should be designed to allow the reservoir to either freeze or remain unfrozen, which means that the boundary effects can be studied while also yielding data suitable for further validation of the model.

The current model formulation assumes a linear elastic behavior of the concrete. However, if the degree of liquid saturation reaches a critical level, the material is damaged during freezing, and this assumption is no longer valid [5]. Hence, a non-linear mechanical description of the concrete is required to capture the actual response under such conditions. In Example 1, it was shown that the model is capable of describing freeze-thaw induced deformations of air-entrained concrete. Consequently, it should be possible to capture internal frost damage in concrete exposed to one or more freeze-thaw cycles, including the influence of dissolved salt, following such an extension. Moreover, based on the results in Example 2, the presence of an external reservoir can also be studied.

Although the aim of the current study was not specifically to model surface deterioration, the developed model can also aid theoretical investigations of mechanisms connected to salt-frost scaling. For instance, in Example 2, an accumulation of liquid was observed in the surface region, which is considered to be of significant importance for salt-frost scaling damage according to, e.g., Lindmark [12] and Powers [14]. However, to model the mechanism outlined by the glue-spall theory, the mechanics of the ice layer and its interaction with the surface must also be considered in addition to the non-linear behavior of the concrete. The current model can, though, be used as a basis for such extensions since it has been shown to adequately describe many of the other processes that are believed to be important.

7. Conclusions

This study presents a hygro-thermo-mechanical multiphase model that describes the freeze-thaw behavior of partially saturated air-entrained concrete, which also considers the influence and transport of dissolved salt in the pore liquid. The freezing and melting of the pore liquid, including the hysteresis in such cycles, were modeled by adopting both an equilibrium and a non-equilibrium approach.

Two examples are presented to verify the behavior of the proposed model and to show its capabilities. The simulations in the first example agree well with experimentally measured strains, and it can be concluded that the model replicates the observed smaller contraction of the specimens with an increasing salt concentration in the pore liquid. Moreover, results obtained using the equilibrium and the non-equilibrium approach for the ice formation are compared, and it was shown that they yield almost equivalent results in the studied case. Since the studied freezing rate is higher than those usually observed in northern Europe, either of the two approaches seems suitable to use in real-world applications.

Results from the second example show a larger absorbed volume of liquid from external reservoirs during repeated freeze-thaw cycles with an increasing concentration of dissolved NaCl in the reservoir. The same observation is made regardless of whether the boundary is closed or remains open during freezing temperatures. Comparing the results with measurements performed under similar conditions, though, indicates that a closed boundary better represents the real conditions. However, to fully verify these capabilities of the model and to further investigate how to describe the real boundary conditions adequately, additional experimental work is needed.

The current model formulation needs to be extended with a non-linear mechanical description of the concrete to be able to describe progressive internal frost damage caused by repeated freeze-thaw cycles. Such an extension would also enable further studies of the various proposed mechanisms related to salt-frost scaling since the model already includes many of the important processes. However, for the glue-spall mechanism, it is also required to include the mechanics of the ice layer and its interaction with the concrete. In addition, to further improve the accuracy and applicability of the model, future extensions should also aim to include the osmotic transport, the influence of varying salt concentration on all relevant physical parameters of the liquid phase and a partially saturated capillary pore system.

CRediT authorship contribution statement

Daniel Eriksson: Methodology, Software, Validation, Formal analysis, Writing - Original Draft, Writing - Review & Editing, Visualization.

David Wahlbom: Writing - Review & Editing.

Richard Malm: Conceptualization, Resources, Writing - Review & Editing, Supervision, Project administration, Funding acquisition.

Katja Fridh: Conceptualization, Resources, Writing - Review &

Editing, Supervision.

Declaration of competing interest

The authors declare that they have no known competing financial interests or personal relationships that could have appeared to influence the work reported in this paper.

Acknowledgements

The research presented was carried out as a part of Swedish Hydropower Centre - SVC. SVC has been established by the Swedish Energy Agency, Energiforsk and Svenska Kraftnät together with Luleå University of Technology, KTH Royal Institute of Technology, Chalmers University of Technology and Uppsala University. www.svc.nu. The authors would also like to acknowledge the financial support of Nanocem, The Industrial-Academic Nanoscience Research Network for Sustainable Cement and Concrete.

References

[1] G. Fagerlund, A service life model for internal frost damage in concrete, in: Report TVBM-3119, Division of Building Materials, LTH, Lund University, 2004.
[2] T. Sandström, K. Fridh, M. Emborg, M. Hassanzadeh, The influence of temperature on water absorption in concrete during freezing, Nordic Concr. Res. 45 (1) (2012) 45–58.
[3] J.J. Valenza, G.W. Scherer, A review of salt scaling: II. Mechanisms, Cem. Concr. Res. 37 (7) (2007) 1022–1034, https://doi.org/10.1016/j.cemconres.2007.03.003.
[4] K. Fridh, Internal Frost Damage in Concrete - Experimental Studies of Destruction Mechanisms (PhD thesis), Division of Building Materials, LTH, Lund University, 2005.
[5] G. Fagerlund, The international cooperative test of the critical degree of saturation method of assessing the freeze/thaw resistance of concrete, Mater. Constr. 10 (4) (1977) 231–253, https://doi.org/10.1007/bf02478694.
[6] G. Fagerlund, The long time water absorption in the air-pore structure of concrete, in: Report TVBM-3051, Division of Building Materials, LTH, Lund University, 1993.
[7] C. Hall, Anomalous diffusion in unsaturated flow: fact or fiction? Cem. Concr. Res. 37 (3) (2007) 378–385, https://doi.org/10.1016/j.cemconres.2006.10.004.
[8] S. Jacobsen, E.J. Sellevold, Frost/salt scaling testing of concrete - importance of absorption during test, Nordic Concr. Res. 14 (1994) 26–44.
[9] S. Jacobsen, Scaling and Cracking in Unsealed Freeze/Thaw Testing of Portland Cement and Silica Fume Concretes (PhD thesis), Norwegian Institute of Technology, 1995.
[10] D.H. Bager, Freeze-thaw damage and water-uptake in low water/cement ratio concrete, in: J.F. Olesen (Ed.), Papers in Structural Engineering and Materials - A Centenary Celebration, Department of Structural Engineering and Materials, Technical University of Denmark, 2000, pp. 119–130.
[11] R. Auberg, M.J. Setzer, Influence of water uptake during freezing and thawing, in: M.J. Setzer, R. Auberg (Eds.), Frost Resistance of Concrete - Proceedings of the International Rilem Workshop on Resistance of Concrete to Freezing and Thawing With or Without De-icing Chemicals, Chapman & Hall, London, 1997, pp. 232–245.
[12] S. Lindmark, Mechanisms of Salt Frost Scaling on Portland Cement-bound Materials: Studies and Hypothesis (PhD thesis), Division of Building Materials, LTH, Lund University, 1998.
[13] Z. Liu, W. Hansen, F. Wang, Pumping effect to accelerate liquid uptake in concrete and its implications on salt frost durability, Constr. Build. Mater. 158 (2018) 181–188, https://doi.org/10.1016/j.conbuildmat.2017.09.154.
[14] T.C. Powers, Freezing effects in concrete, in: C.F. Scholer, E. Farkas (Eds.), Durability of Concrete vol. SP 47, ACI, 1975, pp. 1–12, https://doi.org/10.14359/17603.
[15] Z. Liu, W. Hansen, A hypothesis for salt frost scaling in cementitious materials, J. Adv. Concr. Technol. 13 (9) (2015) 403–414, https://doi.org/10.3151/jact.13.403.
[16] M.J. Setzer, Micro-ice-lens formation in porous solid, J. Colloid Interface Sci. 243 (1) (2001) 193–201, https://doi.org/10.1006/jcis.2001.7828.
[17] J.J. Valenza, G.W. Scherer, Mechanism for salt scaling, J. Am. Ceram. Soc. 89 (4) (2006) 1161–1179, https://doi.org/10.1111/j.1551-2916.2006.00913.x.
[18] M. Koniorczyk, Coupled heat and water transport in deformable porous materials considering phase change kinetics, Int. J. Heat Mass Transf. 81 (2015) 260–271, https://doi.org/10.1016/j.ijheatmasstransfer.2014.10.031.
[19] M. Koniorczyk, D. Gawin, B.A. Schrefler, Modeling evolution of frost damage in fully saturated porous materials exposed to variable hygro-thermal conditions, Comput. Methods Appl. Mech. Eng. 297 (2015) 38–61, https://doi.org/10.1016/j.cma.2015.08.015.
[20] B. Zuber, J. Marchand, Modeling the deterioration of hydrated cement systems exposed to frost action - part 1: description of the mathematical model, Cem. Concr. Res. 30 (12) (2000) 1929–1939, https://doi.org/10.1016/S0008-8846(00)00405-1.
[21] B. Zuber, J. Marchand, Predicting the volume instability of hydrated cement systems upon freezing using poro-mechanics and local phase equilibria, Mater. Struct. 37 (4) (2004) 257–270, https://doi.org/10.1007/bf02480634.
[22] O. Coussy, P.J.M. Monteiro, Poroelastic model for concrete exposed to freezing temperatures, Cem. Concr. Res. 38 (1) (2008) 40–48, https://doi.org/10.1016/j.cemconres.2007.06.006.
[23] T. Fen-Chong, A. Fabbri, M. Thiery, P. Dangla, Poroelastic analysis of partial freezing in cohesive porous materials, J. Appl. Mech. 80 (2) (2013), https://doi.org/10.1115/1.4007908 (020910–020910–8).
[24] D. Eriksson, T. Gasch, R. Malm, A. Ansell, Freezing of partially saturated air-entrained concrete: a multiphase description of the hygro-thermo-mechanical behaviour, Int. J. Solids Struct. 152-153 (2018) 294–304, https://doi.org/10.1016/j.ijsolstr.2018.07.004.
[25] Q. Zeng, T. Fen-Chong, P. Dangla, K. Li, A study of freezing behavior of cementitious materials by poromechanical approach, Int. J. Solids Struct. 48 (22–23) (2011) 3267–3273, https://doi.org/10.1016/j.ijsolstr.2011.07.018.
[26] F. Gong, S. Jacobsen, Modeling of water transport in highly saturated concrete with wet surface during freeze/thaw, Cem. Concr. Res. 115 (2019) 294–307, https://doi.org/10.1016/j.cemconres.2018.08.013.
[27] Q. Zeng, L. Li, X. Pang, Q. Gui, K. Li, Freeze-thaw behavior of air entrained cement paste saturated with 10 wt.% NaCl solution, Cold Reg. Sci. Technol. 102 (2014) 21–31, https://doi.org/10.1016/j.coldregions.2014.02.003.
[28] Q. Zeng, T. Fen-Chong, K. Li, Freezing behavior of cement pastes saturated with NaCl solution, Constr. Build. Mater. 59 (2014) 99–110, https://doi.org/10.1016/j.conbuildmat.2014.02.042.
[29] Z. Liu, W. Hansen, Freezing characteristics of air-entrained concrete in the presence of deicing salt, Cem. Concr. Res. 74 (2015) 10–18, https://doi.org/10.1016/j.cemconres.2015.03.015.
[30] D. Gawin, F. Pesavento, M. Koniorczyk, B.A. Schrefler, Non-equilibrium modeling hysteresis of water freezing: ice thawing in partially saturated porous building materials, J. Build. Phys. 43 (2) (2019) 61–98, https://doi.org/10.1177/1744259119855100.
[31] G.W. Scherer, Crystallization in pores, Cem. Concr. Res. 29 (8) (1999) 1347–1358, https://doi.org/10.1016/S0008-8846(99)00002-2.
[32] O. Coussy, Poromechanics of freezing materials, J. Mech. Phys. Solids 53 (8) (2005) 1689–1718, https://doi.org/10.1016/j.jmps.2005.04.001.
[33] Z. Sun, G.W. Scherer, Pore size and shape in mortar by thermoporometry, Cem. Concr. Res. 40 (5) (2010) 740–751, https://doi.org/10.1016/j.cemconres.2009.11.011.
[34] H.-y. Lin, L.-s. Lee, Estimations of activity coefficients of constituent ions in aqueous electrolyte solutions with the two-ionic-parameter approach, Fluid Phase Equilib. 237 (1) (2005) 1–8, https://doi.org/10.1016/j.fluid.2005.08.005.
[35] M. Brun, A. Lallemand, J.-F. Quinson, C. Eyraud, A new method for the simultaneous determination of the size and shape of pores: the thermoporometry, Thermochim. Acta 21 (1) (1977) 59–88, https://doi.org/10.1016/0040-6031(77)85122-8.
[36] Q. Zeng, K. Li, Quasi-liquid layer on ice and its effect on the confined freezing of porous materials, Crystals 9 (5) (2019) 1–16, https://doi.org/10.3390/cryst9050250.
[37] G. Fagerlund, Determination of pore-size distribution from freezing-point depression, Mater. Constr. 6 (3) (1973) 215–225, https://doi.org/10.1007/bf02479036.
[38] Z. Sun, G.W. Scherer, Effect of air voids on salt scaling and internal freezing, Cem. Concr. Res. 40 (2) (2010) 260–270, https://doi.org/10.1016/j.cemconres.2009.09.027.
[39] D.H. Bager, E.J. Sellevold, Ice formation in hardened cement paste, part I - room temperature cured pastes with variable moisture contents, Cem. Concr. Res. 16 (5) (1986) 709–720, https://doi.org/10.1016/0008-8846(86)90045-1.
[40] M. Wu, B. Johannesson, Impact of sample saturation on the detected porosity of hardened concrete using low temperature calorimetry, Thermochim. Acta 580 (2014) 66–78, https://doi.org/10.1016/j.tca.2014.02.002.
[41] Y. Farnam, D. Bentz, A. Sakulich, D. Flynn, J. Weiss, Measuring freeze and thaw damage in mortars containing deicing salt using a low-temperature longitudinal guarded comparative calorimeter and acoustic emission, Adv. Civ. Eng. Mater. 3 (1) (2014) 316–337, https://doi.org/10.1520/ACEM20130095.
[42] D. Eriksson, T. Gasch, A. Ansell, A hygro-thermo-mechanical multiphase model for long-term water absorption into air-entrained concrete, Transp. Porous Media 127 (1) (2019) 113–141, https://doi.org/10.1007/s11242-018-1182-3.
[43] M. Hassanizadeh, W.G. Gray, General conservation equations for multiphase systems: 1. Averaging procedure, Adv. Water Resour. 2 (1979) 131–144, https://doi.org/10.1016/0309-1708(79)90025-3.
[44] R.W. Lewis, B.A. Schrefler, The Finite Element Method in the Static and Dynamic Deformation and Consolidation of Porous Media, second edn., John Wiley & Sons, Chichester, 1998.
[45] W.G. Gray, C.T. Miller, Thermodynamically constrained averaging theory approach for modeling flow and transport phenomena in porous medium systems: 1. Motivation and overview, Adv. Water Resour. 28 (2) (2005) 161–180, https://doi.org/10.1016/j.advwatres.2004.09.005.
[46] S.M. Hassanizadeh, Derivation of basic equations of mass transport in porous media, Part 2. Generalized Darcy's and Fick's laws, Adv. Water Resour. 9 (4) (1986) 207–222, https://doi.org/10.1016/0309-1708(86)90025-4.
[47] T.M. van Genuchten, A closed-form equation for predicting the hydraulic conductivity of unsaturated soils, Soil Sci. Soc. Am. J. 44 (1980) 892–898.
[48] T.C. Powers, A working hypothesis for further studies of frost resistance of concrete, J. Am. Concr. Inst. 16 (4) (1945) 245–272, https://doi.org/10.14359/8684.

[49] T.C. Powers, R.A. Helmuth, Theory of volume changes in hardened portland-cement paste during freezing, in: Proceedings of the Highway Research Board vol. 32, Portland Cement Association, 1953, pp. 285–297.
[50] T.C. Powers, The air requirement of frost-resistant concrete, in: Proceedings of the Highway Research Board vol. 29, Portland Cement Association, 1949, pp. 184–211.
[51] K.A. Snyder, A numerical test of air void spacing equations, Adv. Cem. Based Mater. 8 (1) (1998) 28–44, https://doi.org/10.1016/S1065-7355(98)00007-8.
[52] H.M. Jennings, A. Kumar, G. Sant, Quantitative discrimination of the nano-pore-structure of cement paste during drying: new insights from water sorption isotherms, Cem. Concr. Res. 76 (2015) 27–36, https://doi.org/10.1016/j.cemconres.2015.05.006.
[53] G. Lin, Y. Liu, Z. Xiang, Numerical modeling for predicting service life of reinforced concrete structures exposed to chloride environments, Cem. Concr. Compos. 32 (8) (2010) 571–579, https://doi.org/10.1016/j.cemconcomp.2010.07.012.
[54] A.V. Saetta, R.V. Scotta, R.V. Vitaliani, Analysis of chloride diffusion into partially saturated concrete, ACI Mater. J. 90 (5) (1993) 441–451, https://doi.org/10.14359/3874.
[55] H. Wang, C. Lu, W. Jin, Y. Bai, Effect of external loads on chloride transport in concrete, J. Mater. Civ. Eng. 23 (7) (2011) 1043–1049, https://doi.org/10.1061/(ASCE)MT.1943-5533.0000265.
[56] Q. Zeng, Poromechanical Behavior of Cement-based Materials Subjected to Freeze-thaw Actions With Salts: Modeling and Experiments (PhD thesis), Université Paris-Est, 2011.
[57] COMSOL, COMSOL Multiphysics ver 5.5 Documentation, COMSOL AB, Stockholm, 2019.
[58] O.C. Zienkiewicz, R.L. Taylor, J.Z. Zhu, The Finite Element Method: Its Basis and Fundamentals, seventh edn., Butterworth-Heinemann, Oxford, 2013 https://doi.org/10.1016/B978-1-85617-633-0.00019-8.
[59] J. Rumble, CRC Handbook of Chemistry and Physics, 98th edn., CRC Press, Boca Raton, 2017.
[60] P.V. Hobbs, Ice Physics, Clarendon Press, Oxford, UK, 1974.
[61] T.R. Butkovich, Thermal expansion of ice, J. Appl. Phys. 30 (3) (1959) 350–353, https://doi.org/10.1063/1.1735166.
[62] D.P. Bentz, Transient plane source measurements of the thermal properties of hydrating cement pastes, Mater. Struct. 40 (10) (2007) 1073–1080, https://doi.org/10.1617/s11527-006-9206-9.
[63] Y. Xu, D.D.L. Chung, Effect of sand addition on the specific heat and thermal conductivity of cement, Cem. Concr. Res. 30 (1) (2000) 59–61, https://doi.org/10.1016/S0008-8846(99)00206-9.
[64] D.G. Archer, R.W. Carter, Thermodynamic properties of the NaCl + H2O system. 4. Heat capacities of H2O and NaCl(aq) in cold-stable and supercooled states, J. Phys. Chem. B 104 (35) (2000) 8563–8584, https://doi.org/10.1021/jp0003914.
[65] K.S. Pitzer, J.C. Peiper, R.H. Busey, Thermodynamic properties of aqueous sodium chloride solutions, J. Phys. Chem. Ref. Data 13 (1) (1984) 1–102, https://doi.org/10.1063/1.555709.
[66] S.A. Grant, Physical and chemical factors affecting contaminant hydrology in cold environments, in: Report TR-00-21, ERDC/CRREL, 2000.
[67] K.A. Riding, M.D.A. Thomas, K.J. Folliard, Apparent diffusivity model for concrete containing supplementary cementitious materials, ACI Mater. J. 110 (6) (2013) 705–714, https://doi.org/10.14359/51686338.
[68] G. Fagerlund, Effect of the freezing rate on the frost resistance of concrete, Nordic Concr. Res. 11 (1) (1992) 20–36.
[69] Z. Liu, W. Hansen, Moisture uptake in concrete under freezingthawing exposure, Mag. Concr. Res. 68 (12) (2016) 619–631, https://doi.org/10.1680/jmacr.15.00193.
[70] I. Medved, R. Černý, Osmosis in porous media: a review of recent studies, Microporous Mesoporous Mater. 170 (2013) 299–317, https://doi.org/10.1016/j.micromeso.2012.12.009.
[71] M. Koniorczyk, D. Gawin, Heat and moisture transport in porous building materials containing salt, J. Build. Phys. 31 (4) (2008) 279–300, https://doi.org/10.1177/1744259107088003.

Appendix 2 - Paper II

Cryosuction experiments on concrete containing ground granulated blast-furnace slag; influence of temperature, air entrainment and salt

David Wahlbom[1], Katja Fridh[2]

[1] Division of Building Materials, Lund University, Sweden

[2] Department of Materials Science and Applied Mathematics, Malmö University, Sweden

E-mail: david.wahlbom@byggtek.se

Version: 2022-04-25

Abstract:

Frost deterioration of concrete is an important durability issue for structures exposed to high degree of saturation, low temperatures and de-icers. The material can then be severely damaged with internal cracking and/or scaling of the surface, which can lead to e.g. reduced protection of the reinforcement and loss of bearing capacity. One interesting aspect of frost deterioration is cryosuction, the process in which the absorption of water into a material is increased because of temperature cycling. Experiments with liquid uptake in concrete using different temperature cycles was made to study this phenomenon. The material used was concrete with different air content and different replacement levels of ground granulated blast-furnace slag (GGBS). The concrete samples were preconditioned by capillary suction. Three temperature conditions were used: constant temperatures of +20 °C and -20 °C, and temperature that cycled between -20 °C and +20 °C. As liquid medium, deionized water and a 3% NaCl salt solution were

used. The temperature in the liquid was never below 3 °C. Samples were in contact with the liquid on their bottom parts. The top and sides were moisture sealed and in contact with the respective temperature conditions controlled through the air. The results showed that the moisture uptake of the samples exposed to freezing temperatures (-20 °C or cycling between -20 °C and +20 °C) had a significantly higher spread, with some samples reaching much higher liquid uptakes than other samples. The liquid uptake in the +20 °C samples was significantly more uniform. We hypothesize that the higher liquid uptake in some samples was caused by the filling of stochastically distributed large pores in the freezing zone. Air entrainment generally increased the liquid uptake. The amount of GGBS and the NaCl concentration in the liquid did not have any significant impact on the liquid uptake in these experiments.

Key Words: Concrete, Frost Action, Supplementary Cementitious Materials, Cryosuction, Durability, Testing

---

1 INTRODUCTION

Concrete is the most used building material in the world and the cement industry releases 5-8% of the total man-made carbon dioxide emissions [1]. These emissions can be reduced by using SCM, supplementary cementitious materials, such as ground granulated blast furnace slag (GGBS), to replace a part of the cement used when casting concrete. When using different SCMs, the changes in chemical and material properties need to be taken under consideration e.g. the hydration progress is often slowed down [2] and with GGBS the pore structure of the concrete becomes denser [3], [4] unless it is carbonated [5]. The capillary suction properties are highly dependent on the pore structure and the denser pore structure of a concrete with GGBS results in an increased discontinuity and tortuosity in the material [6]. There is an observed correlation between the capillary suction properties of a concrete surface and frost scaling resistance [7], where a low liquid uptake from capillary suction results in higher frost scaling resistance.

The concrete can be protected by a proper air void system since this allows the pore liquid to be sucked into the air voids and freeze without creating any pressure on the surrounding material as explained by Powers and Helmuth [8]. But if there is an increase of liquid uptake the protective effect decreases. The positive effect on the air void system when using air entrainment agent have been shown in several studies [9] [10] [11].

Fagerlund presented the theory of critical degree of saturation [12], which predicts that a concrete will get internal damage due to freezing conditions when it has an actual degree of liquid saturation that is higher than a critical degree of saturation. The effective spacing factor is increased with a progressive saturation of the air voids from the liquid uptake, starting by the smallest air voids, which increases the distance between unsaturated air voids

[13]. Large air voids are almost never saturated through liquid uptake from capillary suction at non-freezing temperatures.

At non-freezing temperatures, capillary suction is the controlling transport property for unsaturated concrete [14], [15]. In 1921, Washburn presented the liquid uptake into a porous material with the assumption that the pores have an cylindrical shape with different radii [16]. The air voids with smaller radii are filled with liquid before the larger air voids start to take up liquid [13].

There is an observed increase of liquid uptake when a porous material is exposed to freezing temperatures, compared to non-freezing temperatures, if there is access to an external reservoir of liquid [17]. Taber presented the theory of frost heave in soil in 1930: if a porous material is exposed to freezing temperatures on one side and non-freezing temperature on the other, there will be a transport of unfrozen liquid towards the colder regions, where the liquid will freeze and form an ice lens, due to the difference in chemical potential between the ice and the liquid [18]. This phenomenon is described in concrete as the macroscopic ice lens theory. It has been shown by Rosenqvist and Lindmark that a growing ice lens can create damage to concrete with high water/binder ratios [9], [19]. A thin film of unfrozen water covers the interface between ice and the inside porous concrete, this thin film allows liquid to flow and supply the ice lenses [19]. For an ice lens to grow, the concrete needs an external liquid reservoir, otherwise the growing ice lens will drain the surrounding pores of liquid and the growth of the ice lens will cease [9]. Note that there will be no scaling damage on a concrete surface in the absence of an external liquid [9].

There is also an observed pumping effect during multiple freeze thaw cycles that results in an increased liquid uptake [20]. The pumping effect is a result of the thermodynamic non-equilibrium between the ice inside the air voids and the liquid in contact with these, which requires that the liquid pressure is below atmospheric pressure [21]. As a consequence, liquid

flows towards the air pores as they act as pumps in the material during freezing [21]. During freezing, ice crystallization starts from the largest air voids containing liquid, and as the temperature continues to decrease, the liquid in successively smaller air voids freezes [21].

The phenomenon of increased liquid uptake during freezing has been described by different models based on the poromechanical equations by Coussy [22]. Eriksson developed a hygro-thermo-mechanical multiphase model that can simulate air-entrained concrete in 3D, including phase change and hydraulic pressure in samples with non-saturated air voids [21], [23]. Unfortunately, there is at present a lack of experiments against which to validate poromechanical models.

This paper presents experiments of the liquid uptake in concrete with different amounts of GGBS and different NaCl concentrations in the liquid during freezing to assess the gradual filling of the pore system during multiple freeze thaw cycles. Results will hopefully cast more light on the mechanism of liquid uptake to better understand the complex topic of frost durability and may be of use to validate poromechanical models [23].

2 CRYOSUCTION EXPERIMENT

The objective of the experiment was to quantify the effect of cryosuction by exposing samples to three different air-controlled temperature conditions, a temperature cycling between -20 and +20 °C, a constant temperature of -20 °C and a constant temperature of +20 °C. The bottom of each sample is in contact with an unfrozen liquid. This set up makes it possible to avoid the influence of an ice-layer on the exposed surface, which is an important part of the scaling mechanism [9], and have a better chance to capture the influence of cryosuction only.

2.1 Materials

The recipes for the concrete are presented in Table 1. For each binder composition there were two concretes cast, with and without air-entrainment agent (AEA). An air-entrainment agent, Sika Air pro 5%, and a Super plasticizer (SP), Sika Viscocrete RMC 520, were used to get a desired air content and slump, Table 1. The target value was 5% air content when using AEA and 165 mm slump [5]. The air content and slump were measured on fresh concrete according to standards EN 12350-7 [24] and EN 12350-2 [25].

TABLE 1 CONCRETE RECIPE

Material	**W/B** -	**Cement** [1)] kg/m^3	**GGBS** kg/m^3	**0-8 mm** kg/m^3	**8-11 mm** kg/m^3	**11-16 mm** kg/m^3	**Air Content** Volume-%	**Slump mm**	**SP** [2)]	**AEA** [2)]
1	0.4	430	0	966	285	536	2.30	145	1.1	-
2	0.4	430	0	966	285	536	5.30	130	1.1	0.45
3	0.4	280	150	966	285	536	1.60	155	1.1	-
4	0.4	280	150	966	285	536	5.50	140	1.1	0.45
5	0.4	129	301	966	285	536	2.30	190	1.1	-
6	0.4	129	301	966	285	536	5.50	205	1.1	0.45

[1)] CEM 1 42,5 N SR3 MH/LA. (Slite, anläggningscement, Cementa AB)

[2)] The amount of admixture was dosed in % of binder weight

The materials were cast in molds of 400 mm × 400 mm × 150 mm, moisture sealed for 24 hours, then demolded and water cured in 20 °C lime saturated water for 2.5 months. Samples were then drilled and sawed to cylinders with sawed surfaces on top and bottom, and with the dimensions of 50 mm diameter and 50 mm height. The samples were then stored in 20 °C lime saturated water for an additional 3 months.

2.2 Method

The samples were moisture sealed on top and sides using a 1 mm thick butyl tape that had been tested to be very water vapor tight (Isola-Platon AB), leaving the sawed bottom exposed. The surface was dried in air for 15-30 min to ensure that the tape adhered well.

2.2.1 Experimental set-up

The samples were placed on a plastic grid, and in contact with deionized water or 3% NaCl solution. There were two different set-ups depending on if the samples were exposed to freezing temperatures or not. The set-up at constant +20 °C had a glass lid to prevent moisture loss by evaporation.

The set-ups for constant -20 °C and cycling between +20 °C and -20 °C used an insulated container, with a 50 mm thick XPS insulation that covered the bottom and sides, as is seen in Figs. 1 - 2. A 20 mm XPS insulation in which the samples were placed, was placed 8 mm above the plastic grid, to ensure that the insulation was not in contact with the liquid. Half of each sample were above the insulation and exposed to the temperature-controlled air. A heating coil was used to prevent the liquid from freezing. The heating coil was attached underneath the plastic grid. The plastic grid was supported and levelled by four screws standing on the bottom of the container. The liquid temperature was regulated with a PI-regulator to not decrease below 3 °C. The temperature gradient was quantified by temperature measurements

at three heights (top, middle and bottom) in two dummy samples, Fig. 2, that were never weighted, one for constant temperature of -20 °C and one for cycling temperature between +20 °C and -20 °C. The temperature of the dummy samples were measured inside the material. Holes was drilled to the centre of the sample (25 mm depth) at the three heights, and the sensors were placed inside and the holes were filled with cement paste to keep the sensors in place.

FIGURE 1 SET-UP FOR -20 °C AND FOR CYCLING BETWEEN +20 AND -20 °C WITH ONLY ONE SAMPLE INSERTED.

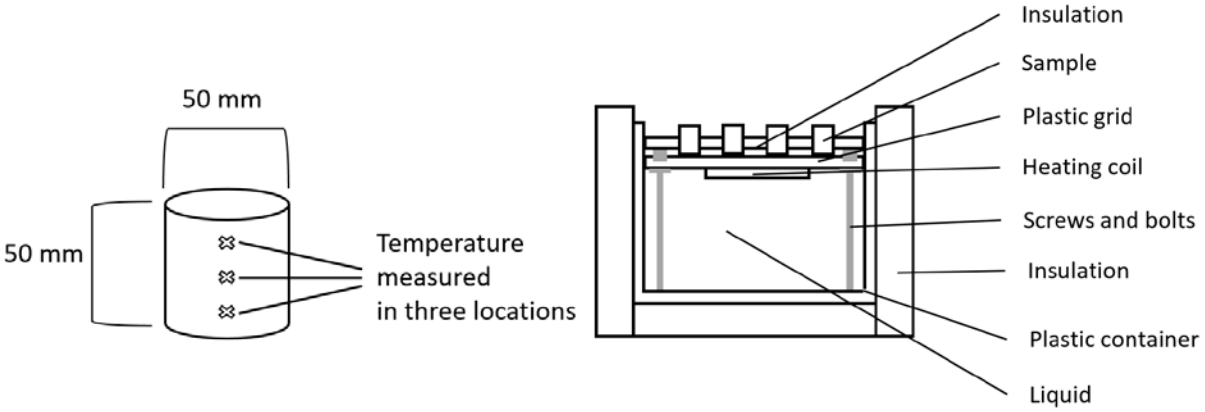

FIGURE 2 LOCATION OF TEMPERATURE SENSORS ON TEMPERATURE DUMMY (LEFT) AND CROSS SECTION OF SET-UP FOR -20 °C AND CYCLING +20/-20 °C EXPERIMENT (RIGHT).

The liquid uptake of the samples was measured at regular intervals. The samples were taken out of the containers, dried with a wet cloth and weighed on a ±0.001 g balance. Samples in constant +20 °C and cycling between +20 °C and -20 °C were weighed once a week. Samples at constant -20 °C were weighed once a month. Samples exposed to freezing temperatures were weighted in a thawed state.

3 RESULTS AND DISCUSSION

The result is presented in Figs. 4 - 7 as liquid uptake per area (kg/m^2) of the bottom of the samples as a function of time. The main interest in the evaluation is the effect of the NaCl solution, the replacement level of GGBS, the three different temperatures conditions and the air entrainment.

As the samples were preconditioned by capillary saturation, the moisture uptake that is studied in this paper is small compared to the moisture content achieved during sample preparation, as is schematically shown in Fig. 3.

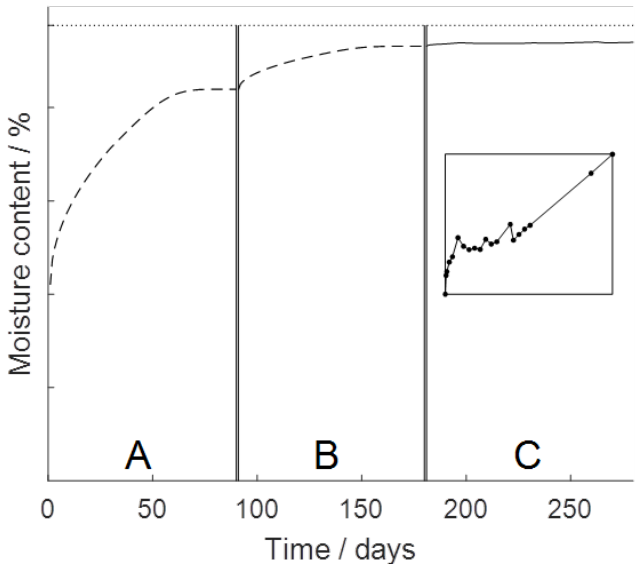

FIGURE 3 SCHEMATIC DESCRIPTION OF HOW THE MOISTURE CONTENT OF A SAMPLE CHANGES DURING SAMPLE PREPARATION AND MEASUREMENT. PHASE A IS THE WATER STORAGE AFTER CASTING; B IS THE WATER STORAGE OF THE CORE DRILLED SPECIMEN; C IS AN EXAMPLE OF THE MEASUREMENTS PRESENTED IN THIS PAPER. INSERT IN C SHOWS EXAMPLE OF UPTAKE DURING PHASE C.

3.1 General observations

In Fig. 4, the raw data from selected measurements are presented for material 4 from Table 1 with three replicate samples for each temperature condition. The measured liquid uptake is small, and as the samples are dried by hand with a wet cloth before each weighing, there are

small differences in how much liquid that remain on the surface of the sample, and this is the most probable cause of the scatter in some curves.

The dashed lines are linear regressions of the data between 10 days and the end of measurement. The results presented in Figs. 6-7 are based on linear regressions at 100 days and not the actual measurement at 100 days, this is to reduce the noise in the measurement.

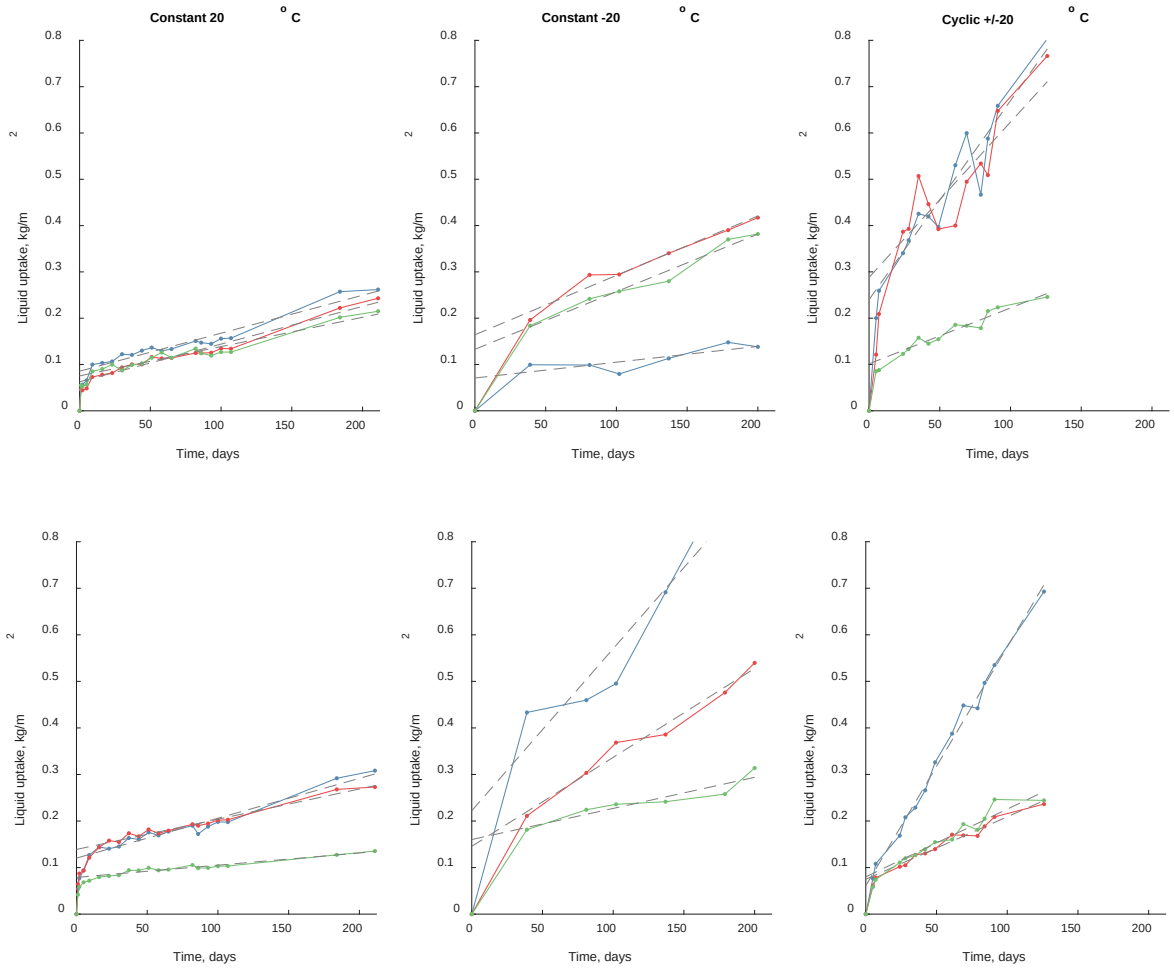

FIGURE 4 EXAMPLE OF EXPERIMENTAL RESULT. RESULTS FOR MATERIAL 4 WITH DEIONIZED WATER (TOP) AND A 3% NACL SOLUTION (BOTTOM) FOR THE THREE TEMPERATURE CONDITIONS. FOR EACH TEMPERATURE CONDITION AND NACL CONCENTRATION, THREE SPECIMENS WERE TESTED.

The results generally show larger spread and larger mean value for the cases with freezing temperatures (constant -20 °C and cycling between +20 °C and -20 °C) compared to the case at constant +20 °C.

3.2 The effect of air entrainment on liquid uptake

When an air entrainment agent (AEA) is used in concrete, it produces more air pores [26] with a diameter of 5 – 100 μm that results in a higher porosity and a more open pore system [26]. The effect this has on liquid uptake in the present experiment is shown in Fig. 5, which shows an overview of the results of all the measurements. In Fig. 5A-C it is seen that the spread in the result is significantly lower for the +20 °C exposure than for the other exposures, and that the samples with entrained air generally have a higher liquid uptake as the grey dashed lines are generally above the black lines. It is also seen in Fig. 5A-C that the samples exposed to freezing temperatures generally have a more rapid liquid uptake.

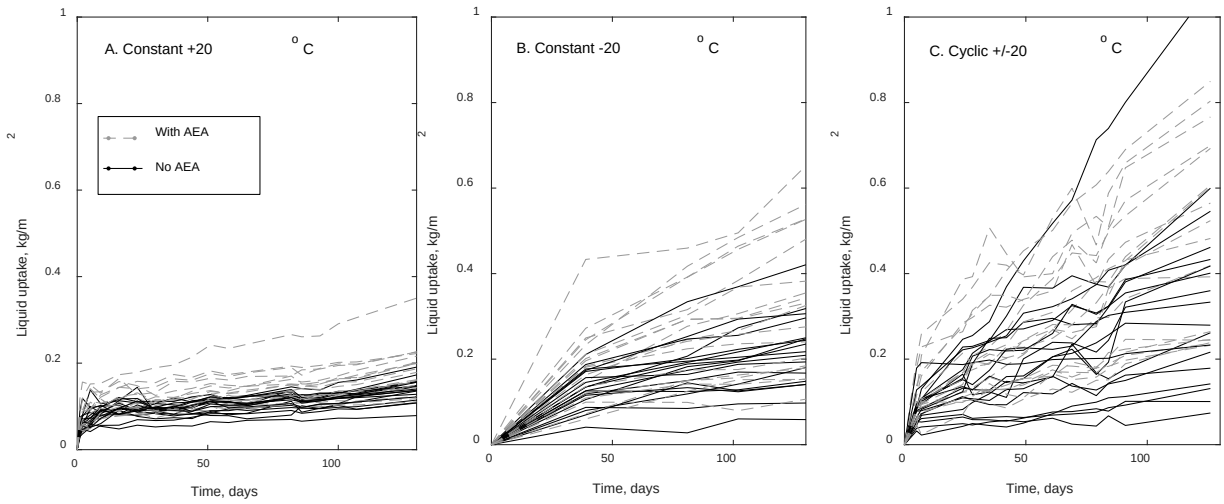

FIGURE 5 LIQUID UPTAKE IN THE CRYOSUCTION MEASUREMENTS. A-C. ALL MEASUREMENTS FOR THE THREE DIFFERENT TEMPERATURE CONDITIONS, GREY DASHED LINES FOR SAMPLES WITH AEA AND BLACK LINES FOR THOSE WITHOUT.

3.3 The effect of replacement level of GGBS for liquid uptake

With an increasing replacement level of GGBS the pore structure becomes denser, but this does not seem to have any effect on the liquid uptake in the present study, see Fig. 6 A-C. The results are presented as the liquid uptake after 100 days (on the linear regressions). When we look at

the different materials, there are mixed results concerning which replacement level of GGBS that gives the highest liquid uptake and in some cases the results are almost the same for all three cases.

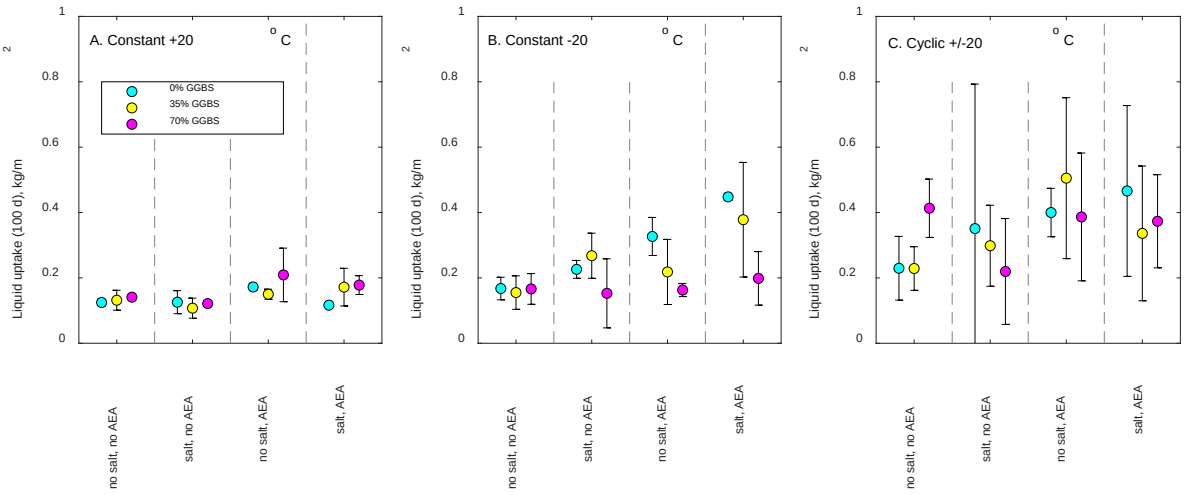

FIGURE 6 THE MEAN LIQUID UPTAKE AFTER 100 DAYS FROM LINEAR REGRESSION OF THE CRYOSUCTION MEASUREMENTS ON THREE SAMPLES WITH THREE LEVELS OF GGBS REPLACEMENT. MEASUREMENTS FOR THE THREE DIFFERENT TEMPERATURE CONDITIONS ARE GIVEN IN A-C. THE X-AXIS SHOW IF AIR ENTRAINMENT AGENT WAS USED (AEA) OR NOT (NO AEA), AND IF THE LIQUID RESERVOIR WAS DE-IONIZED WATER (NO SALT) OR 3 WEIGHT-% NACL (SALT).

3.4 The effect of salt

The effect of salt in the liquid reservoir on the liquid uptake is presented in Fig. 7 A-C. There is no trend for the liquid uptake in the presence or absence of salt. When we look at the different materials, there are mixed results concerning if de-ionized water or a 3% NaCl solution in the liquid reservoir gives the highest liquid uptake.

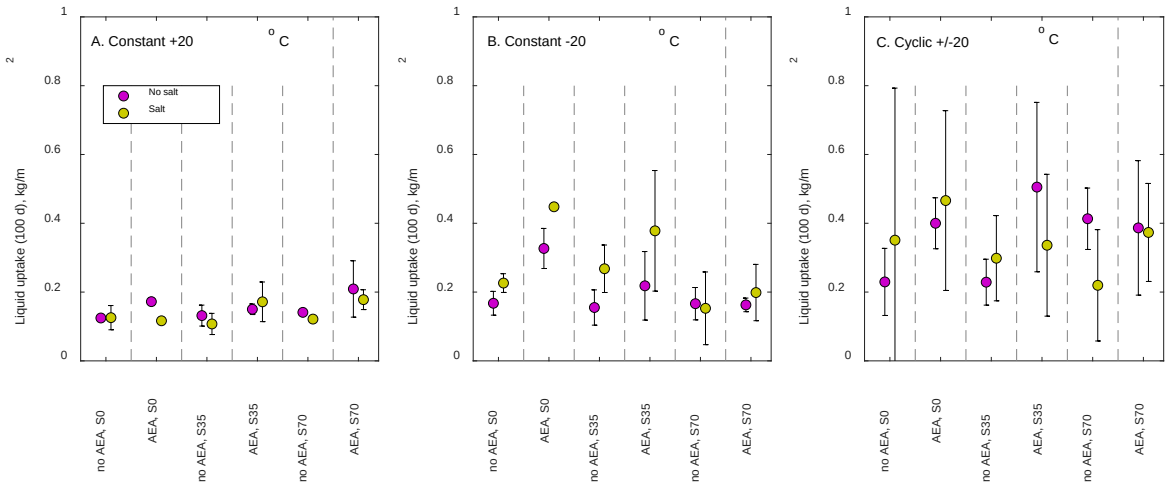

FIGURE 7 THE MEAN LIQUID UPTAKE AFTER 100 DAYS FROM CRYOSUCTION MEASUREMENTS, ON THREE SAMPLES WITH EITHER DE-IONIZED WATER (NO SALT) OR 3 WEIGHT-% NACL (SALT) IN THE LIQUID RESERVOIR. MEASUREMENTS FOR THE THREE DIFFERENT TEMPERATURE CONDITIONS IN A-C. THE X-AXIS DESCRIBES THE CONDITION OF THE SAMPLE: IF AIR ENTRAINMENT AGENT WAS USED OR NOT, AND WHAT THE REPLACEMENT LEVEL OF GGBS IN WEIGHT-% (S0 = 0 %, S35 = 35 % AND S70 =70 %)

3.5 General discussion

The reason for the larger spread in the results during freezing temperatures could be that the higher liquid uptake in some samples was caused by the filling of stochastically distributed large pores (diameter of 1 mm or more) in the freezing zone filled through cryosuction. The samples were stored in lime saturated water 3 months before the experiment began so most of the pores that should be filled with liquid through capillary suction at room temperature, were already filled at the start of the experiment.

Tomography-results of a mortar that have been exposed to capillary suction at room temperature are presented in Fig. 8. Note that this mortar does not have the same recipe as the concrete used in the present study. The Tomography is performed by the author, but not in this project for this article. The tomography results have been processed in ImageJ, and the tomograph is a Zeiss Xradia XRM520.

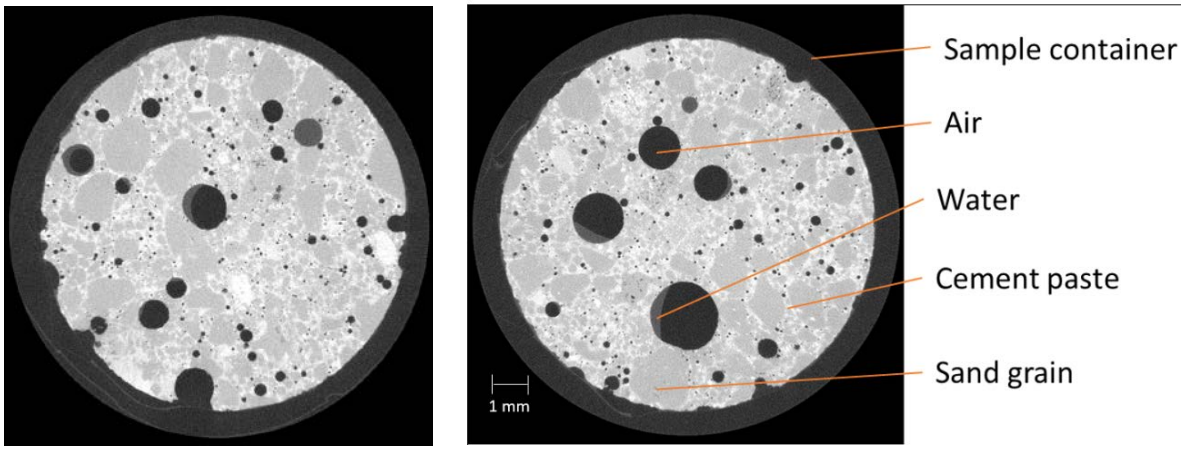

FIGURE 8 TOMOGRAPH PICTURE OF CEMENT MORTAR THAT HAVE BEEN STORED IN WATER AND HAVE TAKEN UP LIQUID THROUGH CAPILLARY SUCTION FROM ALL SIDES. SAMPLE SIZE 10MM X 10 MM [INSERT REFERENCE TO STEVEN HALL, AND JONAS ENGQVIST].

Fig. 8 shows that there still is air in the larger air voids of the material even though it is capillary saturated. Observation and estimation of the large pores of 1mm and larger on the surfaces of the samples have been performed, Fig. 9. Several pores of 1-5 mm diameter were found on all concrete samples.

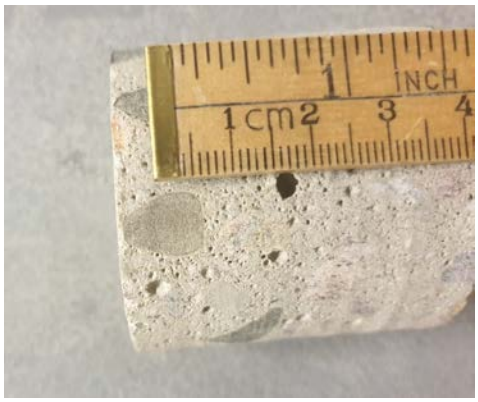

FIGURE 9 EXAMPLE OF LARGER AIR VOIDS ON SURFACE OF CONCRETE SAMPLE, MEASUREMENTS WERE MADE ON 5 SAMPLES FROM EACH MATERIAL.

Tomography examples, Fig. 8, and this surface observation, Fig. 9, can strengthen our hypothesis with larger pores in the freezing zone, can be the reason for the larger standard deviation in freezing temperatures.

3.6 Interpretation of the results and consequences for the effect of frost deterioration

The overall aim of this study was twofold. (1) To make measurements interesting for researchers who build frost models which needs experimental verification. These models help us understand different aspects of the complex deterioration mechanisms behind frost damage. (2) In the research of salt frost scaling there are two rather different explanations for the scaling: too high water content in the surface or damage caused by the ice layer on the surface. With experiments of the liquid uptake in different concrete materials during different temperature cycles, without any ice layer on the surface, will we discuss what circumstances which seems to promote a high water content in the surface and therefore a sensitivity to frost damage [27]. The results will also be discussed together with the results from scaling test performed by Strand [5], as the concrete material in the present study is cast with recipes similar to that study to compare the liquid uptake to the salt frost scaling in a representative material.

This was made to increase our knowledge of the role of liquid uptake in the mechanisms behind freeze-thaw action and the damage it causes to concrete structures. The measurements were made to examine the liquid uptake in concrete with different amount of air entrainment and GGBS when exposed to different temperature conditions and materials.

3.6.1 Temperature condition

In the present study, the liquid uptake is larger during freezing temperatures than at +20 °C. As the samples were stored at lime saturated water for 2.5 months before the experiment began, the samples were already at high moisture levels, and the increased liquid uptake for freezing temperatures is due to the effect of cryosuction.

For the freezing temperatures, the liquid uptake is not significantly larger at temperature cycling than at constant -20 °C as some studies have shown [20] [28]. The difference could be that in the other studies, the liquid reservoir was able to freeze [20]. The increased liquid uptake during freezing temperatures is not a direct indicator of the surface scaling damage, but is more connected to the degree of saturation in the specimen [20]. For a concrete with air entrainment, it takes more time or cycles until the critical degree of saturation is reached, even though the liquid uptake is higher than without AEA, but it still has a greater resistance to frost damage due to the larger air voids from the AEA. And for a concrete without AEA, they have a lower liquid uptake but it takes less time or fewer cycles until the critical degree of saturation is reached and have an higher risk for frost damage [28].

A hypothesis is that the larger uptake and the larger spread in the results of freezing temperatures is due to the occurrence and position of large pores, with a diameter of 1 mm or more in the freezing zone of the samples. For the condition with a cyclic temperature, this freezing zone is changing in position as the temperature changes and activates more of the larger pores, causing a larger spread in the results.

The gradual saturation of the pores through liquid uptake during freezing temperatures is necessary for causing severe damage, as many freeze-thaw cycles are often necessary until damage is observed [29].

3.6.2 Replacement level of GGBS

The pore structure of concrete changes with the addition of SCM´s [2] and, becomes denser with more GGBS [13]. However, the liquid uptake in this study seems to not be affected by the replacement level of GGBS. With the samples already at a high moisture level at the start of the experiment, the additional liquid uptake will mostly happen in the larger pores and due to the cryosuction below freezing temperatures. The study by Strand shows that an increased

slag fraction decreases the permeability by capillary suction measurements of an concrete that has not been aged and dried at the start of the experiment [5]. The effect of GGBS has on frost durability is varied depending on the replacement level and test method, but a denser pore structure gives an lower rate of liquid uptake, which leads to increased frost durability and scaling resistance [27]. The effect of GGBS under standard freeze durability testing of concrete according to ASTMC 672 [30] with a large (50-60%) replacement level of GGBS shows greater scaling, but lower replacement level of GGBS (around 25%) shows less scaling, both compared to concrete made with Portland cement [31]. Studies with the CIF-test show an decrease in scaling due to increased level of GGBS (up to 50%) replacement [32]. The study by Strand show that GGBS decreases the salt frost scaling in non-carbonated concrete (up to 70%) compared to CEM I [5].

3.6.3 salt concentration in the liquid reservoir.

The phenomenon with a NaCl pessimum at low NaCl concentration [5] [9] [33], where the largest salt frost scaling damage occurs [34] [35] [36], cannot be explained by an increased uptake of liquid with salt, as a NaCl concentration of 3% did not give a higher liquid uptake in the present study. Other studies show similar results in that the NaCl concentration does not have a clear increase or decrease in liquid uptake for concrete containing different amount of GGBS at around 0-3% NaCl concentration [14]. The study by Strand shows that the salt frost scaling damage in concrete samples exposed to low NaCl concentrations of 1 or 3% are higher compared with the salt frost scaling damage in the same type of samples exposed to a higher NaCl concentration of 9% or pure water [5], as previous studies have already shown.

4 CONCLUSION

Note that this study investigated the added liquid uptake in samples that were already at high moisture levels before the liquid uptake experiment are started. The surface of the samples in the experiment does not freeze, to isolate the effect of temperature variation on liquid uptake.

- The liquid uptake seems not to be influenced by if the samples are in contact with NaCl solution or pure water.
- The liquid uptake seems not to be influenced with an increased amount of GGBS replacing cement.
- Freezing temperature that cycles between +20 °C and -20 °C and constant -20 °C have a tendency to give higher liquid uptake than constant +20 °C.
- Samples with AEA have a tendency to have a higher liquid uptake than the samples without AEA.
- The samples exposed to cycling between +20 °C and -20 °C, and constant t -20 °C have a significantly higher spread in the liquid uptake than the samples at constant temperature +20 °C.

5 ACKNOWLEDGEMENTS

The authors wish to express their acknowledgement to The Industrial-Academic Nanoscience Research Network for Sustainable Cement and Concrete, Nanocem and the Development Fund of the Swedish Construction Industry, SBUF for financing this project. The authors also want to thank Lars Wadsö for the discussions and help with data evaluation, Martin Rosenqvist for his help with concrete recipes, and thank Steven Hall and Jonas Enqvist for their help with tomography measurements and data evaluation.

References

1. Scrivener, K.L., *Options for the future of cement.* The Indian Concrete Journal 2014 **July 2014**.
2. Lothenbach, B., K. Scrivener, and R.D. Hooton, *Supplementary cementitious materials.* Cement and Concrete Research, 2011. **41**(12): p. 1244-1256.
3. Journals, I., D. Suresh, and K. Nagaraju. *Ground Granulated Blast Slag (GGBS) In Concrete@ A Review*. 2015.
4. Giergiczny, Z., et al., *Air void system and frost-salt scaling of concrete containing slag-blended cement.* Construction and Building Materials, 2009. **23**(6): p. 2451-2456.
5. Strand, M., *Experimental Study of De-icing Salt-frost Scaling in Concrete with Low-calcium Fly Ash or Slag: Influence of Drying and Carbonation, and Air Content Lund: Faculty of Engineering, LTH at Lund University.* 2018.
6. Liu, Z. and W. Hansen, *A Hypothesis for Salt Frost Scaling in Cementitious Materials.* Journal of Advanced Concrete Technology, 2015. **13**(9): p. 403-414.
7. Gagné, R., et al., *Study of the relationship between scaling resistance and sorptivity of concrete.* Canadian Journal of Civil Engineering, 2011. **38**(11): p. 1238-1248.
8. Powers, T.C.a.R.A.H., *Theory of volume changes in hardened portlandcement paste during freezing.* . Proceedings, Highway Research Board 32, PCA Bull 46, 1953.
9. Lindmark, S., *Mechanisms of salt frost scaling on portland cement-bound materials: studies and hypothesis*, in *TVBM 1017*. 1998, Division of Building Materials. p. 272 pages.
10. Utgenannt, P., *The influence of ageing on the salt-frost resistance of concrete*. 2004, Lund University Open Access. p. 346.
11. Powers, *The Air requirement of frost-resistant concrete.* 1949.
12. Fagerlund, G., *Critical degrees of saturation at freezing of porous and brittle materials*. 1973, Division of Building Materials.
13. Fagerlund, G., *The long time water absorption in the air-pore structure of concrete.* Division of Building Materials, LTH, Lund University, 1993.
14. Panesar, D.K. and S.E. Chidiac, *Capillary suction model for characterizing salt scaling resistance of concrete containing GGBFS.* Cement and Concrete Composites, 2009. **31**(8): p. 570-576.
15. Ferraris, C.a.M., N. , , *Capillary Transport in Mortars and Concrete.* Cement and Concrete Research, 1997(27): p. 747-760.
16. Washburn, E.W., *The Dynamics of Capillary Flow.* Physical Review, 1921. **17**(3): p. 273-283.
17. Setzer, M., *MODELING AND TESTING THE FREEZE-THAW ATTACK BY MICRO-ICE-LENS MODEL AND CDF/CIF-TEST.* 2020.
18. Taber, S., *The Mechanics of Frost Heaving.* The Journal of Geology, 1930. **38**(4): p. 303-317.
19. Rosenqvist, M., K. Fridh, and M. Hassanzadeh, *Macroscopic ice lens growth in hardened concrete.* Cement and Concrete Research, 2016. **88**: p. 114-125.
20. Zhichao Liu, W.H.F.W., *Pumping effect to accelerate liquid uptake in concrete and its implications on salt frost durability.* Construction and Building Materials, 2018. **158**: p. 181-188.
21. Eriksson, D., et al., *Freezing of partially saturated air-entrained concrete: A multiphase description of the hygro-thermo-mechanical behaviour.* International Journal of Solids and Structures, 2018. **152-153**: p. 294-304.
22. Coussy, O., *Mechanics and physics of porous solids*. 2010: Chichester, West Sussex, U.K. ; Hoboken, N.J. : Wiley, 2010.
23. Eriksson, D., et al., *Hygro-thermo-mechanical modeling of partially saturated air-entrained concrete containing dissolved salt and exposed to freeze-thaw cycles.* Cement and Concrete Research, 2021. **141**: p. 106314.
24. Institution, B.S., *Testing fresh concrete - Part 7: Air content - Pressure methods, EN 12350-7, .* 2019.
25. Institution, B.S., *Testing fresh concrete - Part 2. Slump test, EN 12350-2.* 2019.

26. Gagné, R., *17 - Air entraining agents*, in *Science and Technology of Concrete Admixtures*, P.-C. Aïtcin and R.J. Flatt, Editors. 2016, Woodhead Publishing. p. 379-391.
27. Liu, Z. and W. Hansen, *Sorptivity as A Measure Of Salt Frost Scaling Resistance Of Air-Entrained Concrete*. Vol. 629-630. 2014.
28. Sandström, T., *Durability of concrete hydropower structures when repaired with concrete overlays*. 2010, Luleå tekniska universitet.
29. Setzer, M.J., *Micro-Ice-Lens Formation in Porous Solid.* Journal of Colloid and Interface Science, 2001. **243**(1): p. 193-201.
30. *Standard test method for scaling resistance of concrete surfaces exposed to de-icing chemicals.* American Society for Testing and Materials. (ASTM C-672-92): p. p. 329–31.
31. Panesar, D. and S.E. Chidiac, *Multi-variable statistical analysis for scaling resistance of concrete containing GGBFS.* Cement and Concrete Composites, 2007. **29**: p. 39-48.
32. Setzer, M., et al., *Test methods of frost resistance of concrete: CIF-Test: Capillary suction, internal damage and freeze thaw test—Reference method and alternative methods A and B.* Mater. Struct., 2004. **37**: p. 743-753.
33. John J. Valenza, G.W.S., *Mechanism for Salt Scaling.* The American Ceramic Society, 2006: p. 1161–1179
34. Liu, Z. and W. Hansen, *Freezing characteristics of air-entrained concrete in the presence of deicing salt.* Cement and Concrete Research, 2015. **74**: p. 10-18.
35. Verbeck, G. and P. Klieger, *STUDIES OF 'SALT' SCALING OF CONCRETE.* Highway Research Board bulletin, 1957.
36. Fagerlund, G., *Studies of the Scaling, the Water Uptake and the Dilation of Mortar Specimens Exposed to Freezing and Thawing in NaCl Solutions.* Freeze-Thaw and De-Icing Resistance of Concrete, Lund Institute of Technology: Lund, Sweden, 1992. **G. Fagerlund and M.J. Setzer, Editors**: p. 36-66.